

2008

# Supply Current Modeling and Analysis of Deep Sub-Micron Cmos Circuits

Tariq B. Ahmad

*University of Massachusetts Amherst*

Follow this and additional works at: <https://scholarworks.umass.edu/theses>

---

Ahmad, Tariq B., "Supply Current Modeling and Analysis of Deep Sub-Micron Cmos Circuits" (2008). *Masters Theses 1911 - February 2014*. 82.

Retrieved from <https://scholarworks.umass.edu/theses/82>

This thesis is brought to you for free and open access by ScholarWorks@UMass Amherst. It has been accepted for inclusion in Masters Theses 1911 - February 2014 by an authorized administrator of ScholarWorks@UMass Amherst. For more information, please contact [scholarworks@library.umass.edu](mailto:scholarworks@library.umass.edu).

**SUPPLY CURRENT MODELING AND ANALYSIS OF DEEP SUB-MICRON  
CMOS CIRCUITS**

**A THESIS PRESENTED**

**by**

**TARIQ BASHIR AHMAD**

**Submitted to the Graduate School of the  
University of Massachusetts Amherst in partial fulfillment  
of the requirements for the degree of**

**MASTER OF SCIENCE IN ELECTRICAL AND COMPUTER ENGINEERING**

**February 2008**

**Electrical and Computer Engineering**

**SUPPLY CURRENT MODELING AND ANALYSIS OF DEEP SUB-MICRON  
CMOS CIRCUITS**

**A THESIS PRESENTED**

**by**

**TARIQ BASHIR AHMAD**

Approved as to style and content by:

---

Sandip Kundu, Chair

---

Wayne P. Burleson, Member

---

Maciej Ciesielski, Member

---

C.V Hollot, Department Head  
Electrical and Computer Engineering

## **DEDICATION**

*Dedicated to my beloved mother, who passed away on April 26, 2007  
(May her soul rest in Eternal Peace (AMIN!))  
The Fulbright Foundation and  
Faisal M.Kashif*

## **ABSTRACT**

# **SUPPLY CURRENT MODELING AND ANALYSIS OF DEEP SUB-MICRON CMOS CIRCUITS**

**FEBRUARY 2008**

**TARIQ BASHIR AHMAD**

**B.S. E.E, GHULAM ISHAQ KHAN INSTITUTE OF ENGINEERING  
SCIENCES, PAKISTAN.**

**M.S. E.C.E, UNIVERSITY OF MASSACHUSETTS AMHERST**

**Directed by: Professor Sandip Kundu**

Continued technology scaling has introduced many new challenges in VLSI design. Instantaneous switching of the gates yields high current flow through them that causes large voltage drop at the supply lines. Such high instantaneous currents and voltage drop cause reliability and performance degradation. Reliability is an issue as high magnitude of current can cause electromigration, whereas, voltage drop can slow down the circuit performance. Therefore, designing power supply lines emphasizes the need of computing maximum current through them. However, the development of digital integrated circuits in short design cycle requires accurate and fast timing and power simulation. Unfortunately, simulators that employ device modeling methods, such as HSPICE are prohibitively slow for large designs. Therefore, methods which can produce good maximum current estimates in short times are critical. In this work a

compact model has been developed for maximum current estimation that speeds up the computation by orders of magnitude over the commercial tools.

## TABLE OF CONTENTS

ABSTRACT .....	iv
LIST OF TABLES .....	viii
LIST OF FIGURES .....	ix
CHAPTER	
1. INTRODUCTION .....	1
1.1 Motivation.....	1
1.2 Background .....	3
1.3 Where does this work fits in?.....	5
2. PREVIOUS WORK.....	6
2.1 Survey of analytical current modeling methods .....	6
2.2 Survey of maximum current estimation techniques.....	8
3. NEW APPROACH OF MODELING SUPPLY CURRENT COMPONENTS ..	12
3.1 Proposed Modeling approach .....	12
3.2 New Model.....	14
4. APPLICATION OF NEW APPROACH OF MODELING SUPPLY CURRENT COMPONENTS.....	19
4.1 Environment set up .....	19
4.1.1 Lookup Table (LUT) generation.....	20
4.1.2 Circuit translation into 2-input NAND gates .....	20
4.1.3 Capacitance extraction .....	21
4.2 Application.....	244
4.3 Algorithm.....	24
5. SIMULATION OF ISCAS-85 BENCHMARKS USING NEW MODELING APPROACH .....	26

5.1 Simulation of ISCAS-85 benchmarks with 250nm Technology(vdd = 2.5V).....	27
5.1.1 Simulation Using Algorithm 1.....	27
5.1.2 Simulation using Algorithm 2.....	37
5.2 Simulation of ISCAS-85 Benchmarks with 90nm Technology (vdd = 1.5V).....	46
5.2.1 Simulation using Algorithm 1.....	46
5.2.2 Simulation using Algorithm 2.....	55
5.3 Simulation of ISCAS-85 benchmarks with 65nm technology (vdd = 1.5V).....	64
5.3.1 Simulation using Algorithm 2.....	64
6. CONCLUSION.....	73
6.1 Comparing run time of new proposed model with hspice .....	73
6.1.1 Comparing C432 Run time in HSPICE and New Model .....	73
6.1.2 Comparing C880 Run time in HSPICE and New Model .....	74
6.1.3 Comparing C2670 Run time in HSPICE and New Model .....	74
6.1.4 Comparison C3540 run time in HSPICE and New Model .....	75
6.1.5 Comparison of C6288 run time in HSPICE and New Model.....	76
6.1.6 Comparison of C7552 run time in HSPICE and New Model.....	76
6.2 Comparing accuracy of results between HSPICE and New Model.....	77
6.2.1 Comparing accuracy between HSPICE and Algorithm1 in New Model for 250nm technology.....	78
6.2.2 Comparing accuracy between HSPICE and Algorithm2 in New Model for 250nm technology.....	79
6.2.3 Comparing accuracy between HSPICE and Algorithm1 in New Model for 90nm technology.....	80
6.2.4 Comparing accuracy between HSPICE and Algorithm2 in New Model for 90nm technology.....	81
6.2.5 Comparing accuracy between HSPICE and Algorithm2 in New Model for 65nm technology.....	82
6.3 Future work.....	83
BIBLIOGRAPHY .....	84



## LIST OF TABLES

Table	Page
1. ISCAS 85 Benchmarks description .....	26

## LIST OF FIGURES

Figure	Page
1. Current consumption trends in Intel Microprocessors. Source Intel .....	1
2. Power density trends in Intel microprocessors. Source Intel .....	2
3. Power supply droop illustration .....	3
4. Effective input signal as the as the average of the inputs .....	7
5. Illustration of load current in gate network.....	12
6. Components of new compact model of capturing switching current waveform .....	13
7. Compact modeling approach with 2-input NAND gate with buffer at inputs.....	15
8. Fall case1(b) Shows input and output transitions, current from the vdd supply and current to the ground.....	16
9. Fall case2. (b) Shows input and output transitions, current from the vdd supply and current to the ground.....	16
10. Rise case1. (b) Shows input and output transitions, current from the vdd supply and current to the ground.....	17
11. Rise case2. (b) Shows input and output transitions, current from the vdd supply and current to the ground.....	17
12. Flow of steps in the environment setup .....	19
13. Flow of converting ISCAS-85 benchmarks into 2-input NAND gate circuits .....	21
14. Flow diagram of application of New Modeling approach to circuits .....	23
15. Levelized simulation example .....	25
16. Flow diagram of algorithm .....	25
17. Flow of Validation .....	27
18. Comparison of C17 benchmark using Algorithm1 in New Model and HSPICE.....	28

19. Comparison of C432 benchmark using Algorithm1 in New Model and HSPICE ....	29
20. Comparison of C880 benchmark using Algorithm1 in New Model and HSPICE ..	30
21. Comparison of C1908 benchmark using Algorithm1 in New Model and HSPICE.....	31
22. Comparison of C2670 benchmark using Algorithm1 in New Model and HSPICE.....	32
23. Comparison of C3540 benchmark using Algorithm1 in New Model and HSPICE.....	33
24. Comparison of C6288 benchmark using Algorithm1 in New Model and HSPICE.....	34
25. Comparison of C7552 benchmark using Algorithm1 in New Model and HSPICE.....	35
26. Histogram of comparison of vdd current between Algorithm 1 in New Model and HSPICE..	36
27. Histogram of comparison of ground current between Algorithm 1 in New Model and HSPICE.....	36
28. Comparison of C17 Benchmark using Algorithm2 in New Model and HSPICE.....	37
29. Comparison of C432 Benchmark using Algorithm2 in New Model and HSPICE.....	38
30. Comparison of C880 Benchmark using Algorithm2 in New Model and HSPICE.....	39
31. Comparison of C1908 Benchmark using Algorithm2 in New Model and HSPICE.....	40
32. Comparison of C2670 Benchmark using Algorithm2 in New Model and HSPICE.....	41
33. Comparison of C3540 Benchmark using Algorithm2 in New Model and HSPICE.....	42
34. Comparison of C6288 Benchmark using Algorithm2 in New Model and HSPICE.....	43

35. Comparison of C7552 Benchmark using Algorithm2 in New Model and HSPICE.....	44
36. Comparison of vdd current in ISCAS-85 benchmarks using Algorithm2.....	45
37. Comparison of ground current in ISCAS-85 benchmarks using Algorithm2.....	45
38. Comparison of C17 Benchmark using Algorithm 1 in New Model and HSPICE (90nm).....	46
39. Comparison of C432 Benchmark using Algorithm 1 in New Model and HSPICE (90nm).....	47
40. Comparison of C880 Benchmark using Algorithm 1 in New Model and HSPICE (90nm).....	48
41. Comparison of C1908 Benchmark using Algorithm 1 in New Model and HSPICE (90nm).....	49
42. Comparison of C2670 Benchmark using Algorithm 1 in New Model and HSPICE (90nm).....	50
43. Comparison of C3540 Benchmark using Algorithm 1 in New Model and HSPICE (90nm).....	51
44. Comparison of C6288 Benchmark using Algorithm 1 in New Model and HSPICE (90nm).....	52
45. Comparison of C7552 Benchmark using Algorithm 1 in New Model and HSPICE (90nm).....	53
46. Histogram of comparison of vdd current using Algorithm 1 in New Model and HSPICE for 90nm technology .....	54
47. Histogram of comparison of ground current using Algorithm 1 in New Model and HSPICE for 90nm technology .....	54
48. Comparison of C17 Benchmark using Algorithm 2 in New Model and HSPICE (90nm).....	55
49. Comparison of C432 Benchmark using Algorithm 2 in New Model and HSPICE (90nm).....	56
50. Comparison of C880 Benchmark using Algorithm 2 in New Model and HSPICE (90nm).....	57

51. Comparison of C1908 Benchmark using Algorithm 2 in New Model and HSPICE (90nm).....	58
52. Comparison of C2670 Benchmark using Algorithm 2 in New Model and HSPICE (90nm).....	59
53. Comparison of C3540 Benchmark using Algorithm 2 in New Model and HSPICE (90nm).....	60
54. Comparison of C6288 Benchmark using Algorithm 2 in New Model and HSPICE (90nm).....	61
55. Comparison of C7552 Benchmark using Algorithm 2 in New Model and HSPICE (90nm).....	62
56. Histogram of Comparison of vdd current using Algorithm2 in New Model and HSPICE (90nm).....	63
57. Histogram of Comparison of ground current using Algorithm2 in New Model and HSPICE (90nm).....	63
58. Comparison of C17 Benchmark using Algorithm 2 in New Model and HSPICE (65nm).....	64
59. Comparison of C432 Benchmark using Algorithm 2 in New Model and HSPICE (65nm).....	65
60. Comparison of C880 Benchmark using Algorithm 2 in New Model and HSPICE (65nm).....	66
61. Comparison of C1908Benchmark using Algorithm 2 in New Model and HSPICE (65nm).....	67
62. Comparison of C2670 Benchmark using Algorithm 2 in New Model and HSPICE (65nm).....	68
63. Comparison of C3540 Benchmark using Algorithm 2 in New Model and HSPICE (65nm).....	69
64. Comparison of C6288 Benchmark using Algorithm 2 in New Model and HSPICE (65nm).....	70
65. Comparison of C7552 Benchmark using Algorithm 2 in New Model and HSPICE (65nm).....	71

66. Histogram of comparison of vdd current using Algorithm 2 in New Model and HSPICE for 65nm technology .....	72
67. Histogram of comparison of ground current using Algorithm 2 in New Model and HSPICE for 65nm technology .....	72
68. Comparison of run time of C432 with HSPICE and New Model.....	74
69. Comparison of run time of C880 with HSPICE and New Model.....	74
70. Comparison of run time of C2670 with HSPICE and New Model.....	75
71. Comparison of run time of C3540 with HSPICE and New Model.....	75
72. Comparison of run time of C6288 with HSPICE and New Model.....	76
73. Comparison of run time of C7552 with HSPICE and New Model.....	77
74. Mean square error in vdd current between HSPICE and Algorithm 1 in New Model (250nm).....	78
75. Mean square error in ground current between HSPICE and Algorithm 1 in New Model (250nm) ..	78
76. Mean square error in vdd current between HSPICE and Algorithm 2 in New Model (250nm).....	79
77. Mean square error in ground current between HSPICE and Algorithm 2 in New Model (250nm) .....	79
78. Mean square error in vdd current between HSPICE and Algorithm 1 in New Model (90nm).....	80
79. Mean square error in ground current between HSPICE and Algorithm 1 in New Model (90nm).....	80
80. Mean square error in vdd current between HSPICE and Algorithm 2 in New Model (90nm).....	81
81. Mean square error in ground current between HSPICE and Algorithm 2 in New Model (90nm).....	81
82. Mean square error in vdd current between HSPICE and Algorithm 2 in New Model (65nm).....	82

83. Mean square error in ground current between HSPICE and Algorithm 2 in New Model (65nm) .....	82
--	----

# CHAPTER 1

## INTRODUCTION

### 1.1 Motivation

As Moore's law continues to hold today, the numbers of transistors per chip continue to grow per generation. As a result gate density increases per generation. An increase in gate density translates into more switching activity. At the same time, voltage gets scaled down per generation. This voltage scaling contributes to faster switching of the transistors which leads to high frequency and thus improved performance. These two trends have led to an increase in the current consumption of a chip. Even though an increase in current consumption is followed by voltage scaling and reduction in transistor size, the net effect is still a huge increase in the current consumption as shown in Figure 1

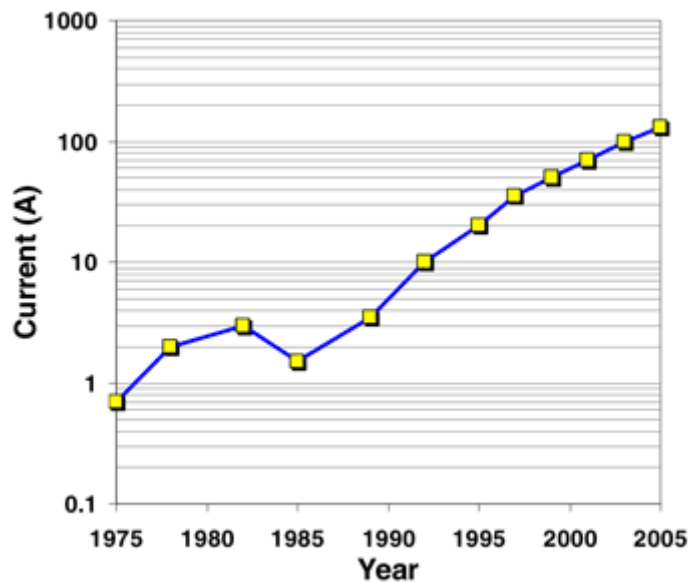
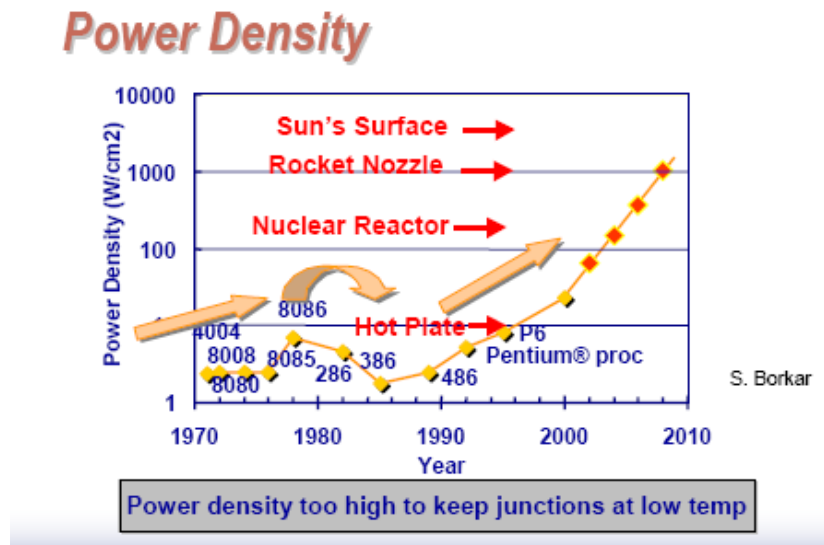


Figure 1 Current consumption trends in Intel Microprocessors. Source Intel



This unintended consequence of Moore's law has led to an exponential increase in current and power densities per generation. Power density has been increasing as much as 80 % per generation while current density has been increasing as much as 225 % per generation. See Figure 2 for power density trend.



**Figure 2 Power density trends in Intel microprocessors. Source Intel**

Power distribution network has not been able to cope up with these trends resulting in compromise in the power delivery such that the power distribution network becomes a bottleneck [1].

Another consequence of Moore's law is the interconnect scaling. The interconnects are becoming more resistive per generation. When large current flows through such thin interconnect lines, it causes voltage drop termed as *IR drop*. This IR drop manifests itself as glitch on power distribution lines and causes erroneous logic signals (*soft errors*) and degradation in switching speed. Further, high sustained current flow can cause electromigration.

In short, in order to avoid logic errors, the circuit needs to be redesigned to mitigate IR drop and reduced noise margins. This highlights the need for efficient CAD tools to estimate IR drop in the power distribution lines. The first step in solving this problem is quantifying the IR drop, which is also referred as *droop*, which is slack in power supply voltage below its nominal value. See Figure 3

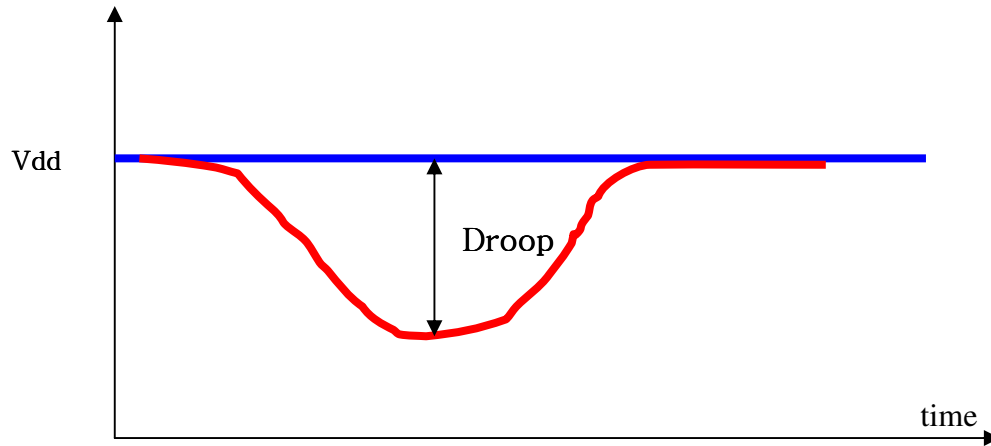


**Figure 3 Power supply droop illustration**

This droop depends upon the switching pattern. To quantify the droop requires modeling switching current waveform, which itself depends upon output load and input drive. Hence modeling worst case switching current will allow us to compute the worst case droop and size the supply lines accordingly. This work is about compact modeling of this switching current waveform and using it to estimate the total supply currents, i.e. supply (vdd) current and ground current.

## **1.2 Background**

Power is distributed to electronic components in an integrated circuit over a network of conductors. Power network design is about designing such power distribution networks with adequate performance and reliability.

IR drop across the network causes the voltage seen by the device to be supply voltage – IR drop. Another kind of voltage drop is caused by package inductance. It is commonly referred as *di/dt drop*. Therefore, the voltage seen by the device gets further reduced by this quantity.

To mitigate voltage drop at supply lines, capacitance is inserted between power and ground lines referred as *decoupling capacitance* or *decaps*. It acts as local charge storage and is helpful in counteracting voltage drop at supply points. However, given the high frequency switching of today's integrated circuits, decoupling capacitor does not provide much relief. Further, parasitic interconnect resistance, decoupling capacitance and package inductance form a complex RLC network with its own resonance frequency. If the resonance frequency gets anywhere close to the frequency of the integrated circuit, large voltage drop can occur.

Another issue in the analysis of power distribution network is the large size of integrated circuit in terms of electronic components. Simulating all such devices is infeasible. Such simulation requires searching for a pattern that causes maximum switching. A circuit with  $n$  inputs requires searching among  $2^{2n}$  patterns which is NP complete problem. An important consideration in the analysis of power distribution network is what these patterns should be. For IR drop, pattern or patterns that cause maximum switching are required. While for electromigration, patterns that cause large sustained current are of interest.

Power grid analysis can be classified into *input vector dependent* methods and *vectorless* methods. 1) The input vector pattern dependent methods employ search techniques to find a set of input patterns which cause the worst drop in the grid. A

number of methods have been proposed in literatures which use genetic algorithms or other search techniques to find vectors or a pattern of vectors that maximize the total current drawn from the supply network. Input vector-pattern dependent approaches are computationally intensive. Furthermore, these approaches are inherently optimistic, underestimating the voltage drop and thus letting some of the supply noise problems go unnoticed. 2) The vectorless approaches, on the other hand, aim to compute an upper bound on the worst-case drop in an efficient manner. These approaches have the advantage of being fast and conservative, but are sometimes too conservative, leading to overdesign [5,6].

### **1.3 Where does this work fits in?**

It is mentioned in [7] that a complete power supply distribution model must include

- 1) Package level power distribution network dominated by Inductance
- 2) On-chip power bus model dominated by Resistance
- 3) On-chip switching activities model for each functional block which means determining the switching current.

From [7], it follows that our work falls in 3), which is modeling switching current waveform of a network.

## CHAPTER 2

### PREVIOUS WORK

#### 2.1 Survey of analytical current modeling methods

Analytical methods for estimating switching current waveform of CMOS gates have been in use since the introduction of CMOS technology. Analytical equations exist both for NMOS and PMOS for each region of their operation and for every technology generation. Moving to a higher level of abstraction, CMOS inverter has been a subject of an extended research [9-12], which is the basic block to which all CMOS circuits can be collapsed. It has been proposed in various research studies that if one could convert a CMOS circuit into an equivalent CMOS inverter that has the same performance, then modeling switching current waveform of the CMOS circuit is equivalent to modeling switching current waveform of an equivalent CMOS inverter.

Analytical modeling of CMOS inverter aim at deriving an output expression based upon input status for each region of operation of each transistor. Various analytical models have been proposed such as Shiman-Hodges square law [9], nth power law [10], and Alpha power law [11-12]. They all suffer from the same problems of complicated expressions and inability to account for deep submicron effects. Hence, they require modification every technology generation.

In the past, estimation techniques focused upon dynamic current flow, caused by the charging or discharging of output load capacitance. However, in the deep submicron era, short circuit current flow can not be neglected. Exactly similar approach has been adopted to model short circuit current as dynamic current. The CMOS circuit is

converted to an equivalent CMOS inverter for estimating short circuit current. The problem here is to determine the size of transistors in the CMOS inverter as well as the effective input signal fed to it. The approach has been to choose fastest input signal as the effective signal for parallel connected MOSFETS and vice versa [15]. This approach may result in erroneous delay information [16]. Another approach of choosing effective input signal of an equivalent CMOS inverter is to heuristically choose the average of the overlapping signals at the inputs as shown in Figure 4. The solid lines represent the original input signals while the dotted line represents the effective input.

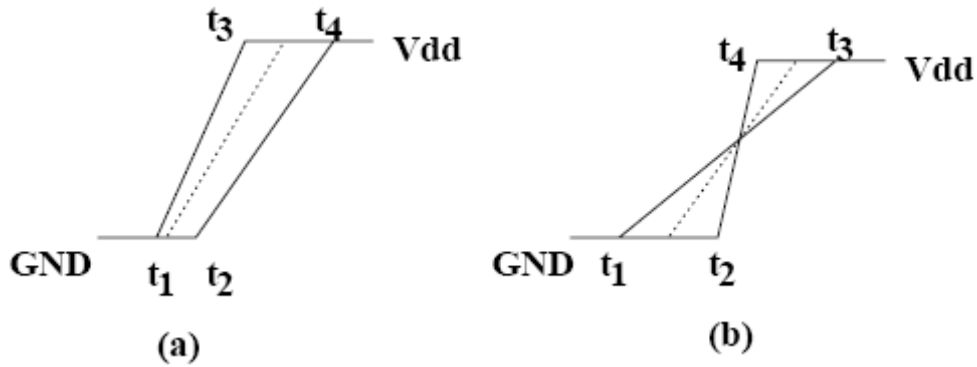


**Figure 4 Effective input signal as the as the average of the inputs**

Similarly, effective channel width of the equivalent CMOS inverter is calculated. Traditionally, the equivalent transistor width of MOSFETs connected in series is the inverse of the sum of reciprocals of the channel width of each individual transistor and vice versa for MOSFETs connected in parallel [16]. A better approximation is proposed in [15], where the equivalent transistor width depends on the relative delays of input signals.

## 2.2 Survey of maximum current estimation techniques

There has been an extensive research done on the estimation of currents in power supply lines for deterministic input patterns [15, 18, 19, and 20]. The proposed methods provide speed up over HSPICE while providing acceptable accuracy of power and ground current waveforms. Thus finding maximum current in power distribution lines translates to running simulation over all possible input patterns and choosing the one that causes maximum current drawn. However, these methods can be applied to small circuits having a few inputs. As the circuit gets larger, the number of input patterns that can be applied grows exponentially and these methods are not practical.

Chowdhury et al [21] have addressed the problem of maximum current estimation for large circuits with large number of inputs. In their proposed method, a large circuit is divided into smaller logic blocks. Then either a search technique i.e., branch or bound or heuristic technique is employed to find maximum transient current for every logic block. The sum of maximum transient currents for each block represents the estimated maximum current for the entire circuit. However, their method suffers from the problem of overestimation. Further, due to large circuit size, their search technique is slow.

Devdas et al [22] have addressed the same problem. They formulate maximum current estimation problem as weighted max-satisfiability problem on a set of multi-output Boolean functions. These functions are derived from the logic description of the circuit. Branch and bound algorithm is employed to solve this N-P complete max satisfiability problem. However, they attempted the problem under the unit gate delay

assumption. Further, the output functions are quite complex and running time is slow. They also didn't attempt to solve for the general gate delay.

From the above survey, it is established that proposed techniques are computationally prohibitive for large VLSI circuits. In such a case, pattern independent algorithms become a natural choice. In the following paragraphs such techniques are being discussed.

Previous work by Farid Najm et al [3] estimates an upper bound of maximum current from the power supply and ground buses by propagating input excitations and time intervals through a levelized gate network. The proposed algorithm termed as 'iMax' calculates maximum current waveform statistically in linear time and is pattern independent. Hence this work has resorted to static approach of current calculation, as simulation of a large input set for larger circuits is prohibitively expensive. However, this work assumes all inputs are independent, all primary inputs switch at time  $t = 0$ , circuit style is combinational, gate delays are fixed and known ahead of time, waveform shape is right angled triangular, various parameters of the transition current waveform such as its peak, duration and the time at which it occurs are calculated in a preprocessing phase from the circuit level parameters of the gate under consideration as well as of the other gates that are connected to its inputs and output. Another assumption is that between the times at inputs when an interval begins or ends, and the next interval begins or ends, the sets of excitations that the inputs can assume do not change and therefore no corresponding uncertainty interval can begin or end at the output during that time shifted by the gate delay  $D$ .



Work by Yi-Min Jiang [2] et al has extended the work done by Farid Najm et al and present four approaches 1) timed-ATPG-based approach, 2) probability based approach, 3) genetic algorithm based approach and 4) integer linear programming based approach for estimating the maximum instantaneous currents through the supply lines. The first three approaches produce a tight lower bound while the fourth approach an exact solution for small circuits and tight upper bounds for large circuit. In timed-ATPG approach, a set of signals whose simultaneous switching produces high current is assigned transitions and timed-ATPG is used to justify the assignments and derive two-vector sequences. But selection of such signals has not been explained and justified. In the probability-based approach, a set of selected gates is assigned weights based on their possible current contribution at a given time. Again, it is not specified how do they select such gates and how do they assign weights? In the ILP-based approach, the problem is modeled as an ILP problem. Solving the corresponding ILP formula allows finding an exact solution. However, this technique is impractical for large circuits. They propose a partition solution for breaking the bigger circuit into smaller sub-circuits and solving ILP for smaller sub-circuits. However, the upper bound found by combining the ILP solutions of sub-circuits is not a tight upper bound. In the genetic algorithm-based (GA) approach, which works at any level of abstraction unlike the previous three approaches that work at the gate level, a search is conducted based on mechanics of natural selection and natural genetics. To use GA, elements in the solution space are coded into finite length strings. Each string has a fitness values associated with it. But it is not defined how to associate a fitness value with a given string. They use three processes of 1) selection, 2) crossover and 3) mutation to generate new strings. The

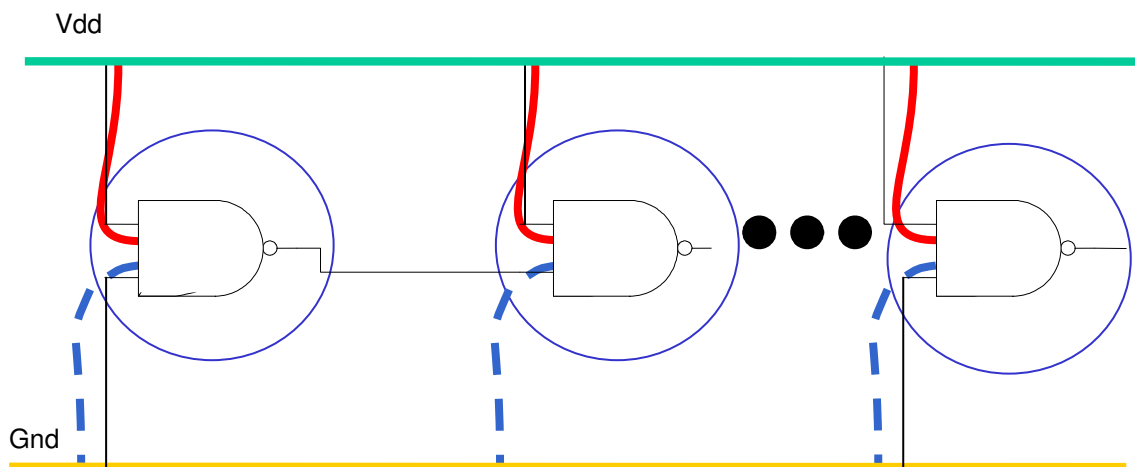
objective is to generate strings with high fitness value. The initial population contains  $N$  random strings of length  $L$ . The fitness value of each string is calculated by a fitness function. Generation of a new population is found by selecting two individuals from the current population, crossing the two selected strings, and mutating the elements of the new strings with a given mutation probability. The process is repeated until the number of strings in the new population is equal to  $N$ . Selection is biased toward individuals with higher fitness values so the average fitness value tends to increase. The next population is generated based on the current population using the same procedure. The process continues until the number of generations reaches a predefined value, or the optimal solution has been found.

## CHAPTER 3

### NEW APPROACH OF MODELING SUPPLY CURRENT COMPONENTS

#### 3.1 Proposed Modeling approach

On the basis of discussion presented in chapter 1, it is established that power supply droop is a dynamic quantity that depends upon the current drawn by the output load also known as load current. This current itself depends upon the output load and input drive. Therefore, modeling load current waveform of a switching network is equal to modeling load current at each and every gate in the network. This idea is illustrated in figure 5



**SOLID** is switching **Vdd** current  
**DASHED** is switching **ground** current

**Figure 5 Illustration of load current in gate network**

Modeling load current requires that load current has a certain associated waveform. In this chapter, a compact model is presented to capture this waveform.

Once this waveform is captured for each gate based on its switching status, they can be added to get the the total switching current waveform.

In our new compact model, switching current waveform is a function of

- 1) Output load capacitance  $l$  at the output of a gate
- 2) Input voltage  $v$  at the gate and
- 3) Slope  $s$  of the transition at the input of the gate.

This is illustrated in the case of a 2-input NAND gate in figure 6.

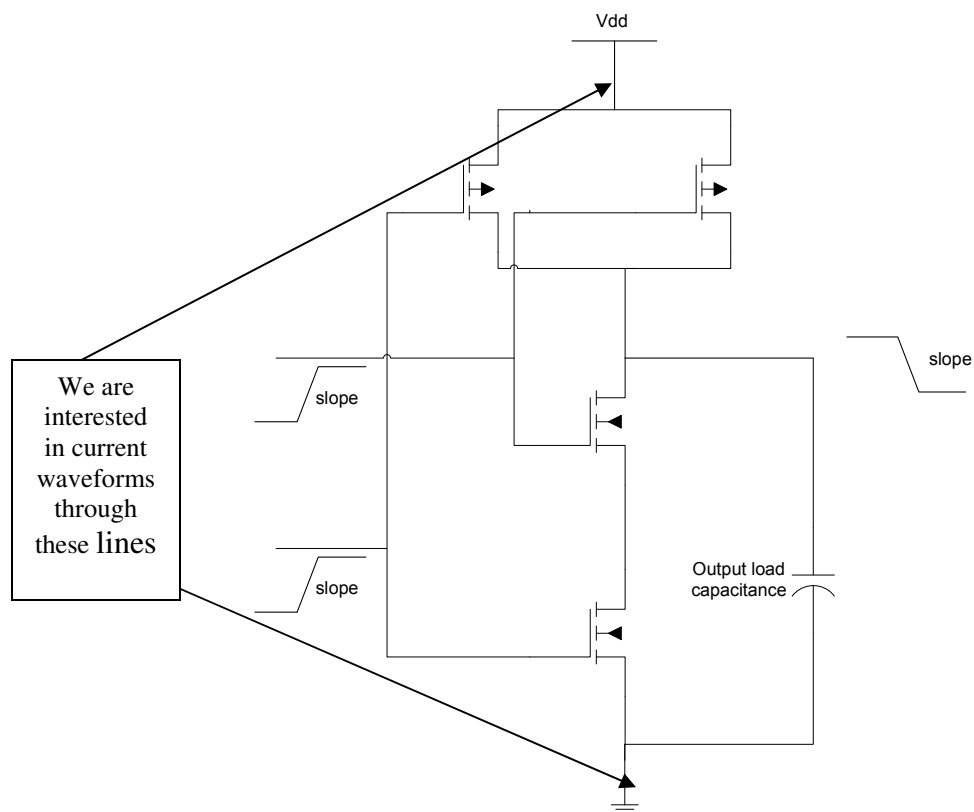


**Figure 6 Components of new compact model of capturing switching current waveform**

Hence,

$$I_{\text{switching}} = \text{function}(l, v, s) \quad \text{Equation 1}$$

Similarly peak supply current is defined by the following equation

$$peak\_current = \max \sum_{i=1}^{|gates|} \max(\text{switching\_currents})$$

Equation 2

For characterizing peak current and total supply current consumption, a vector based circuit simulation is used to find the total supply currents i.e both ground and vdd currents. Unlike the work done by Farid Najm et al [3] and Angela Krystic et al [4], dynamic simulation is used to compute vdd and ground currents for a gate network given a specific input pattern. This is intended to eliminate the need of using HSPICE, which is slow for large circuits and works at a lower level of abstraction. Moreover, HSPICE solves complex differential equations while our compact model uses a simple approach of characterizing switching current waveform as a function of load, slope and input voltage. If working with a particular technology for example 0.25 micron, the supply voltage is known to be 2.5 volts so one can skip voltage, as it is constant and model switching current waveform as a function of slope and output load capacitance.

### 3.2 New Model

To compute switching current waveform of a gate in a network, we use compact modeling approach applied to a 2-input NAND gate with buffer at inputs as our model shown in figure 7. It should be noted that a 2-input NAND gate is chosen because it is a universal gate and many technology mapping tools such as SIS can convert a heterogeneous gate network into a network of only 2-input NAND gates. But nevertheless, our compact modeling approach can be applied to other gate types as well. This part is being skipped here because of the enormity of this.

NAND Gate Model  
Current I = func(output load,input slope,input voltage)

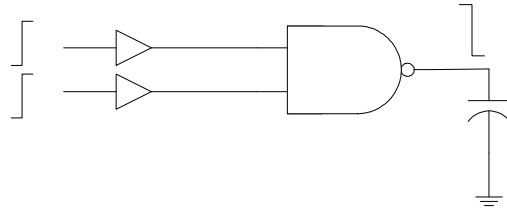


**Figure 7 Compact modeling approach with 2-input NAND gate with buffer at inputs**

The New Model is driven with particular load capacitance at the output, slope and voltage at the input. The New Model is used to compute vdd and gnd currents for different voltages, slopes and load combinations. Note that we are not interested in the current through load capacitance but the total current from the vdd and ground buses. The New Model is not only used to compute peak values of these currents but also propagation delay, width of the current waveforms and output slope. This way one can capture the whole current waveform.

There are four transition cases for a 2-input NAND gate that cause transition at its output: two for the fall transition and two for the rise transition. The two fall transitions are

1) When one of the input changes from 0 to 1 while the other remains at 1 as shown in figure 8 along with the currents that flow from vdd supply and sink in the ground.

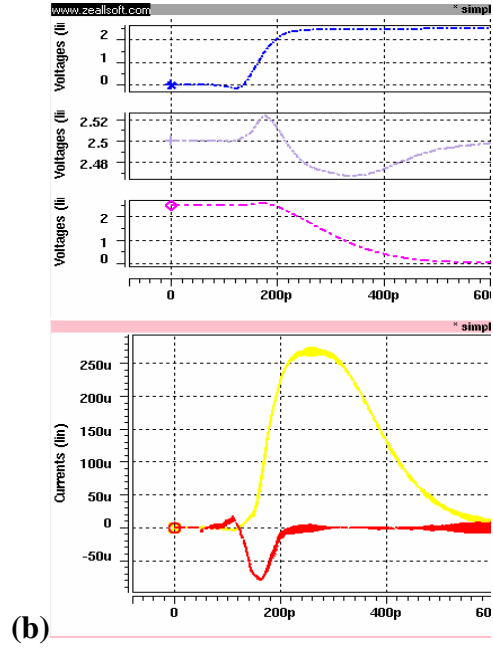
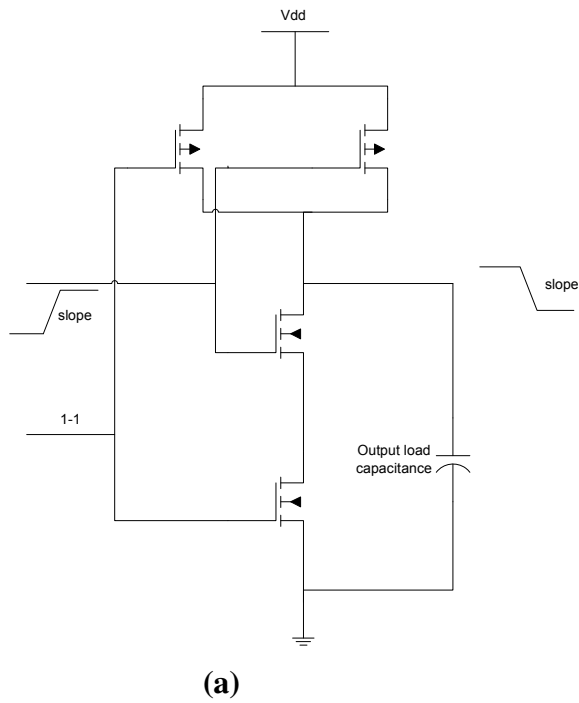


**Figure 8 Fall case1. (b) Shows input and output transitions, current from the vdd supply and current to the ground**

2) When both of the inputs change from 0 to 1 as shown in figure 9

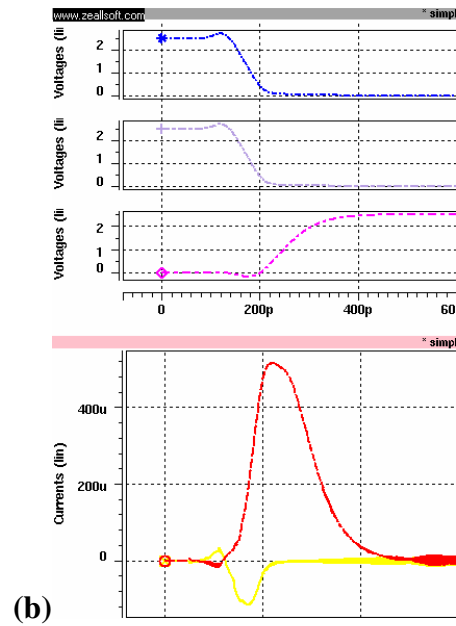
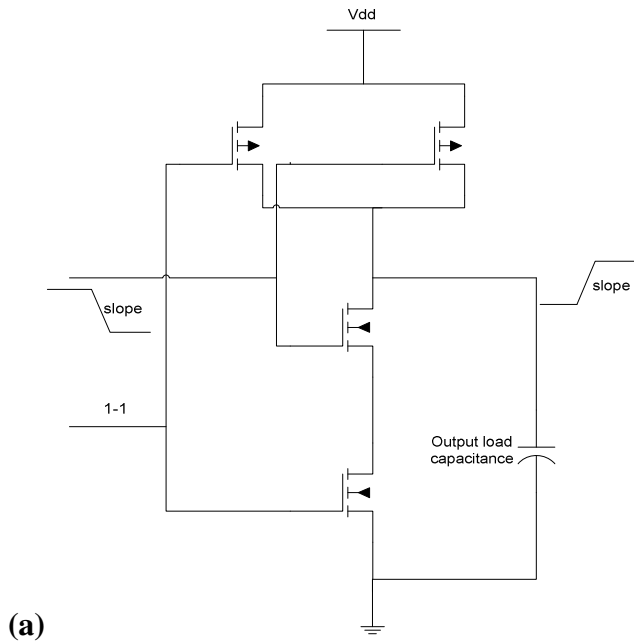


**Figure 9 Fall case2. (b) Shows input and output transitions, current from the vdd supply and current to the ground.**

Similarly the two rise transitions are

- 1) When one of the input changes from 1 to 0 while the other remains at 1 as shown in figure 10.

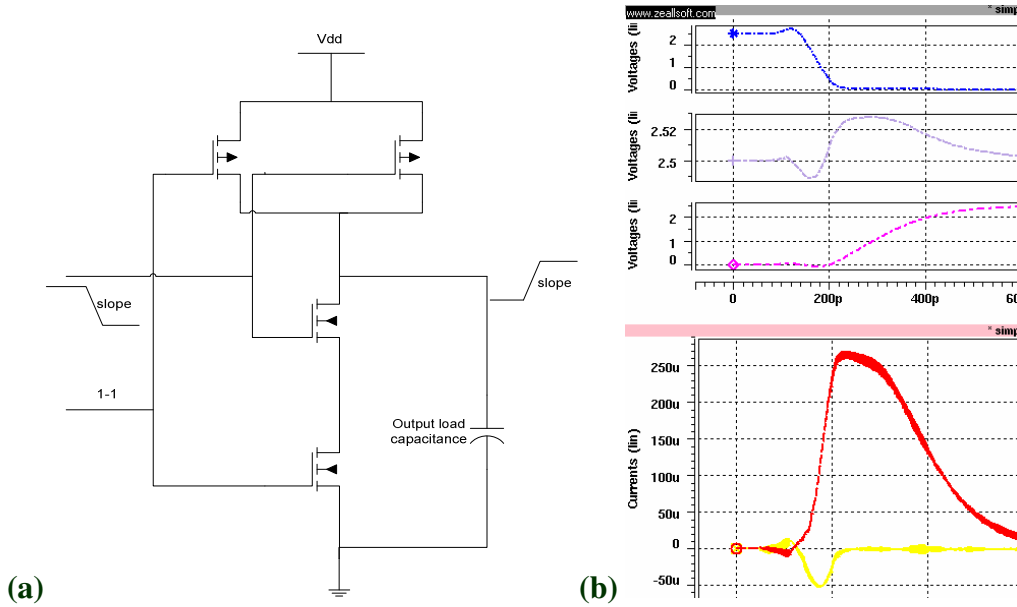


**Figure 10 Rise case1. (b) Shows input and output transitions, current from the vdd supply and current to the ground.**

- 2) When both of the inputs change from 1 to 0 as shown in figure 11

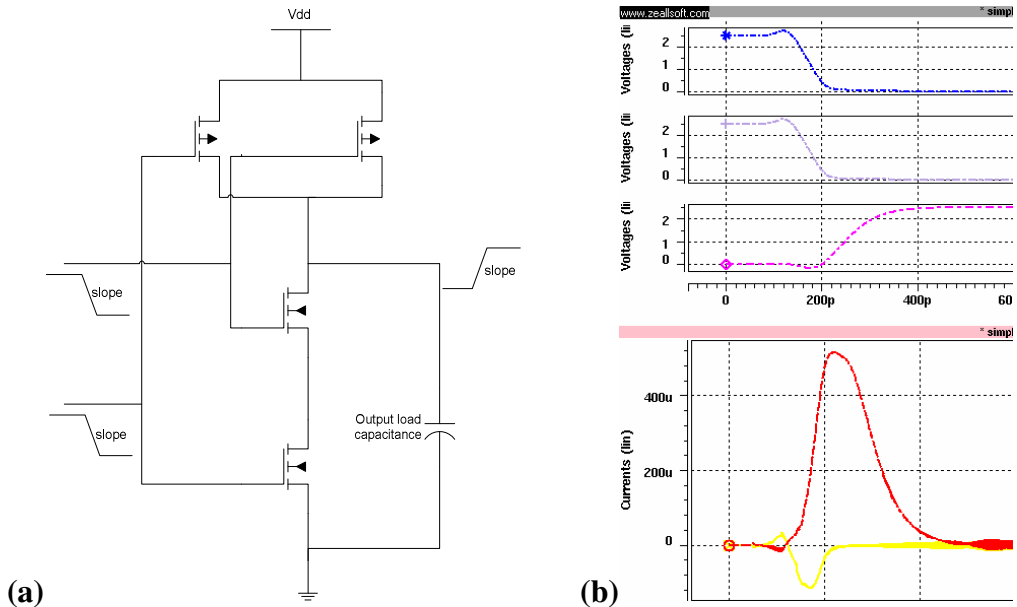


**Figure 11 Rise case2. (b) Shows input and output transitions, current from the vdd supply and current to the ground.**



In the case when output does not switch, a slightly different approach of modeling is used which will be discussed later.

## CHAPTER 4

### APPLICATION OF NEW APPROACH OF MODELING SUPPLY CURRENT COMPONENTS

Now that a compact model of supply currents has been defined, it is necessary to apply this to circuits. But before its application, there are certain steps that should be followed. These steps are called setting up the environment.

#### 4.1 Environment set up

The environment set up consists of three major steps. The following flow diagram describes the three steps.

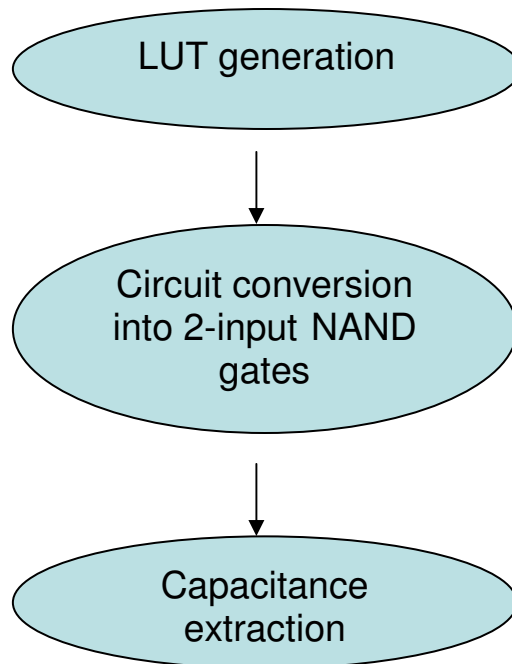


**Figure 12 Flow of steps in the environment setup**

#### **4.1.1 Lookup Table (LUT) generation**

Based on the basis of experiments on a 2-input NAND gate detailed in Appendix A, four lookup tables (LUTs) were generated for the four switching cases. These experiments helped simplify the lookup tables as much as possible. A lookup table is generated for each switching case by keeping slope/s and arrival time/s fixed while varying the output load capacitance. This translates to running HSPICE simulations by just varying the output load and capturing the values that can help plot supply current waveforms. The values that are captured by this table are maximum and minimum values of vdd current, maximum and minimum values of gnd current, widths of the current waveforms, output slope and output delay. Note that all quantities are dynamic.

#### **4.1.2 Circuit translation into 2-input NAND gates**

As discussed in the previous chapter, the model is based on 2-input NAND gate. Hence one can apply this new model onto a 2-input NAND gate network. So either one can build a 2-input NAND gate network from the scratch or convert widely used ISCAS-85 benchmarks to 2-input NAND gates. Following is the flow of converting ISCAS-85 benchmarks to 2-input NAND gates. It should be noted that the proposed model can be applied to other types of gates with different fan in besides a 2 input NAND gate but this part is being skipped because of the enormity of this project and time constraint.

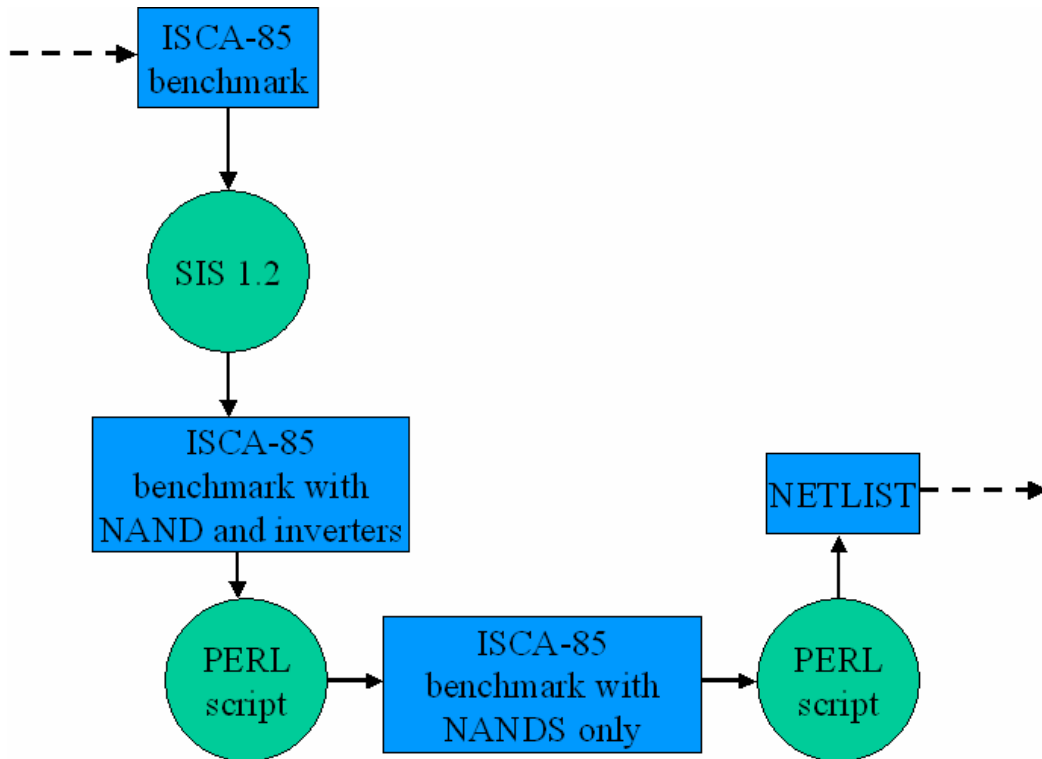


**Figure 13 Flow of converting ISCAS-85 benchmarks into 2-input NAND gate circuits**

#### 4.1.3 Capacitance Extraction

This step is optional. Capacitance of ISCAS-85 benchmark circuits can be extracted using professional tools both in the pre-layout mode as well as in the post-layout mode. While a simpler way to extract capacitance of ISCAS-85 circuits in the pre-layout mode is to run HSPICE simulation of a given ISCAS-85 benchmark circuit with *.captab* option in the HSPICE deck. While running HSPICE simulation, it has been observed that for a particular technology say 0.25u, the capacitance of all intermediate nodes almost remain the same independent of the size of the circuit. Therefore, one can assume the capacitance to be the same for all the intermediate nodes for all ISCAS-85

benchmarks. This assumption greatly reduces the computation time to be discussed later on.

## **4.2 Application**

The following flow diagram in Figure 14 describes the application of proposed New Model to circuits. In order to apply the proposed New Model, all circuit information should be provided to the Model as input. This includes providing primary inputs, primary outputs, gate delay information, load capacitance information, netlist and input pattern for a circuit. The other information that needs to be provided to the New Model is the Lookup Tables (LUT) which is global for a certain technology. Once all this information is presented to the New Model, it processes the information according to an algorithm (to be discussed in the next section) to compute switching current values, widths of switching current waveforms and output gate delay. Once all switching gates are processed in such a manner, waveforms are constructed for each such gate. Both vdd and ground current waveforms are constructed per switching gate. For simplicity, triangular construction is used for both vdd and ground waveforms. Once all these waveforms have been constructed for all switching gates, superposition is applied to superpose all ground waveforms to get one final ground waveform. Similarly, superposition is applied to all vdd waveforms to get one final vdd waveform. The maximum values of these two waveforms estimate the maximum vdd and ground current for a particular pattern in a circuit. Figure 14 also shows an optional step, which is superposition of nonswitching waveforms into the switching waveforms. Non-switching waveform is generated for a 2 input NAND gate when both the inputs make a transition while the output does not make a transition. For example when one input of a

2 input NAND switches from zero to one while the other input of the NAND gate switches from one to zero. In this case, one can add the contribution of such gates by counting the number of such gates and scaling the final ground waveform appropriately.

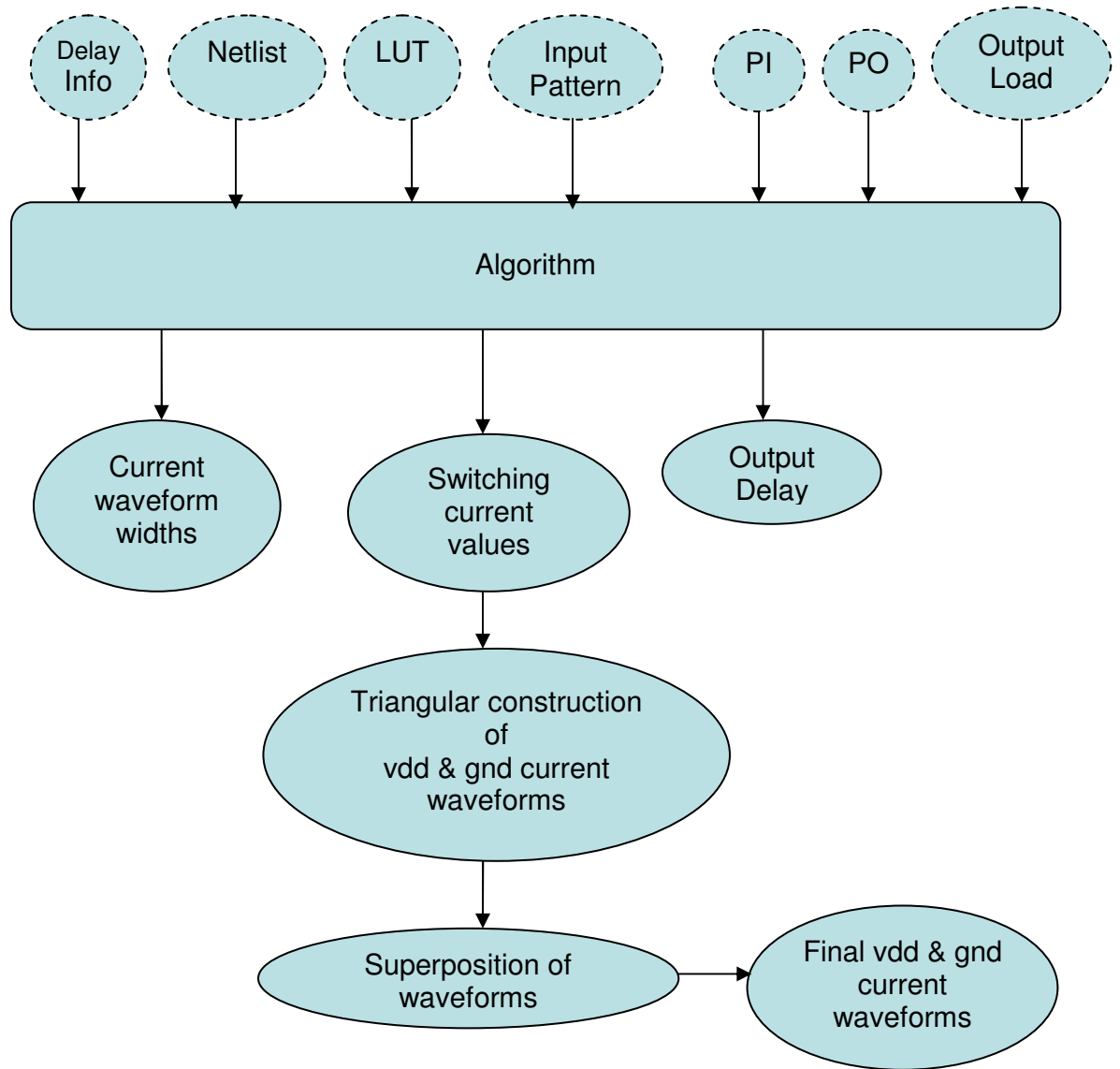


**Figure 14** Flow diagram of application of New Modeling approach to circuits.

### 4.3 Algorithm

Figure 16 discusses the flow of the algorithm which is the core of application of proposed New Modeling approach to the circuits. The algorithm makes several arrays out of the information that is provided to the application as input. The algorithm then calls a procedure *Evaluate\_Netlist* that first initializes all arrays to a condition that marks that no gate has been evaluated. The algorithm then enters into a loop which iterates until all gates are evaluated. The order in which gates are evaluated is *levelized* order shown in figure 15. Levelized order makes sure that a gate is not evaluated until all of its inputs have arrived. Therefore, gates at level 0 are evaluated first then gates at level 1 and so on until all gates have been evaluated. Coming back to the algorithm, when inside the loop, for every gate input transitions are obtained based upon the input pattern. Based upon this information, algorithm falls into one of four switching cases and fetches information from the appropriate Lookup table (LUT) based upon load information. The information obtained from the LUT is used to fill delay and switching waveform arrays. Based upon this information, triangular waveforms are constructed for all switching gates. Once all gates have been evaluated, algorithm exits out of the loop, superposition is done on all vdd waveforms and ground waveforms to get one final vdd waveform and one final ground waveform. The maximum values of vdd waveform and ground waveform estimate the maximum vdd and maximum ground current respectively.

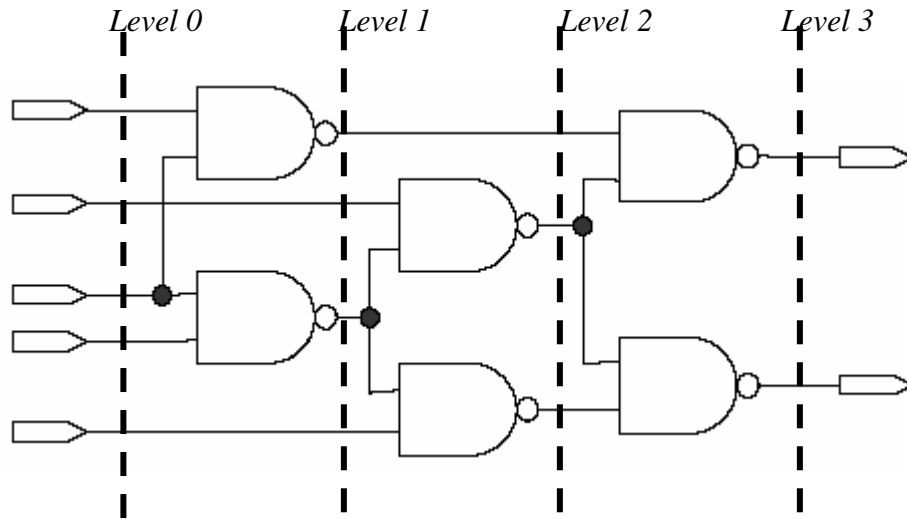


**Figure 15 Levelized simulation example**

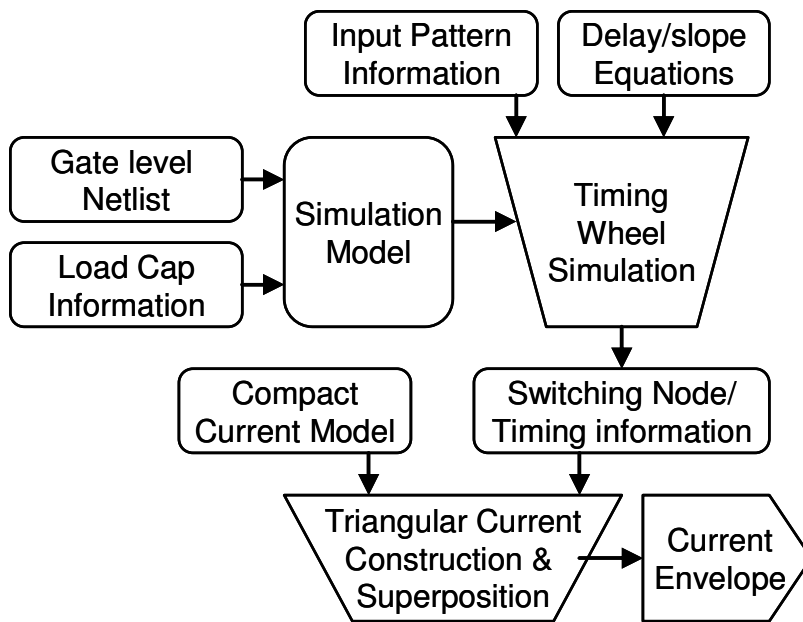


**Figure 16 Flow diagram of algorithm**



## CHAPTER 5

### SIMULATION OF ISCAS-85 BENCHMARKS USING NEW MODELING

#### APPROACH

Now that an application environment has been setup for the proposed New Current Model, its time to apply this to real circuits. The circuit suite chosen for this purpose is ISCAS-85 benchmarks. Following Table 1 describes the ISCAS-85 benchmarks. Please note that for our purpose, ISCAS-85 benchmarks have been converted to pure 2 input NAND gates using flow described in the previous chapter.

<b>Circuit Name</b>	<b>Circuit Function</b>	<b>Total Gates</b>	<b># of Inputs</b>	<b># of outputs</b>
C17	ALU	6	5	2
C432	Priority Decoder	347	36	7
C880	ALU & Control	540	60	26
C1908	ECAT	972	33	25
C2670	ALU & Control	1354	233	144
C3540	ALU & Control	1899	50	22
C6288	16 Bit Multiplier	2399	32	32
C7552	ALU & Control	3870	207	108

**Table 1 ISCAS 85 Benchmarks description**

Further, the following flow in figure 17 describes how validation will be done. As the figure shows, a netlist for any benchmark is given to the New Proposed Model (upper arm of the figure 17) and to a PERL script that converts that netlist into a

transistor level SPICE deck (lower arm of figure 17). The simulation results of the two arms are then compared to see any differences. Note that there are two algorithms shown in the upper arm. The algorithm has been fully discussed in the previous chapter but two versions of the algorithm were created. Algorithm 1 is slower but more accurate while Algorithm 2 is faster and comparatively slightly less accurate.

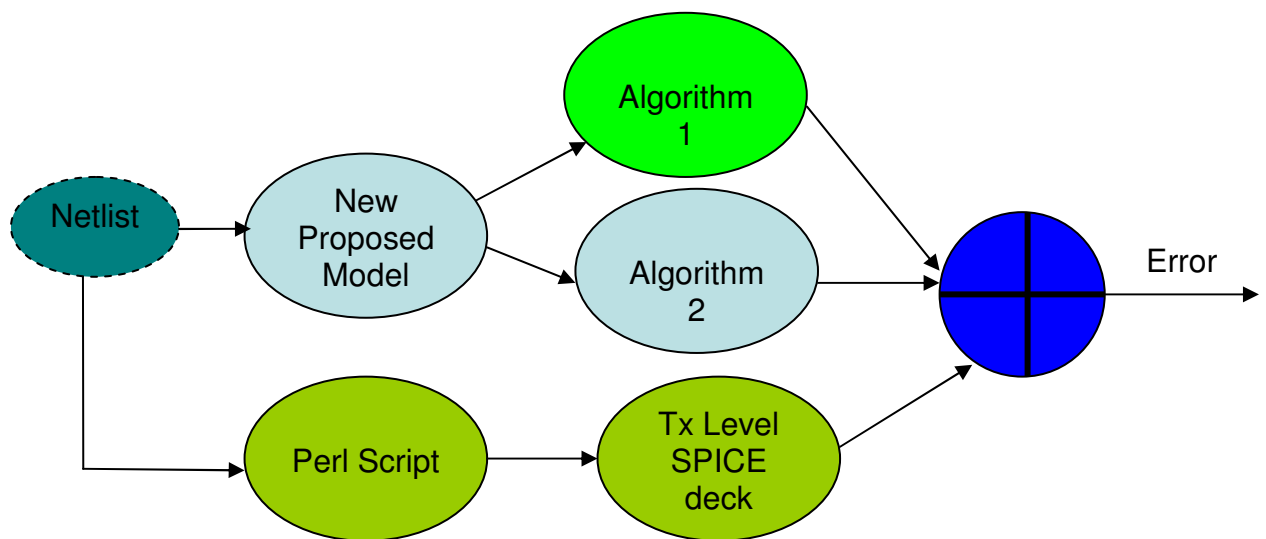


**Figure 17 Flow of Validation**

## **5.1 Simulation of ISCAS-85 benchmarks with 250nm technology (vdd = 2.5V)**

### **5.1.1 Simulation Using Algorithm 1**

First simulation of all benchmarks will be done using Algorithm 1 and the results will be compared with HSPICE simulation. Both waveforms and histogram of the results are shown in the following figures.

### 5.1.1.1 Simulation of C17 Benchmark

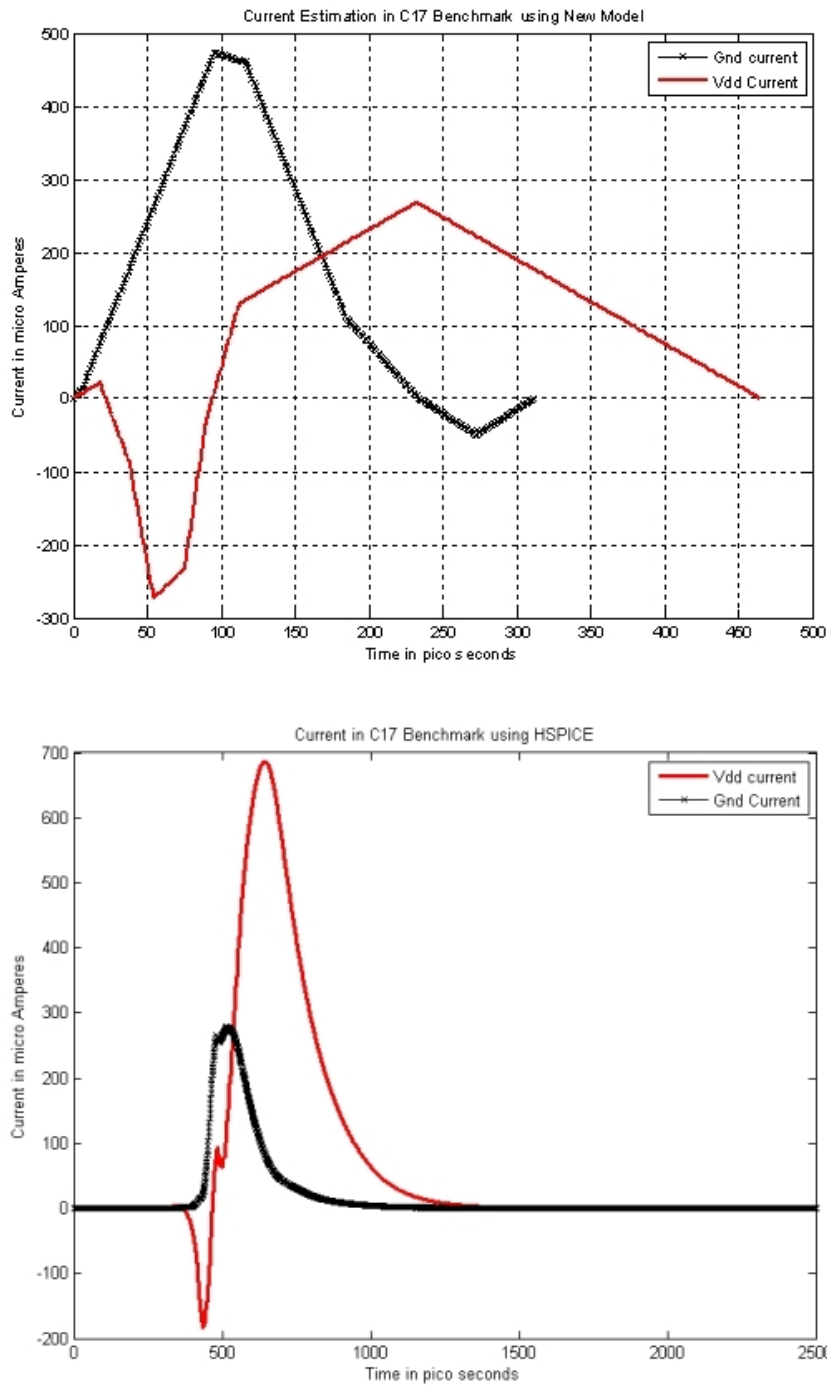


**Figure 18 Comparison of C17 benchmark using Algorithm1 in New Model and HSPICE**

### 5.1.1.2 Simulation of C432 Benchmark

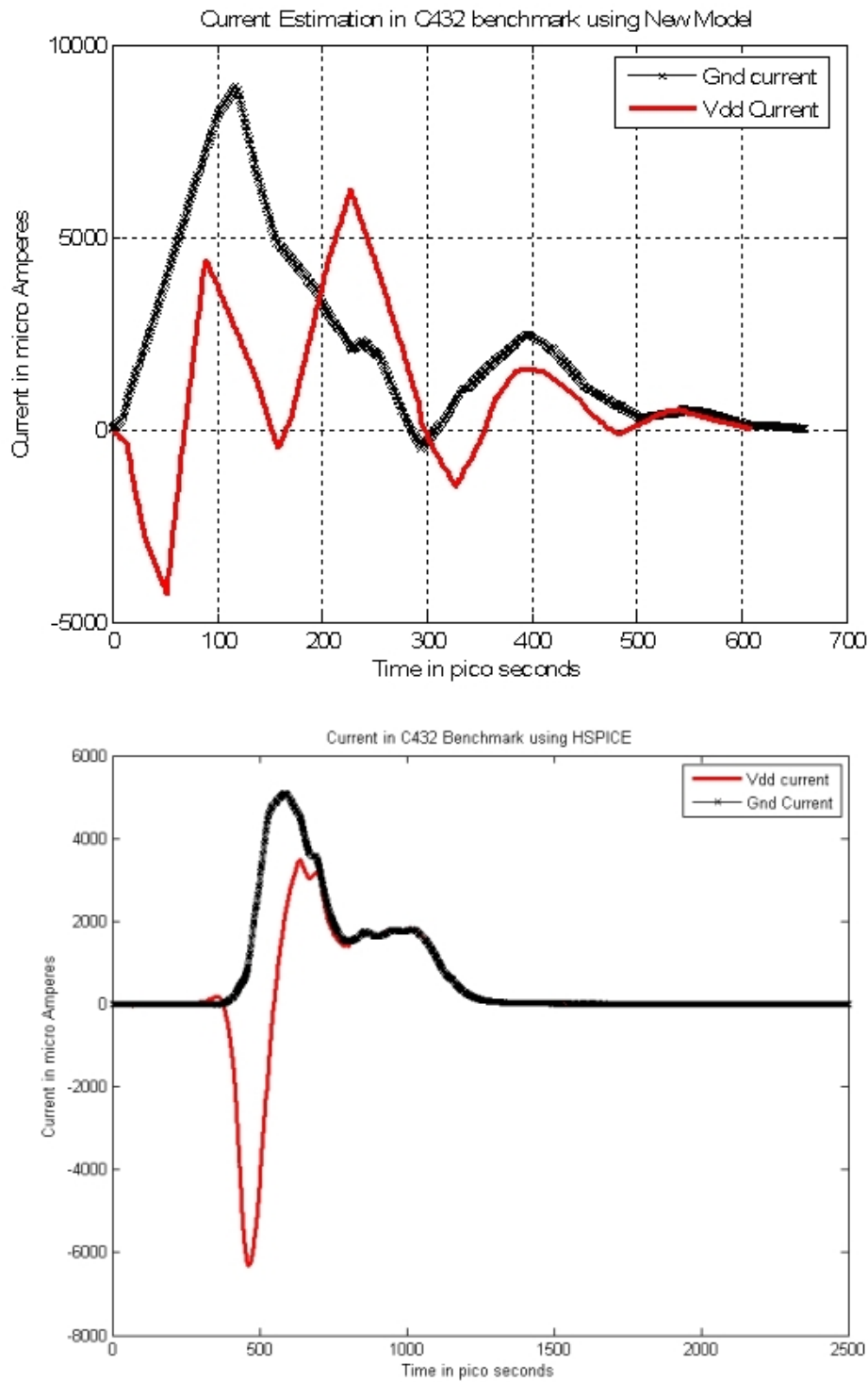


**Figure 19 Comparison of C432 Benchmark using Algorithm 1 in New Model and HSPICE**

### 5.1.1.3 Simulation of C880 Benchmark

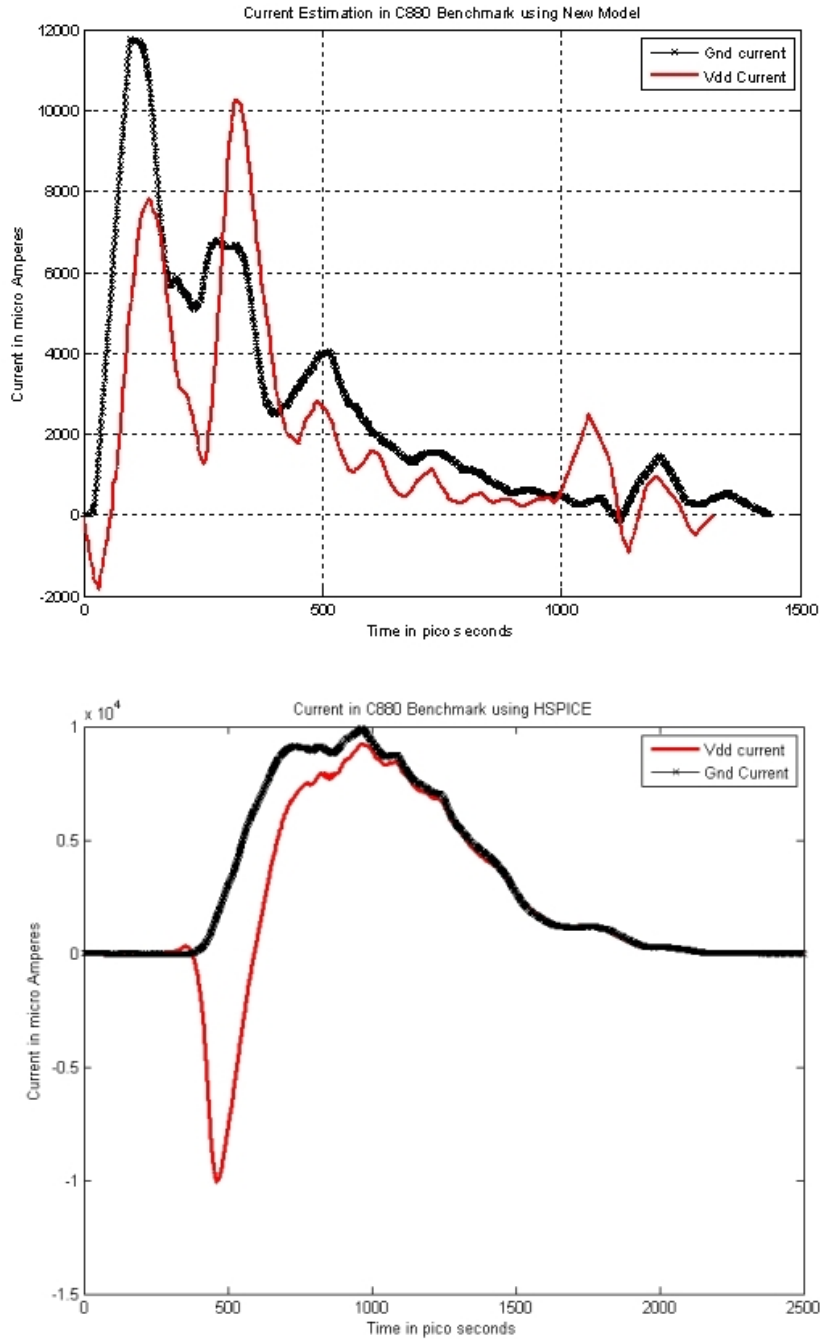


**Figure 20 Comparison of C880 Benchmark using Algorithm 1 in New Model and HSPICE**

### 5.1.1.4 Simulation of C1908 Benchmark

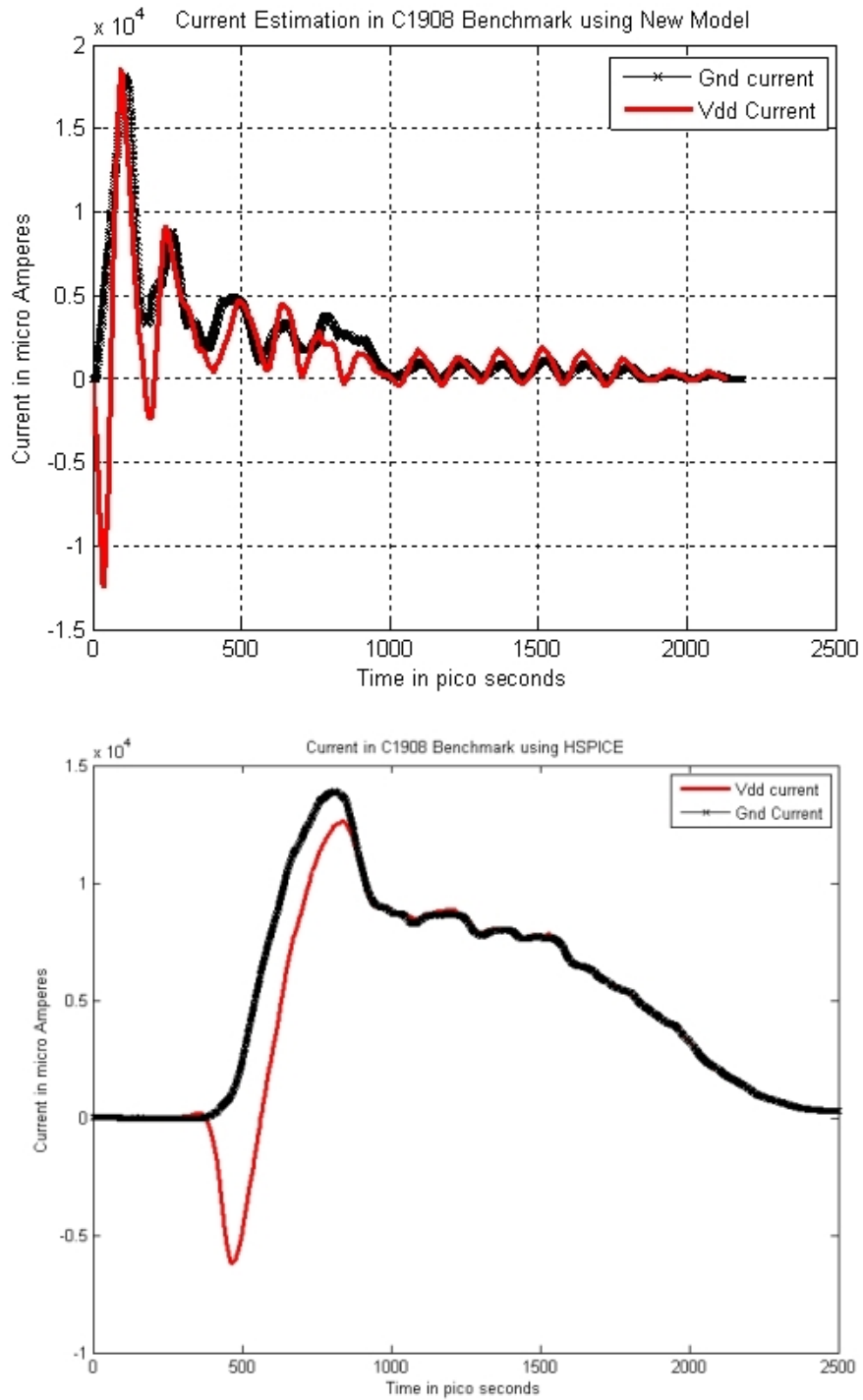


**Figure 21 Comparison of C1908 Benchmark using Algorithm 1 in New Model and HSPICE**

### 5.1.1.5 Simulation of C2670 Benchmark

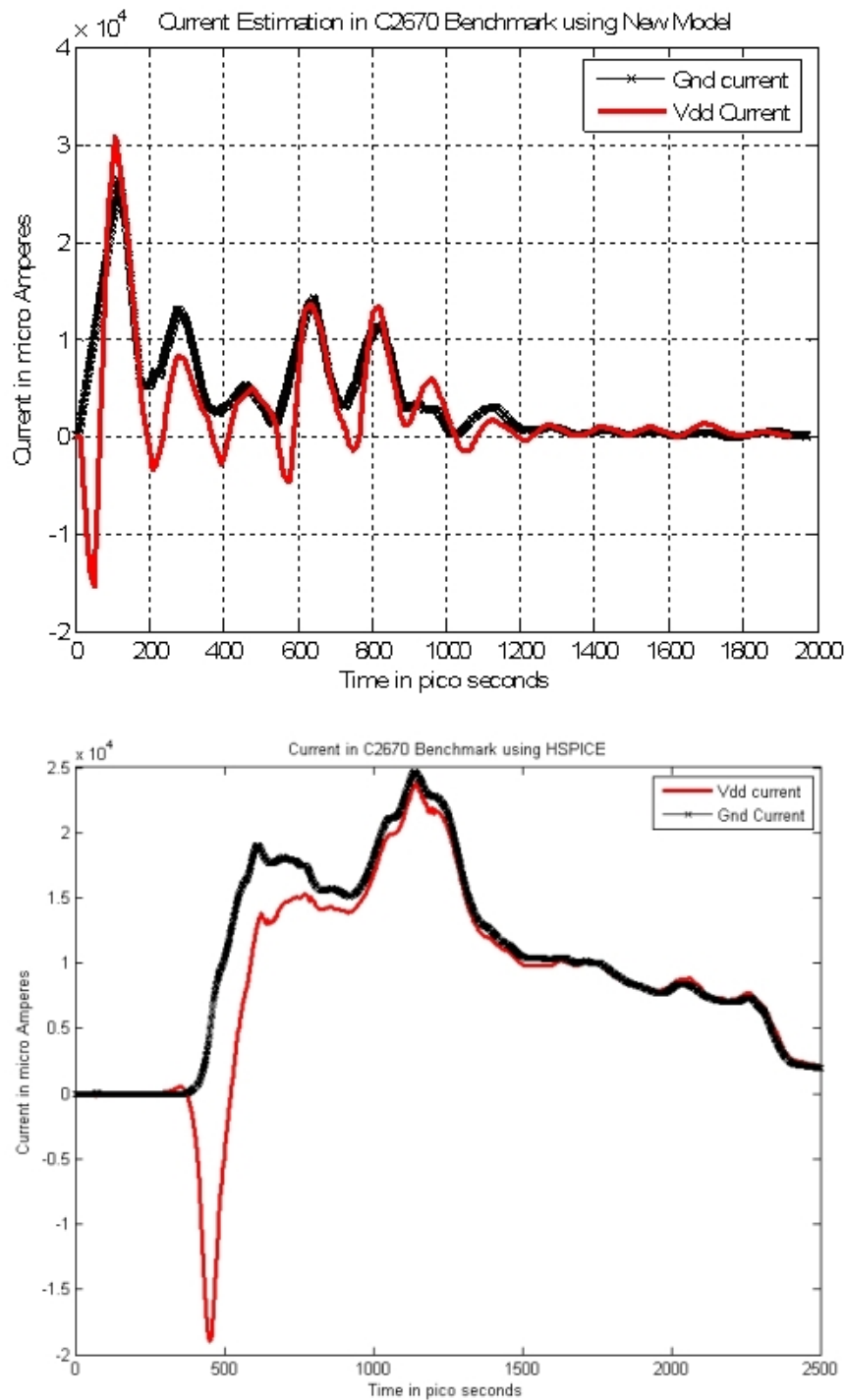


**Figure 22 Comparison of C2670 Benchmark using Algorithm 1 in New Model and HSPICE**

### 5.1.1.6 Simulation of C3540 Benchmark

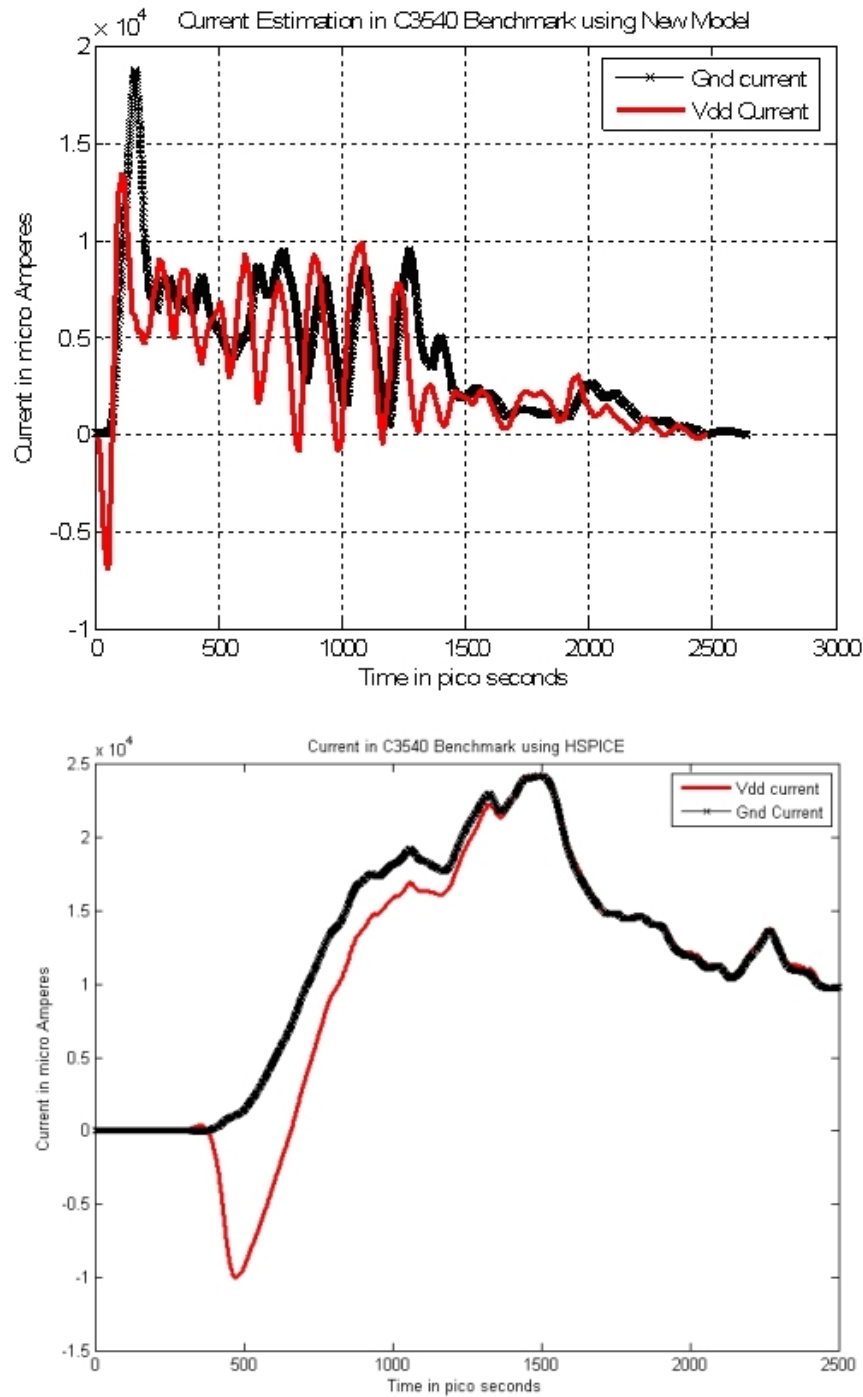


**Figure 23 Comparison of C3540 Benchmark using Algorithm 1 in New Model and HSPICE**



### 5.1.1.7 Simulation of C6288 Benchmark

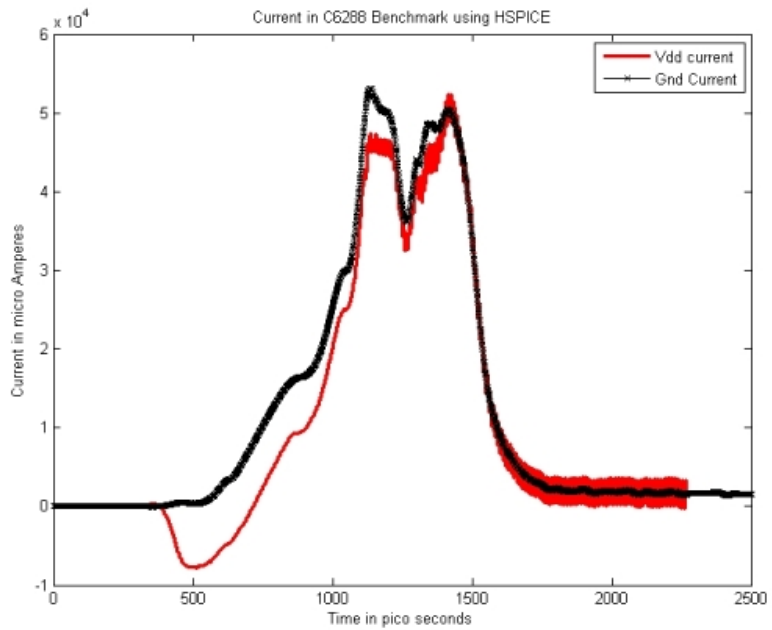
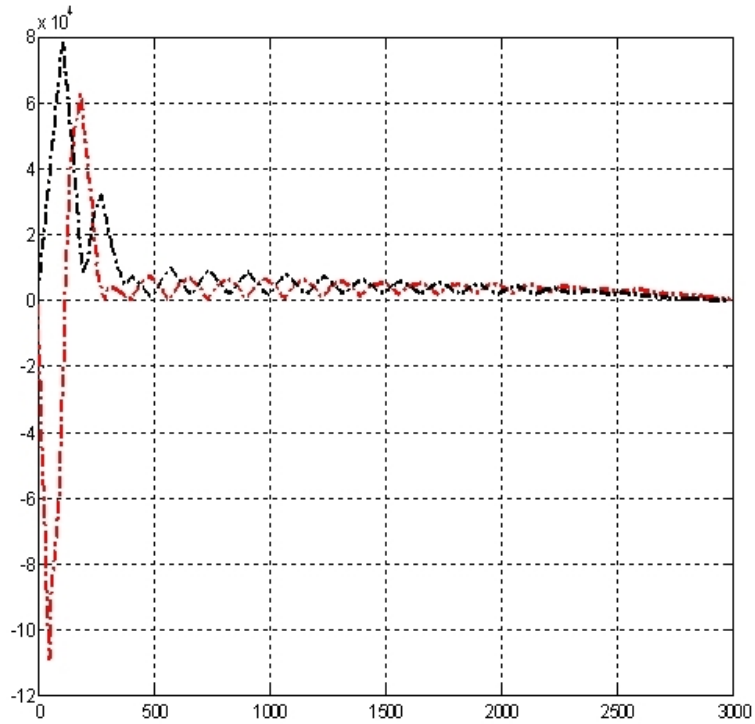


**Figure 24 Comparison of C6288 Benchmark using Algorithm 1 in New Model and HSPICE**

### 5.1.1.8 Simulation of C7552 Benchmark

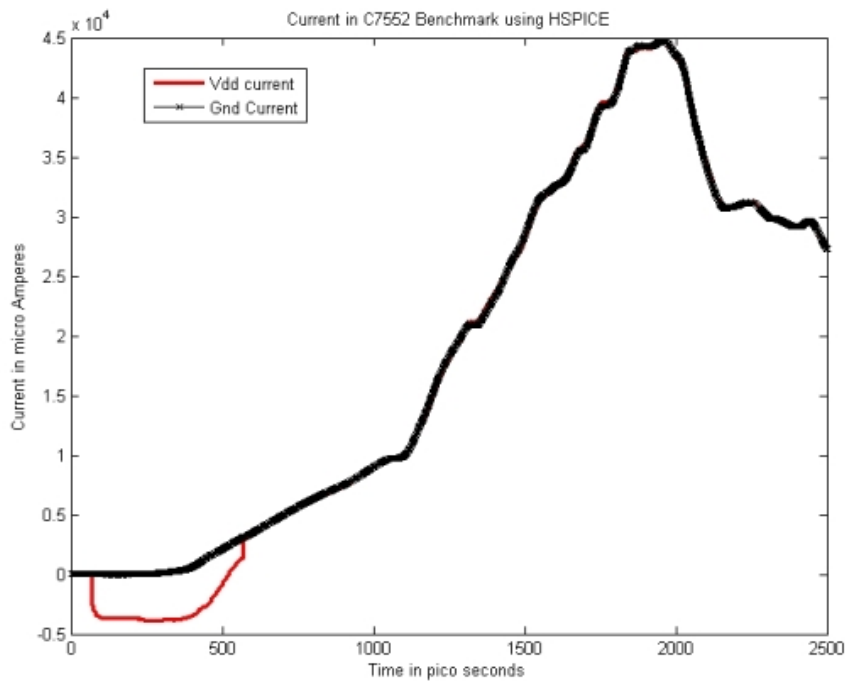
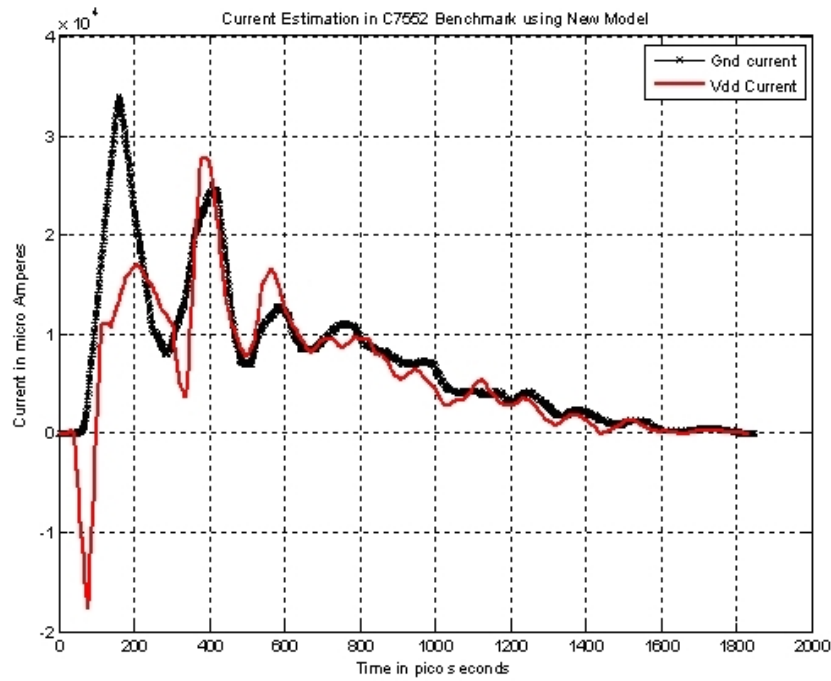


**Figure 25 Comparison of C7552 Benchmark using Algorithm 1 in New Model and HSPICE**

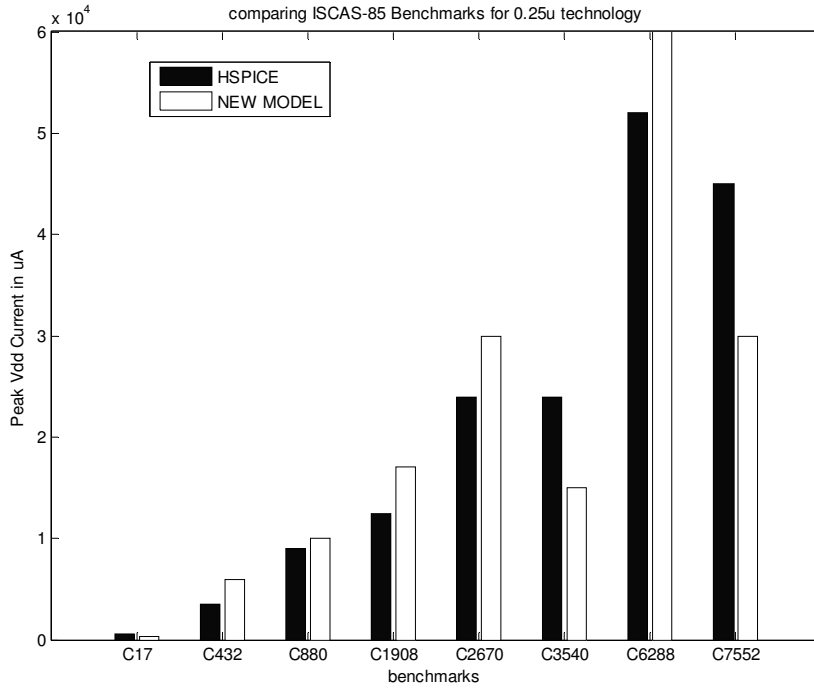


**Figure 26 Histogram of comparison of vdd current between Algorithm 1 in New Model and HSPICE**

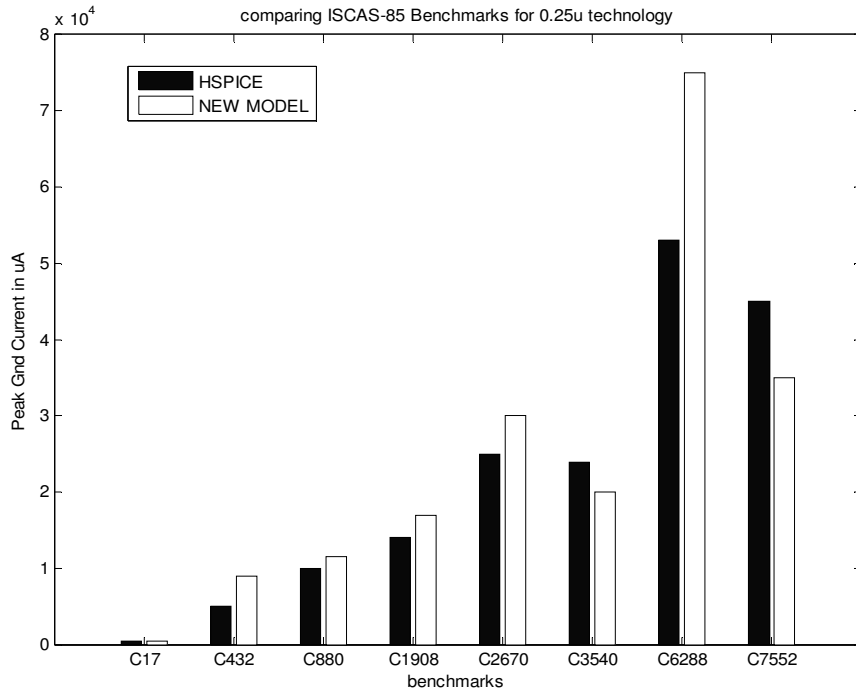


**Figure 27 Histogram of comparison of ground current between Algorithm1 in New Model and HSPICE.**

### 5.1.2 Simulation using Algorithm 2

Now simulation of all benchmarks will be done using Algorithm 2 and the results will be compared with HSPICE simulation. Both waveforms and histogram of the results are shown in the following figures.

#### 5.1.2.1 Simulation of C17 Benchmark

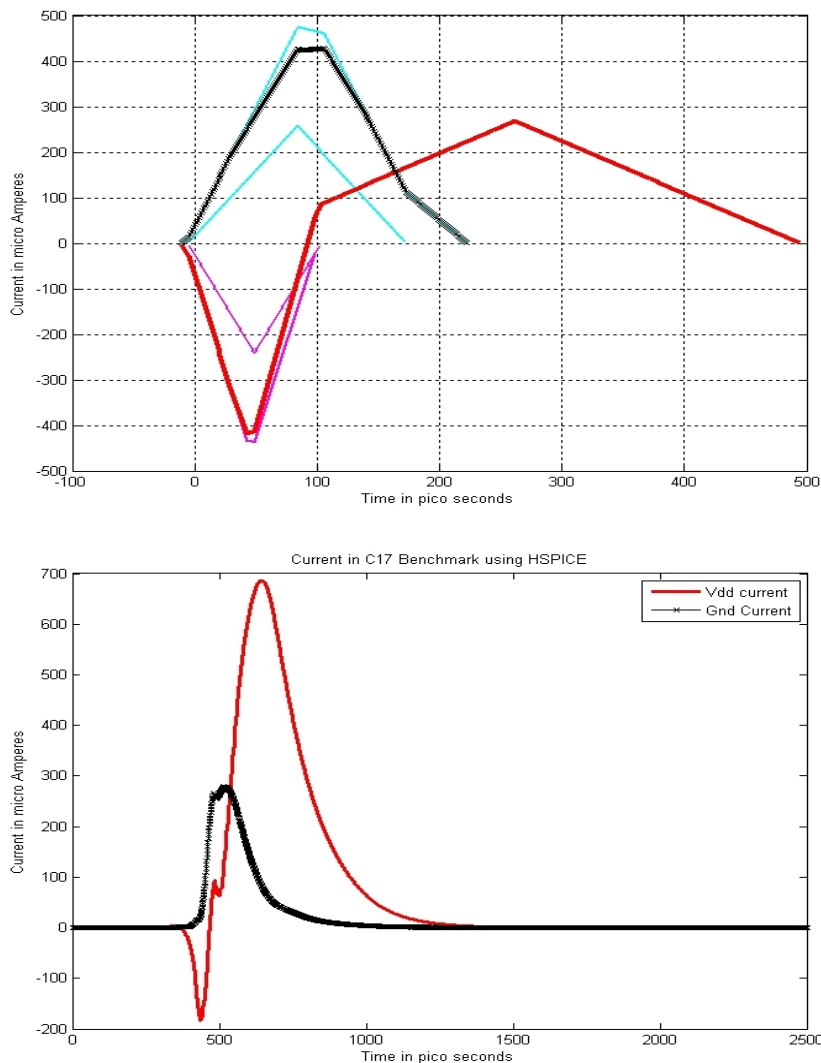
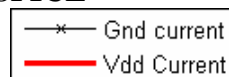


**Figure 28 Comparison of C17Benchmark using Algorithm2 in NewModel and HSPICE**



### 5.1.2.2 Simulation of C432 Benchmark

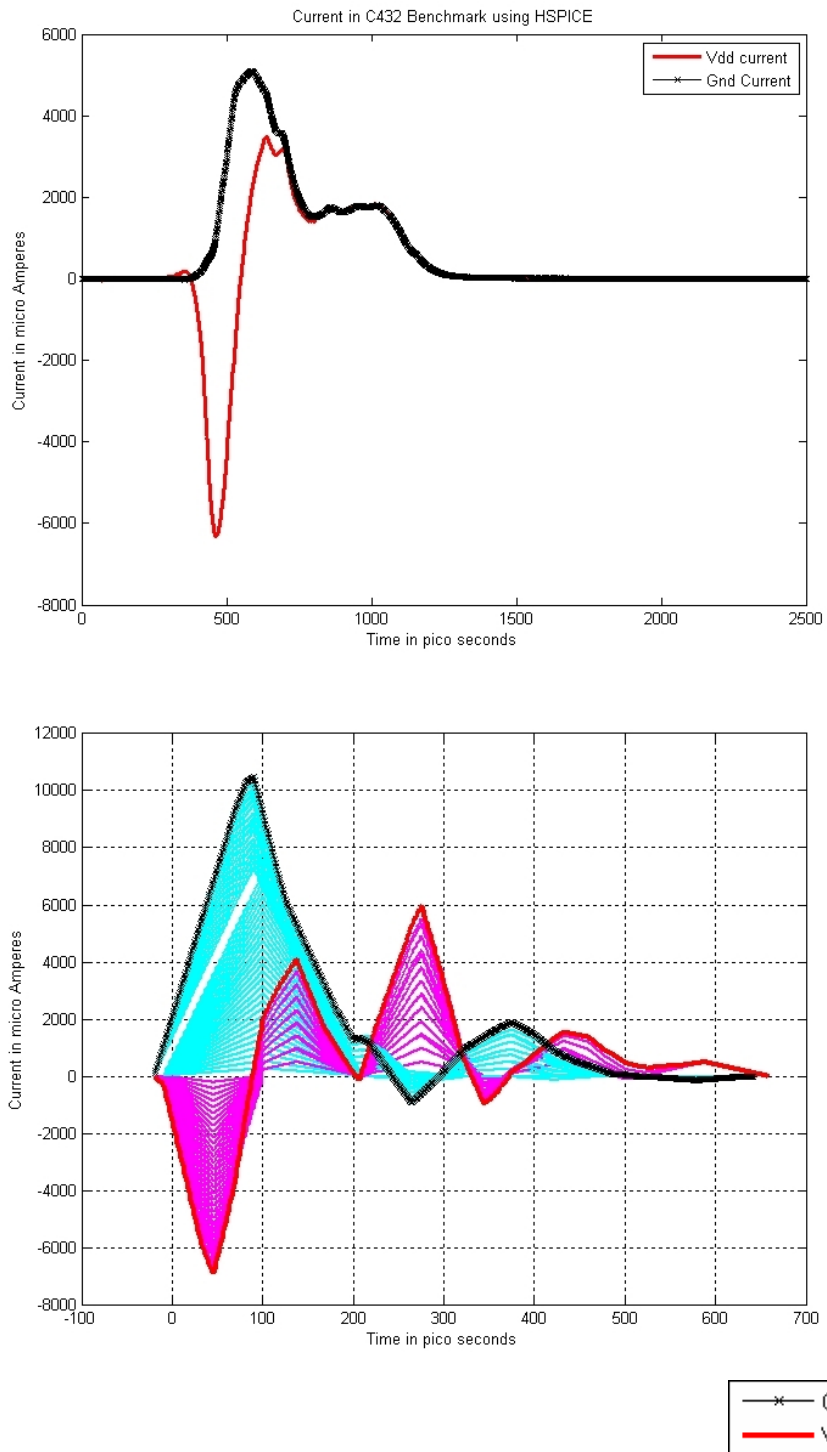


**Figure 29 Comparison of C432Benchmark using Algorithm2 in NewModel and HSPICE**

### 5.1.2.3 Simulation of C880 Benchmark

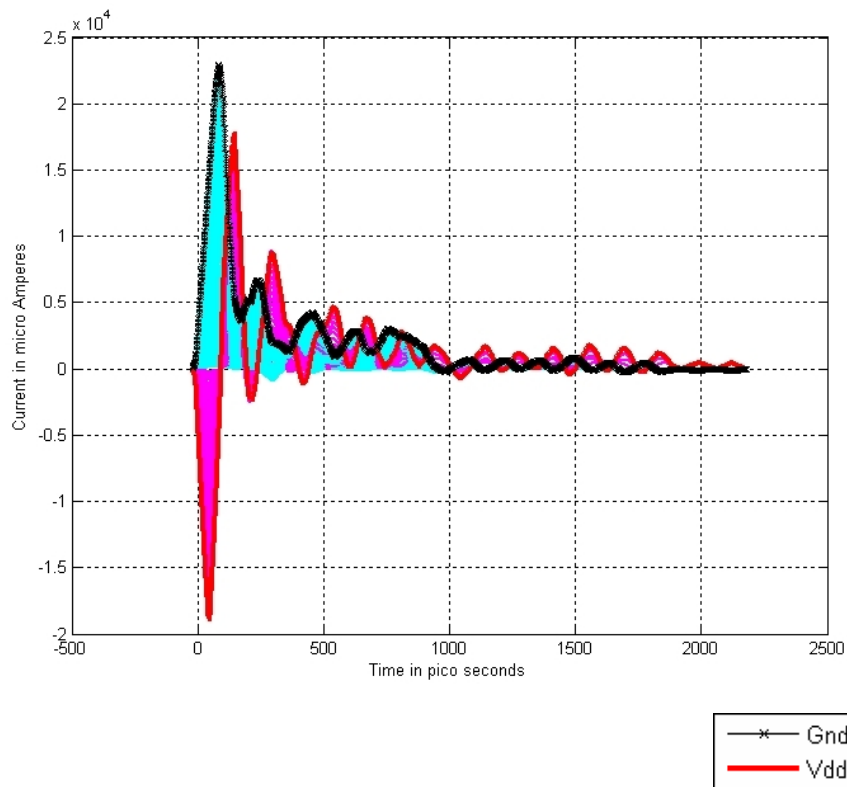
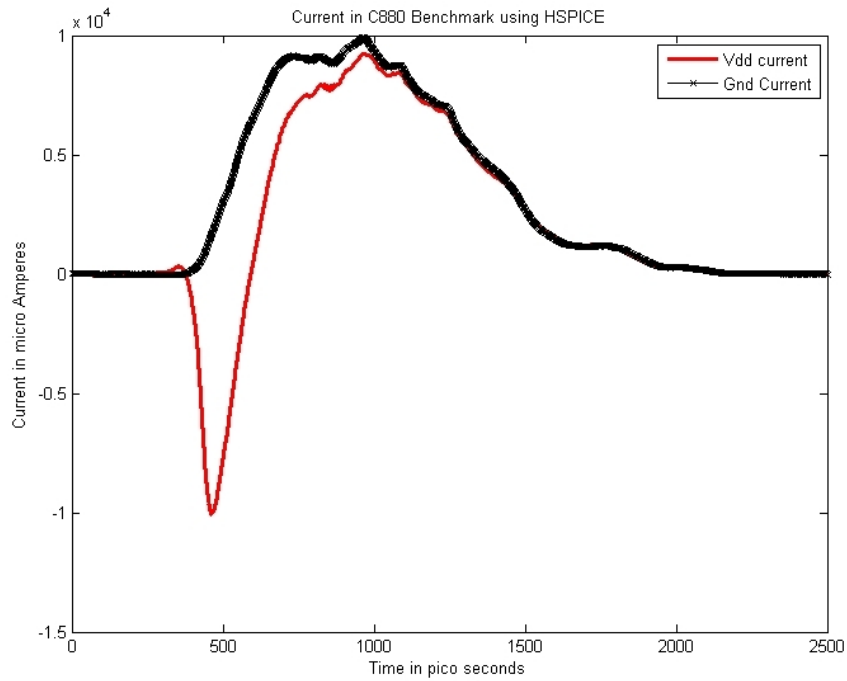


**Figure 30 Comparison of C880 Benchmark using Algorithm 2 in New Model and HSPICE**

### 5.1.2.4 Simulation of C1908 Benchmark

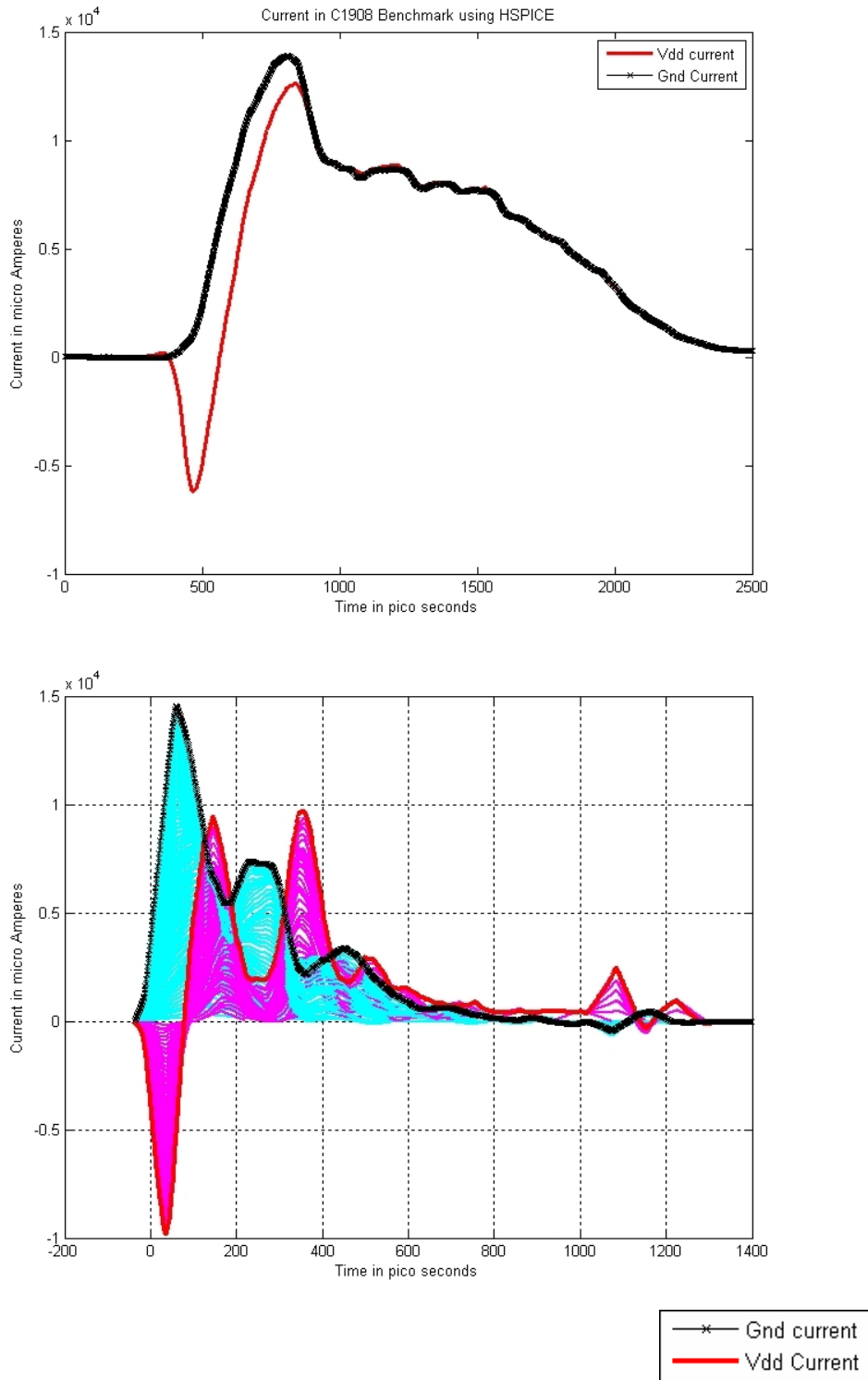


**Figure 31 Comparison of C1908 Benchmark using Algorithm 2 in New Model and HSPICE**

### 5.1.2.5 Simulation of C2670 Benchmark

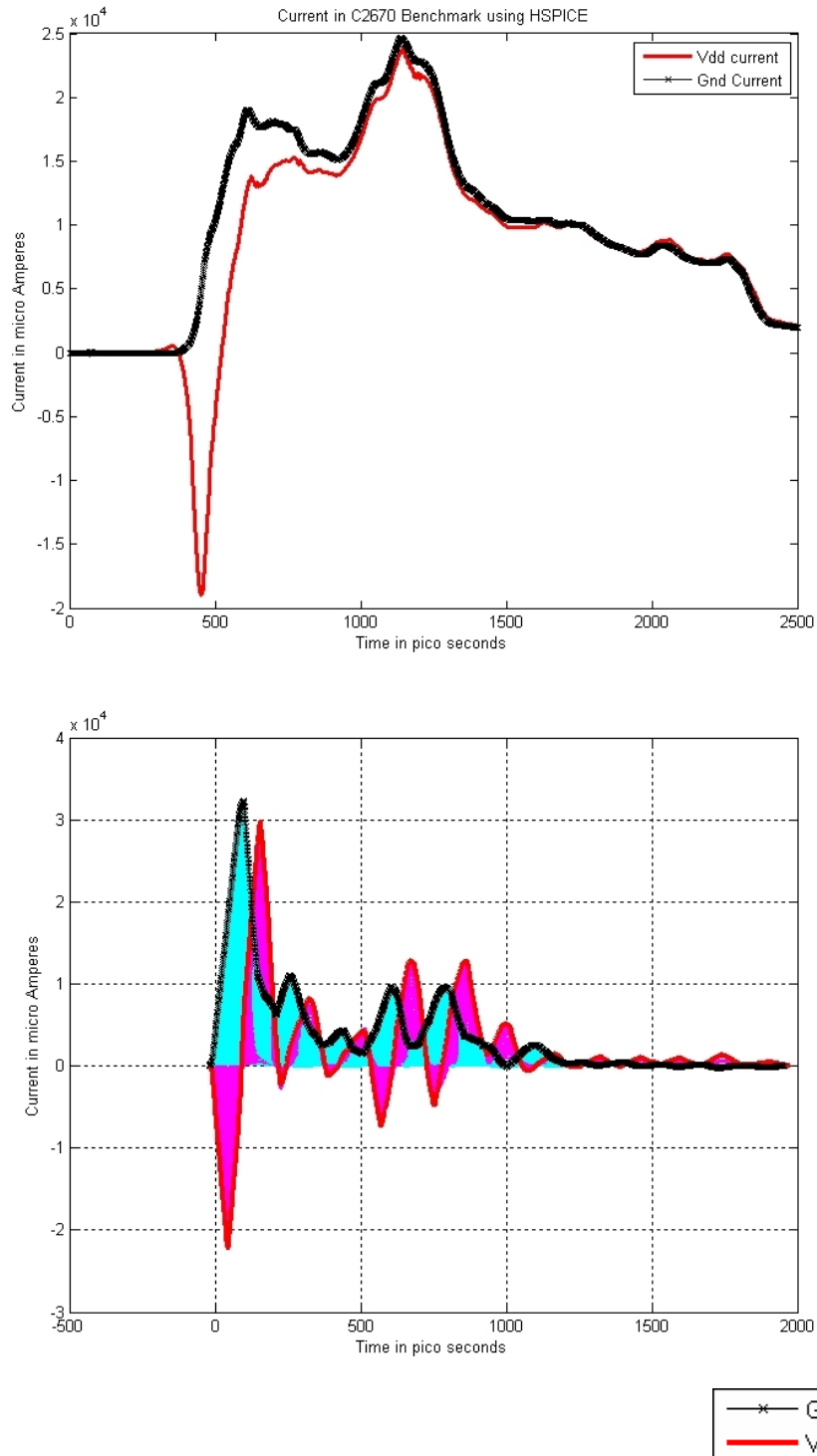


**Figure 32 Comparison of C2670 Benchmark using Algorithm 2 in New Model and HSPICE**



### 5.1.2.6 Simulation of C3540 Benchmark

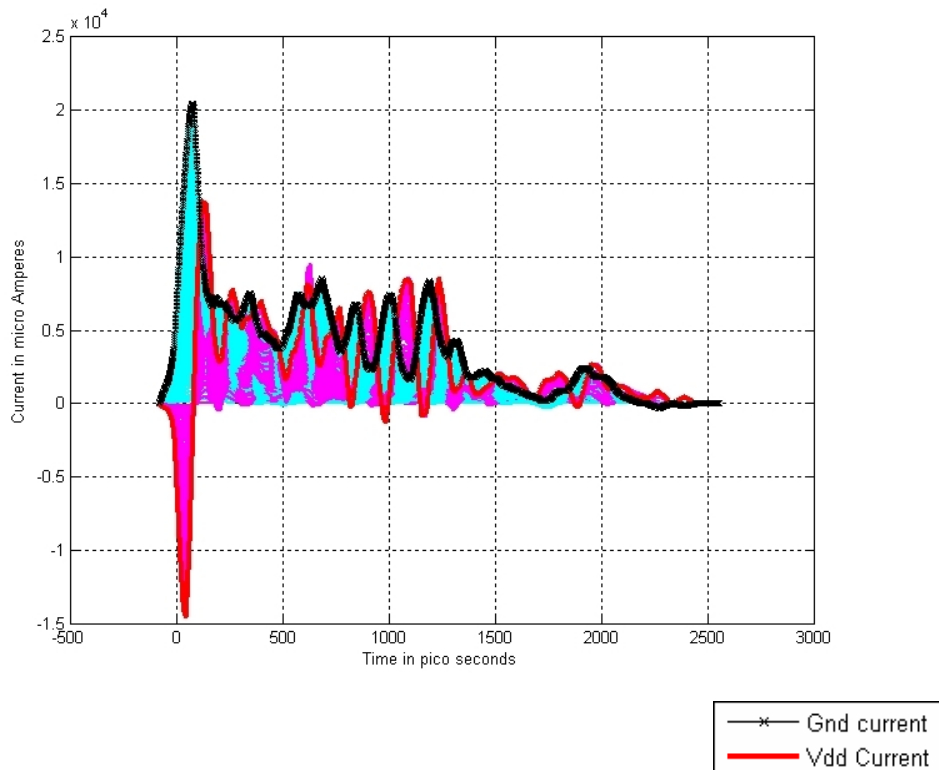
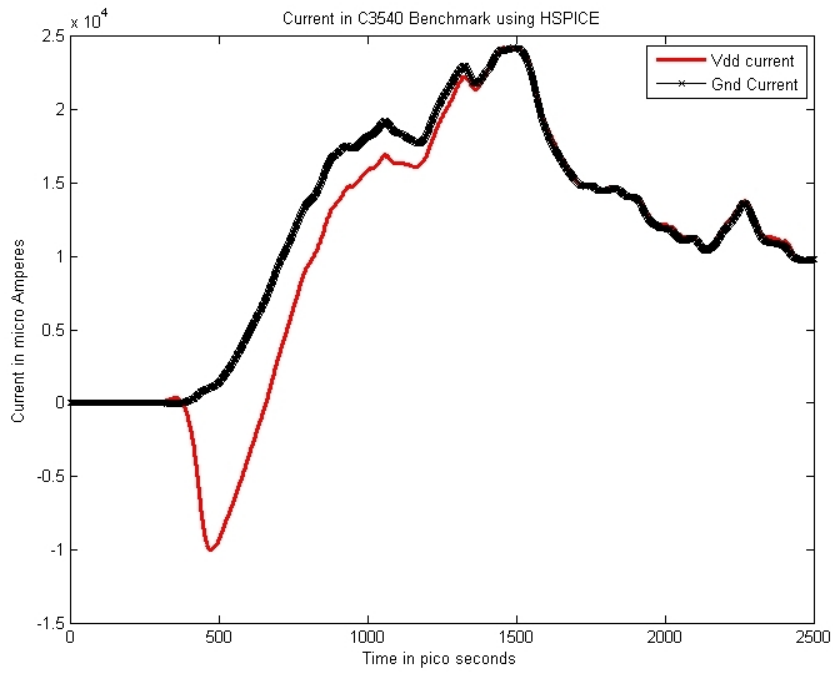


**Figure 33 Comparison of C3540 Benchmark using Algorithm 2 in New Model and HSPICE**

### 5.1.2.7 Simulation of C6288 Benchmark

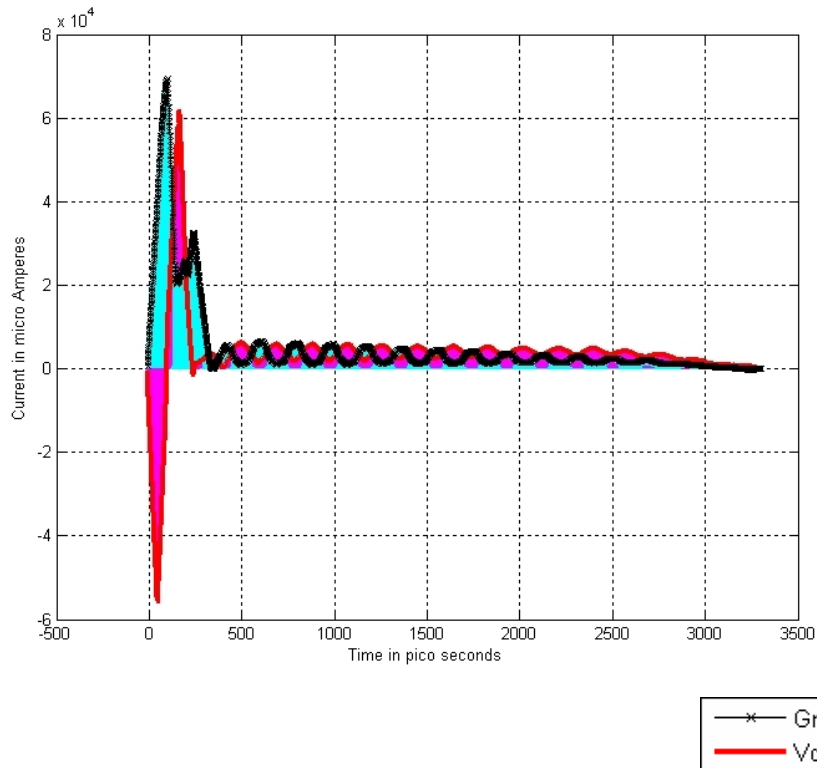
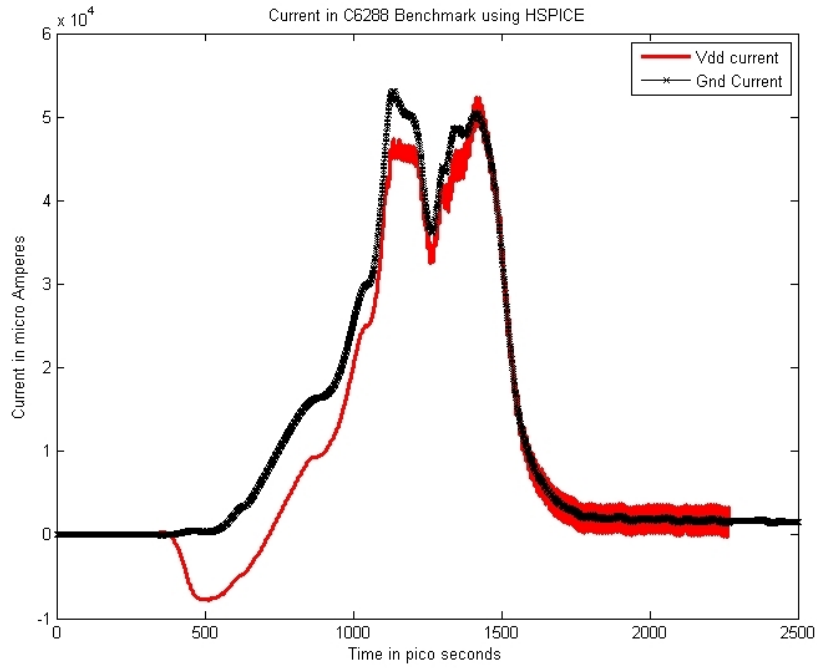


**Figure 34 Comparison of C6288 Benchmark using Algorithm 2 in New Model and HSPICE**

### 5.1.2.8 Simulation of C7552 Benchmark

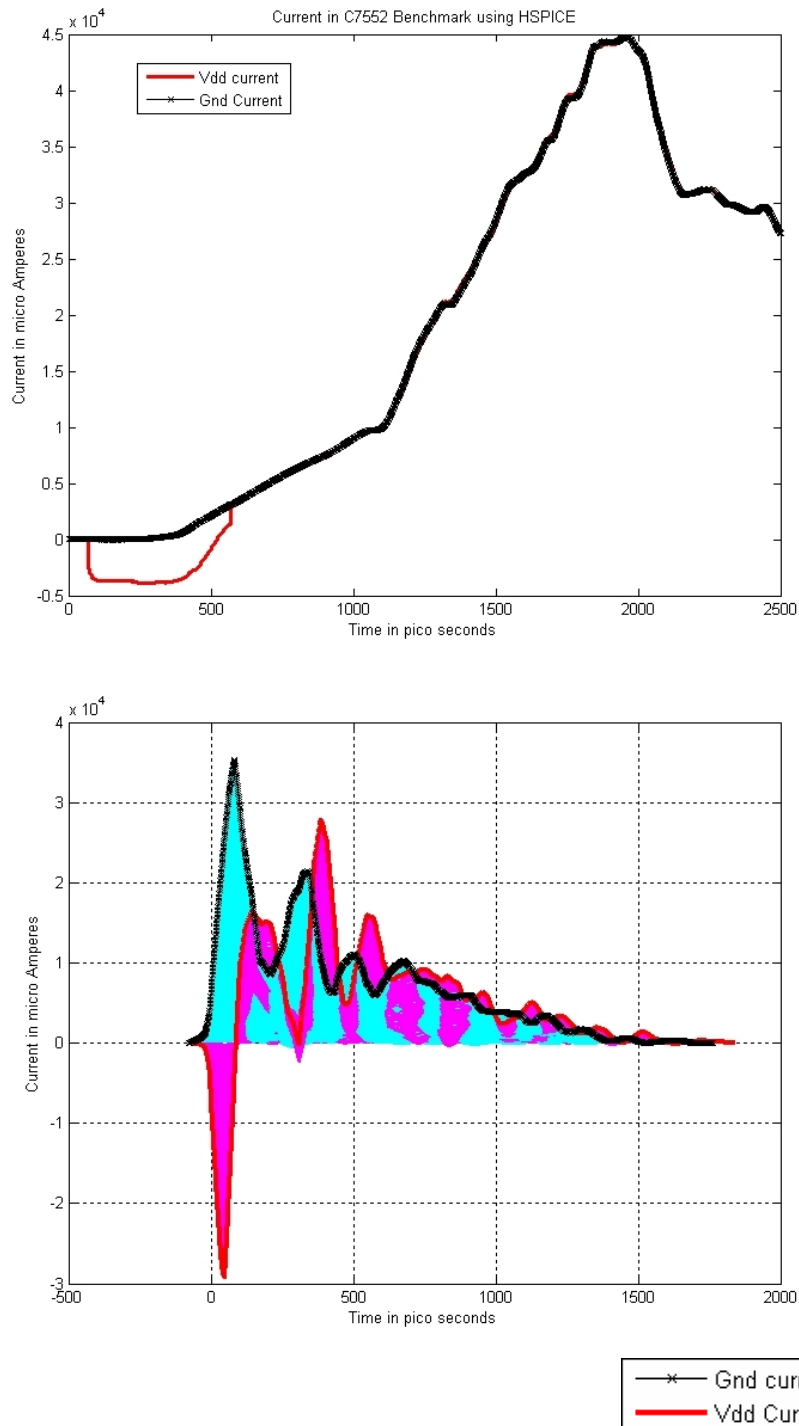


**Figure 35 Comparison of C7552 Benchmark using Algorithm 2 in New Model and HSPICE**

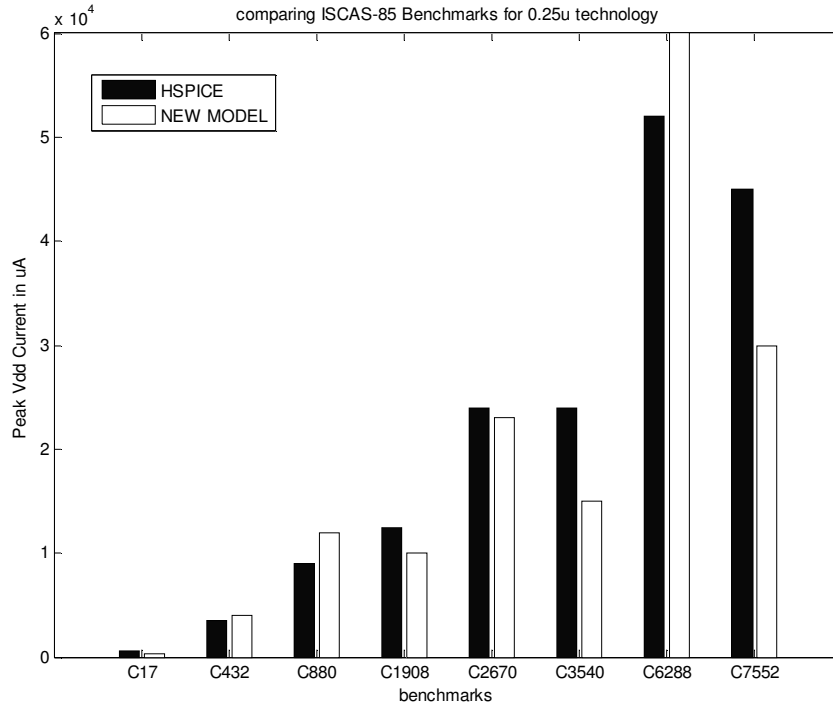


**Figure 36 Comparison of vdd current in ISCAS-85 benchmarks using Algorithm2**

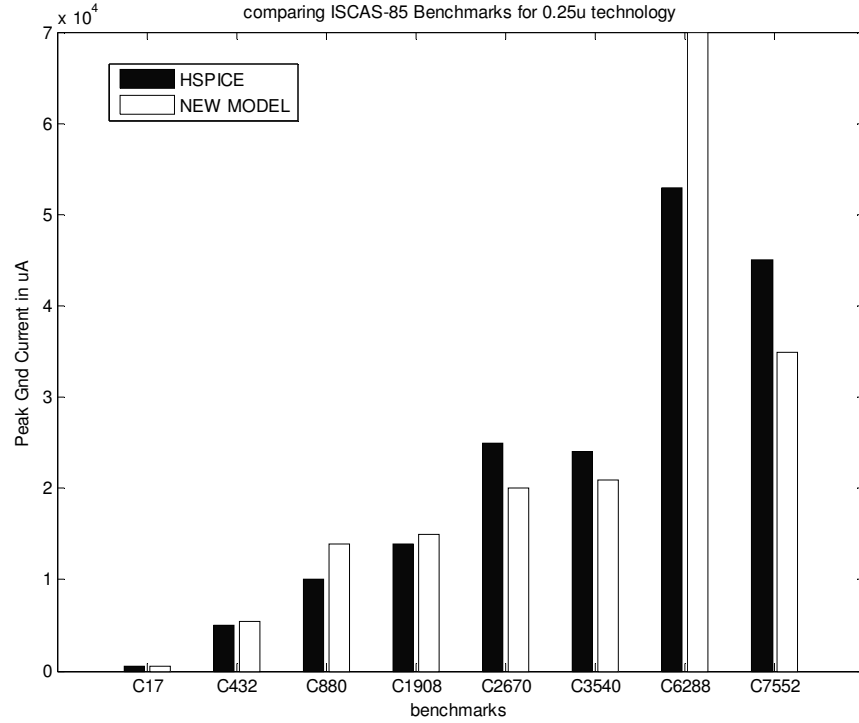


**Figure 37 Comparison of ground current in ISCAS-85 benchmarks using Algorithm2**

## 5.2 Simulation of ISCAS-85 Benchmarks with 90nm Technology (vdd = 1.5V)

### 5.2.1 Simulation using Algorithm 1

#### 5.2.1.1 Simulation of C17 Benchmark

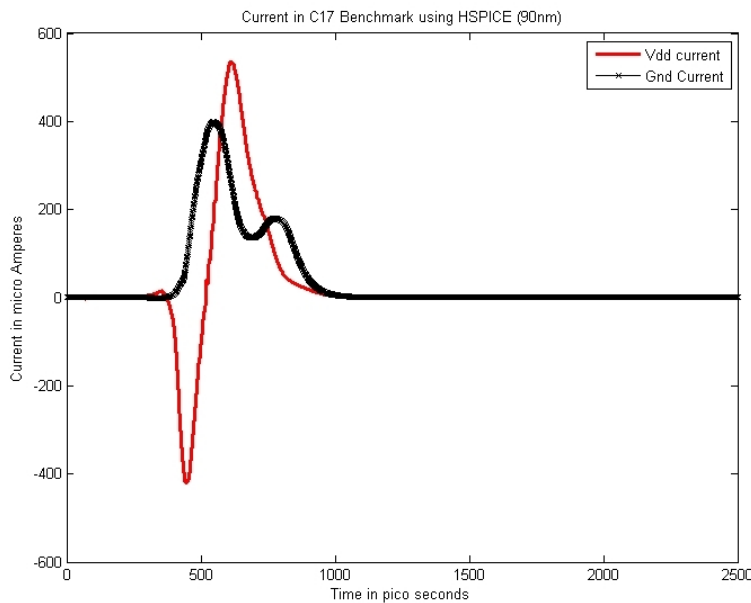
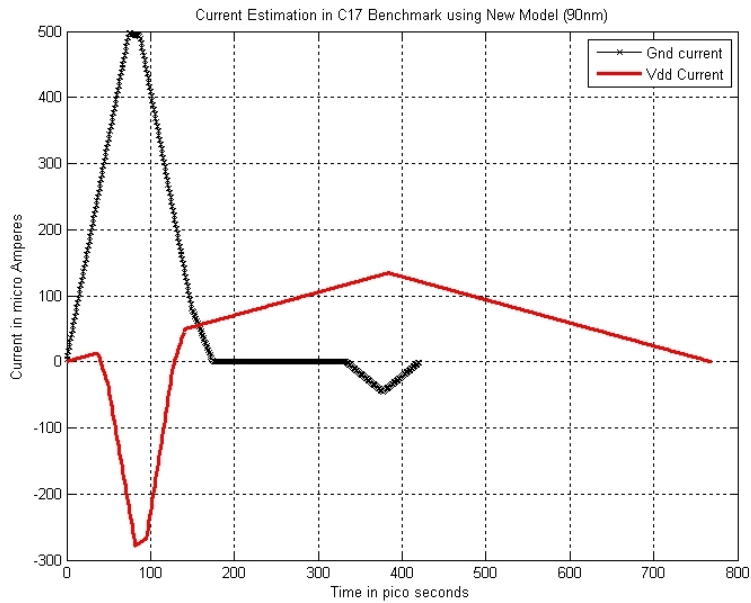


**Figure 38 Comparison of C17 Benchmark using Algorithm 1 in New Model and HSPICE (90nm)**

### 5.2.1.2 Simulation of C432 Benchmark

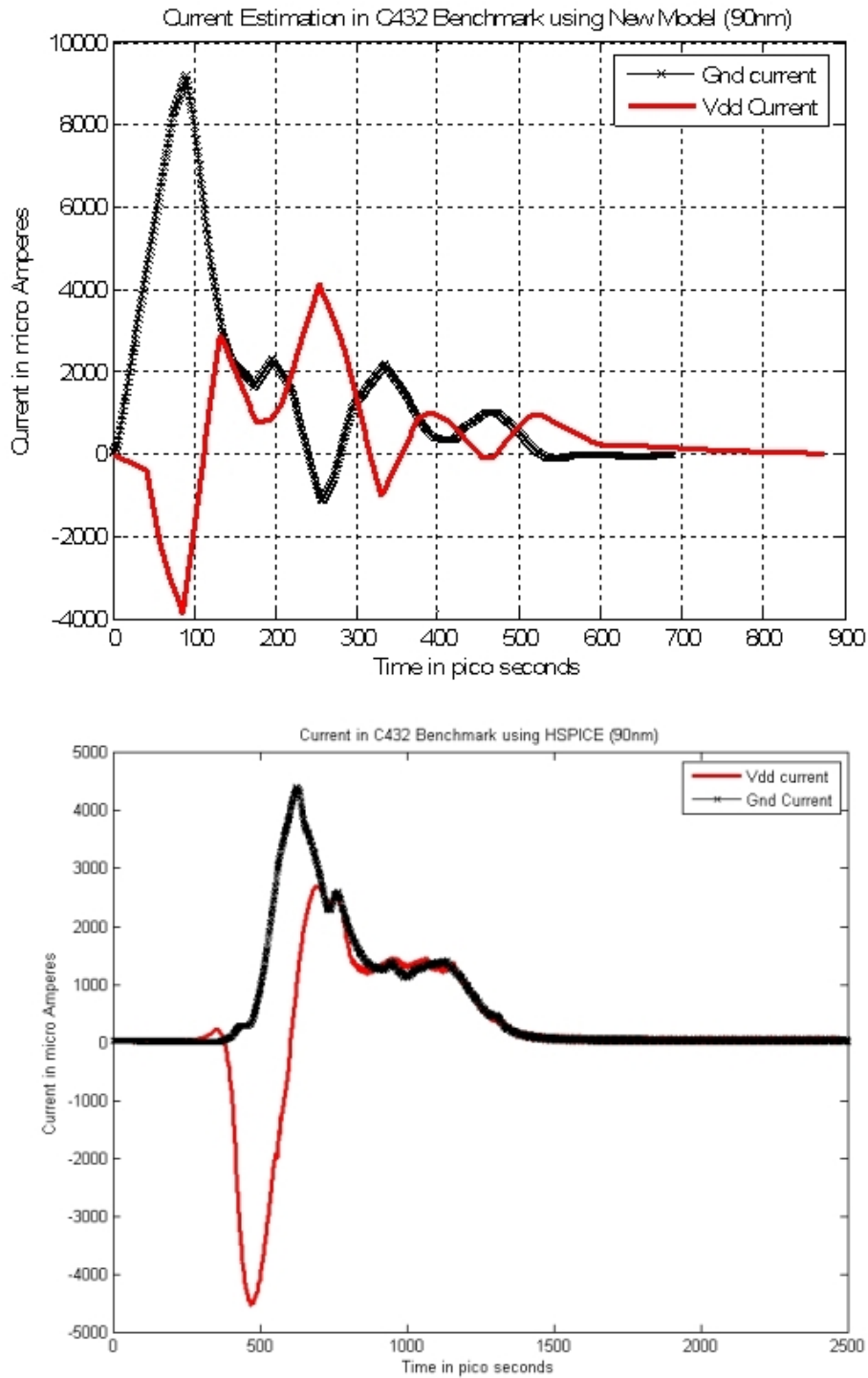


**Figure 39 Comparison of C432 Benchmark using Algorithm 1 in New Model and HSPICE (90nm)**

### 5.2.1.3 Simulation of C880 Benchmark

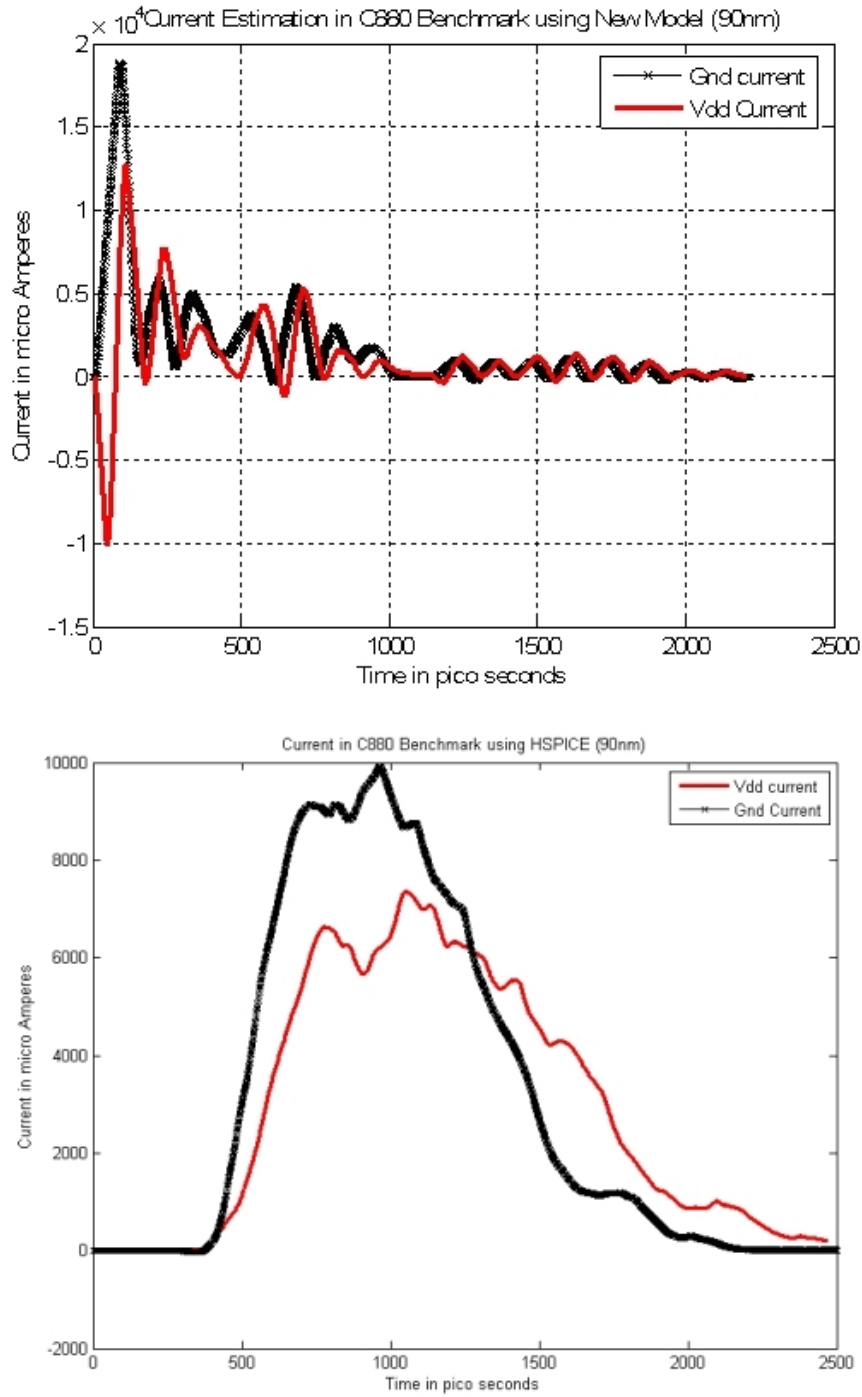


**Figure 40 Comparison of C880 Benchmark using Algorithm 1 in New Model and HSPICE (90nm)**

### 5.2.1.4 Simulation of C1908 Benchmark

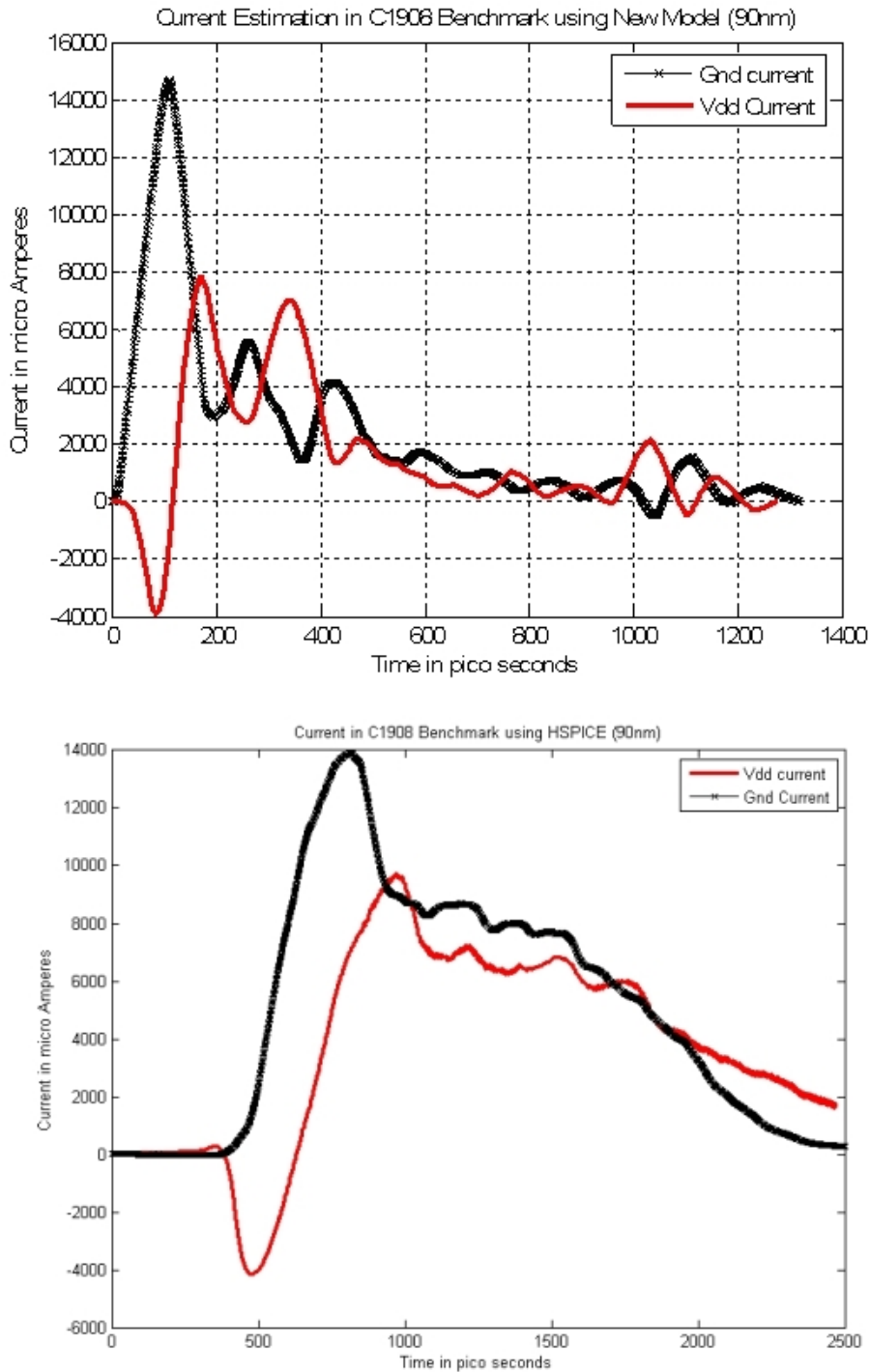


**Figure 41 Comparison of C1908 Benchmark using Algorithm 1 in New Model and HSPICE (90nm)**



### 5.2.1.5 Simulation of C2670 Benchmark

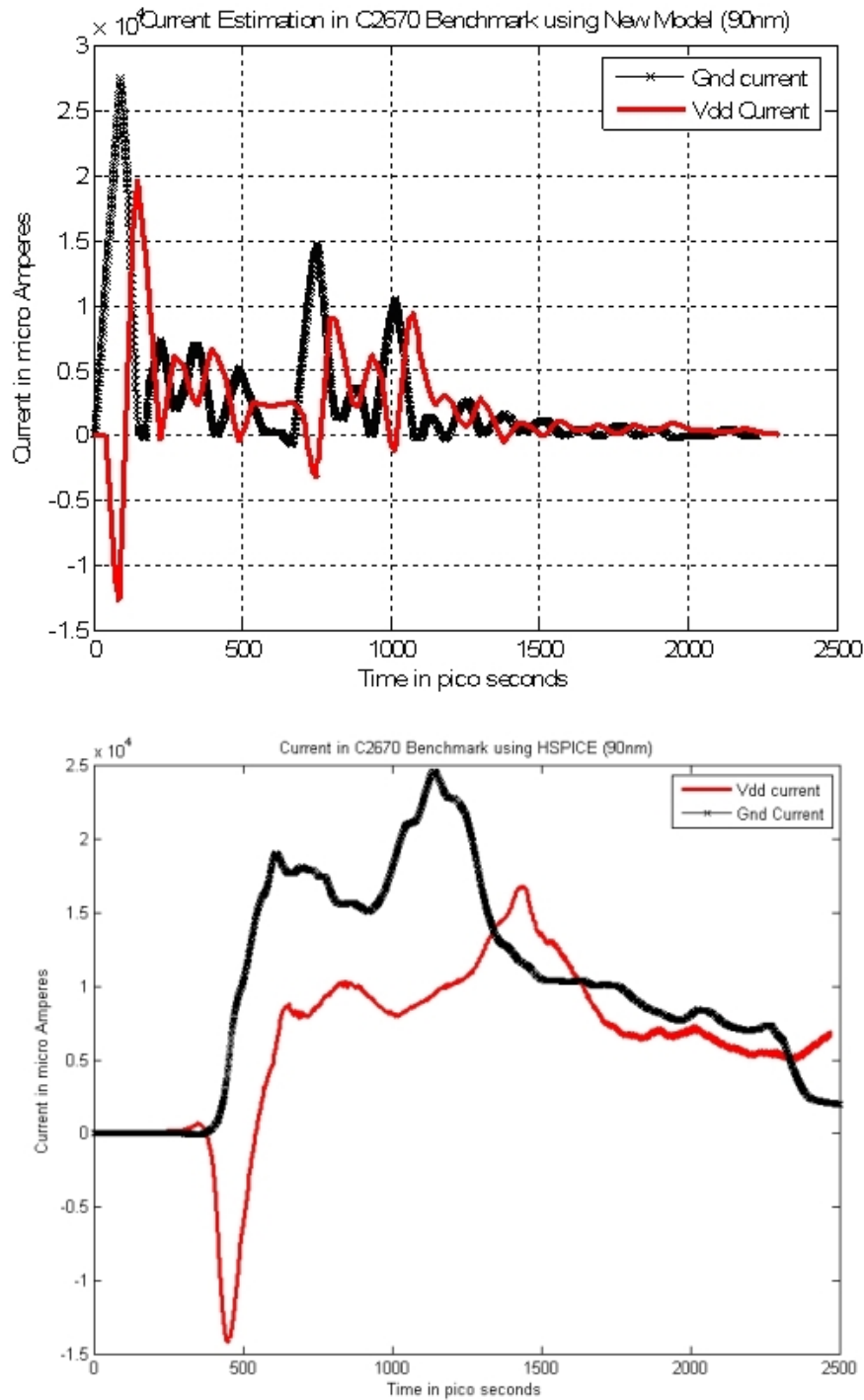


**Figure 42 Comparison of C2670 Benchmark using Algorithm 1 in New Model and HSPICE (90nm)**

### 5.2.1.6 Simulation of C3540 Benchmark

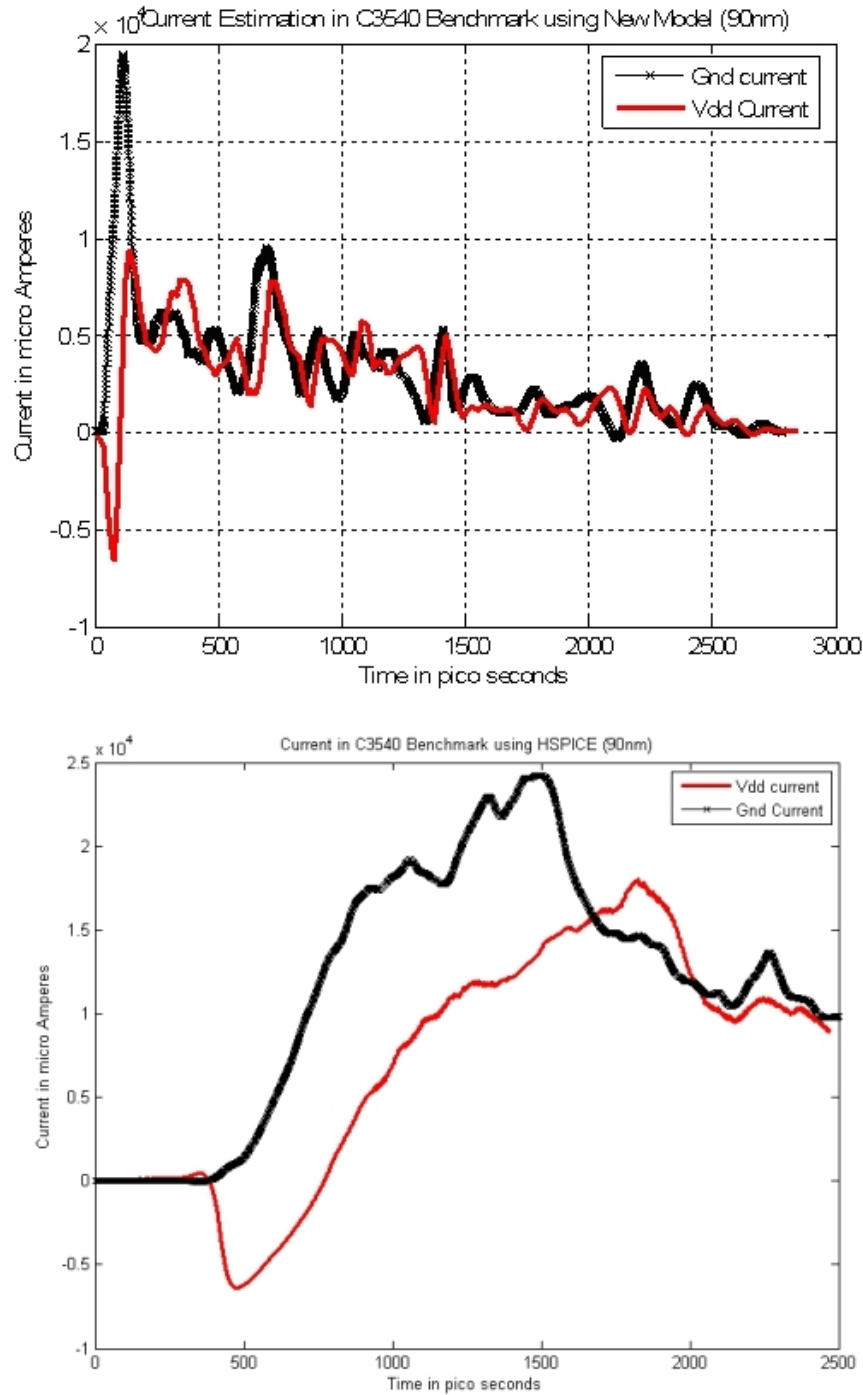


**Figure 43 Comparison of C3540 Benchmark using Algorithm 1 in New Model and HSPICE (90nm)**

### 5.2.1.7 Simulation of C6288 Benchmark

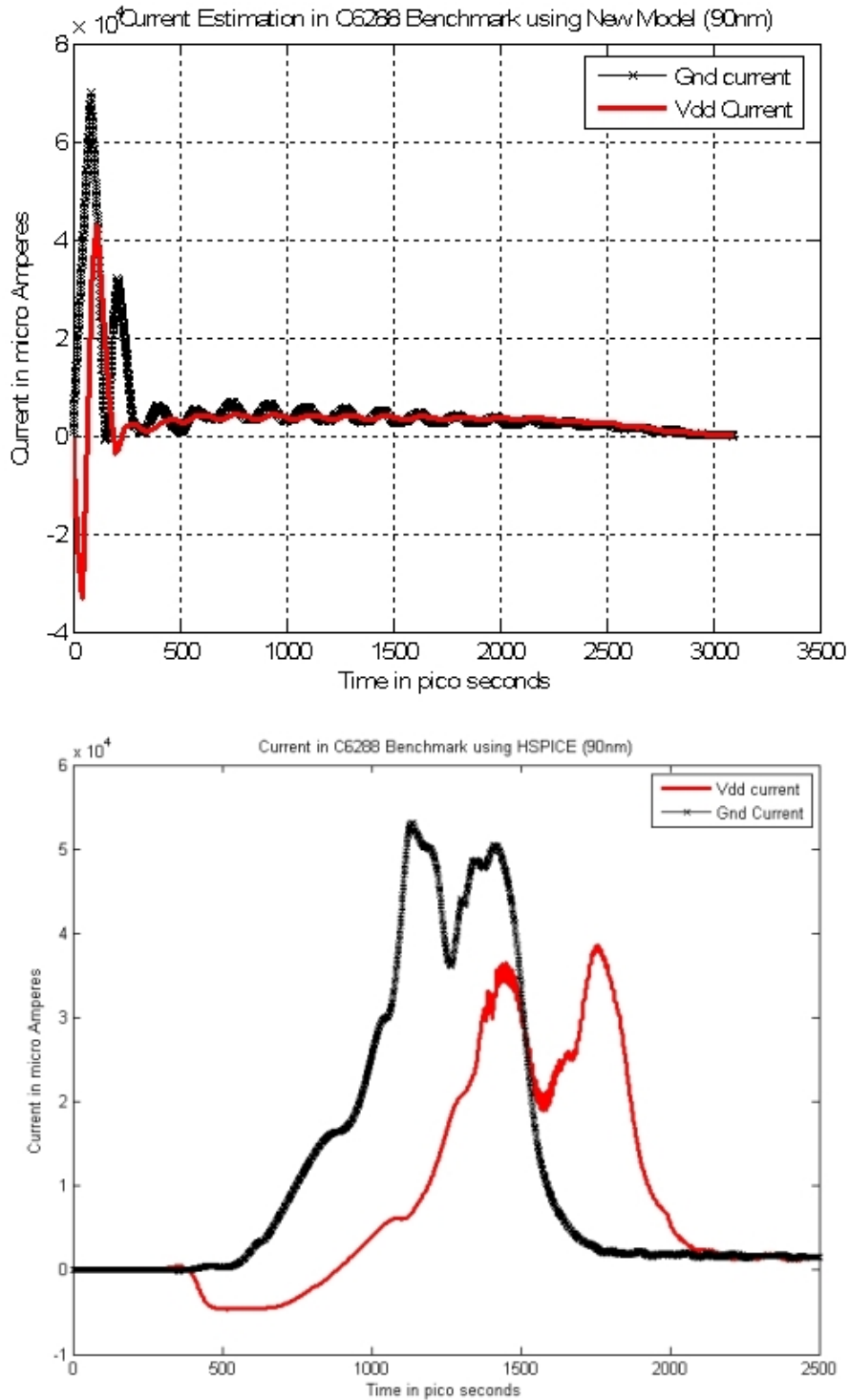


**Figure 44 Comparison of C6288 benchmark using Algorithm 1 in New Model and HSPICE (90nm)**

### 5.2.1.8 Simulation of C7552 Benchmak

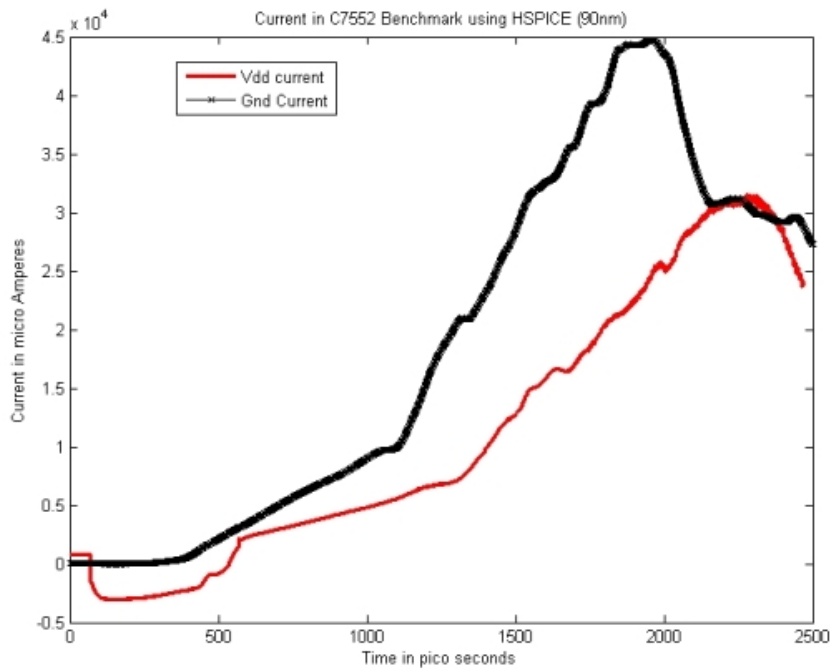
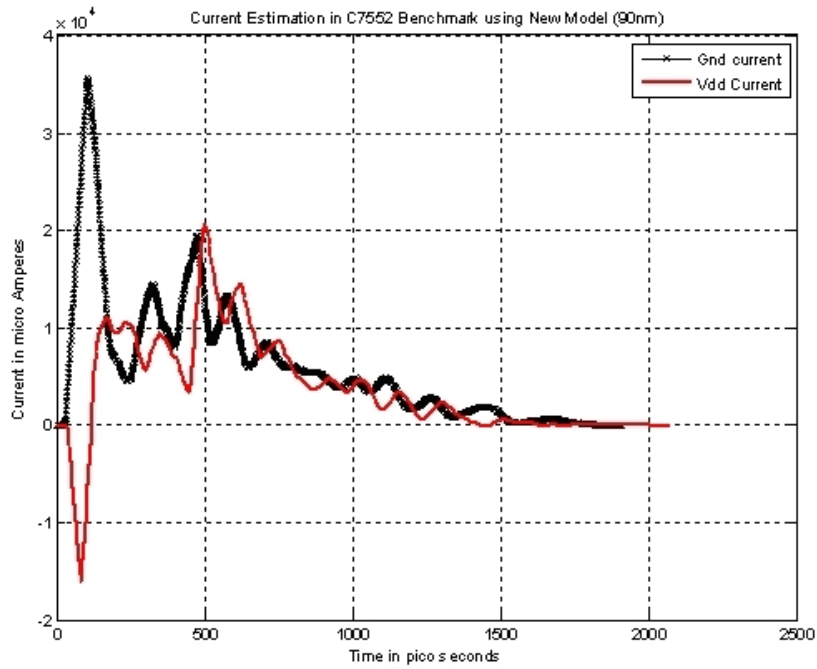


**Figure 45 Comparison of C7552 Benchmark using Algorithm 1 in New Model and HSPICE (90nm)**

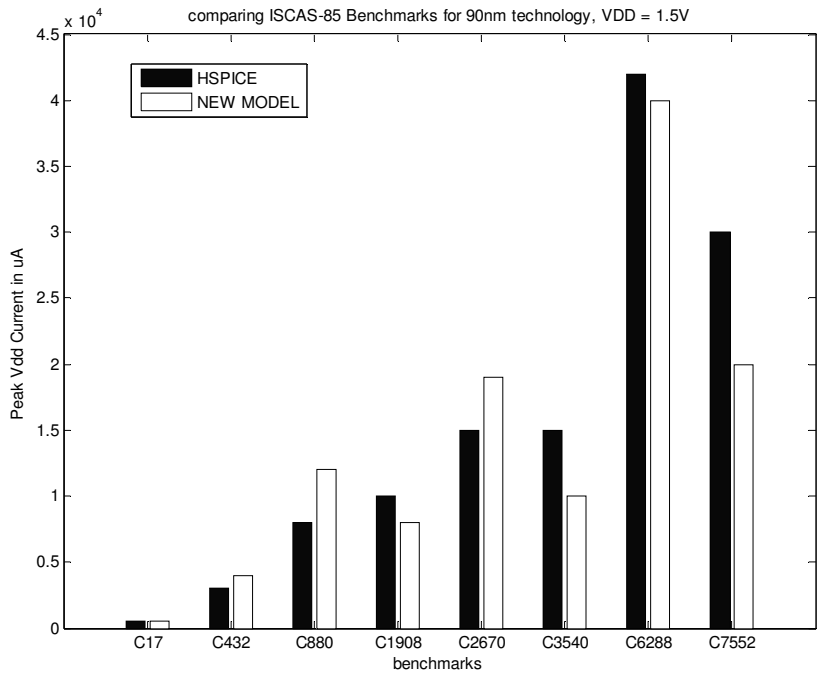


**Figure 46 Histogram of comparison of vdd current using Algorithm 1 in New Model and HSPICE for 90nm technology**

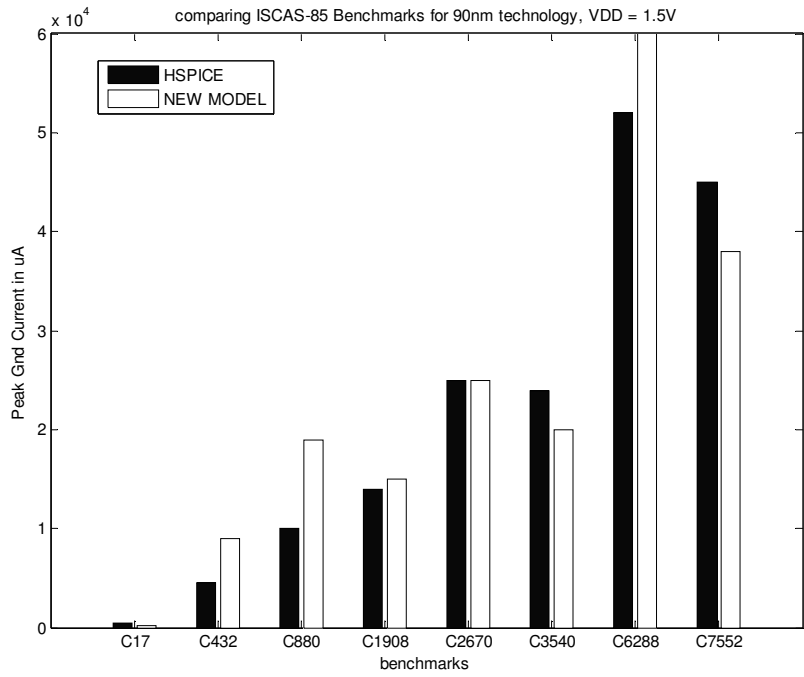


**Figure 47 Histogram of Comparison of ground current using Algorithm1 in New Model and HSPICE for 90nm technology**

## 5.2.2 Simulation using Algorithm 2

### 5.2.2.1 Simulation of C17 Benchmark

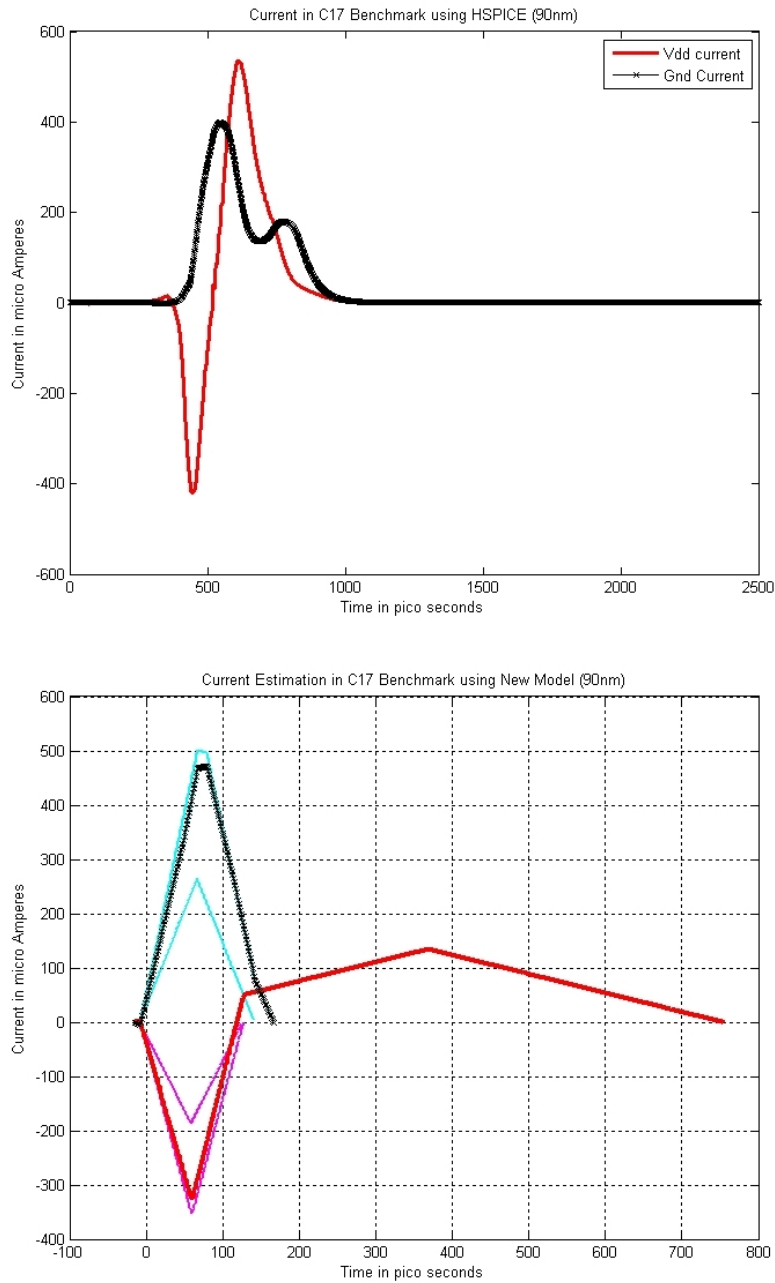


**Figure 48 Comparison of C17 Benchmark using Algorithm 2 in New Model and HSPICE (90nm)**

### 5.2.2.2 Simulation of C432 Benchmark

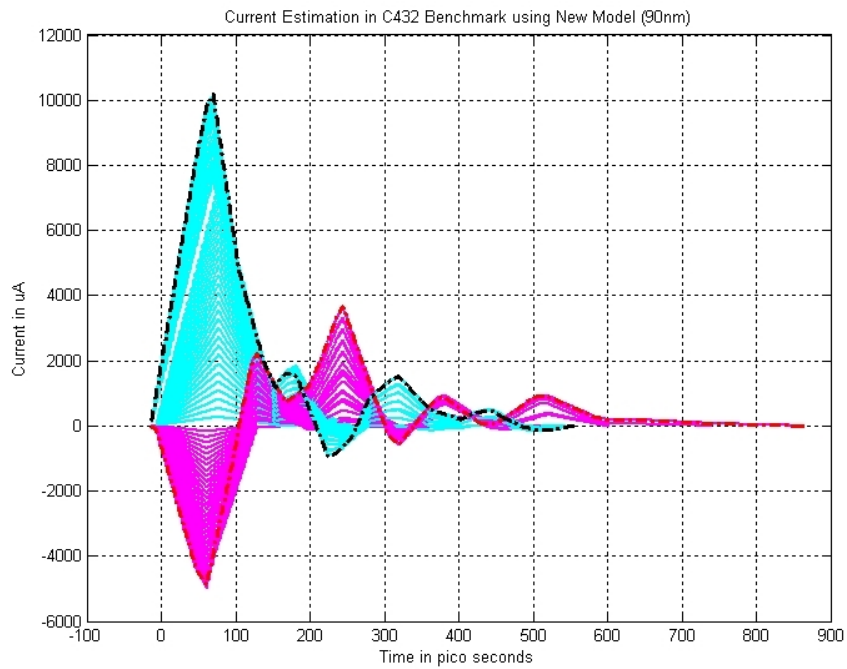
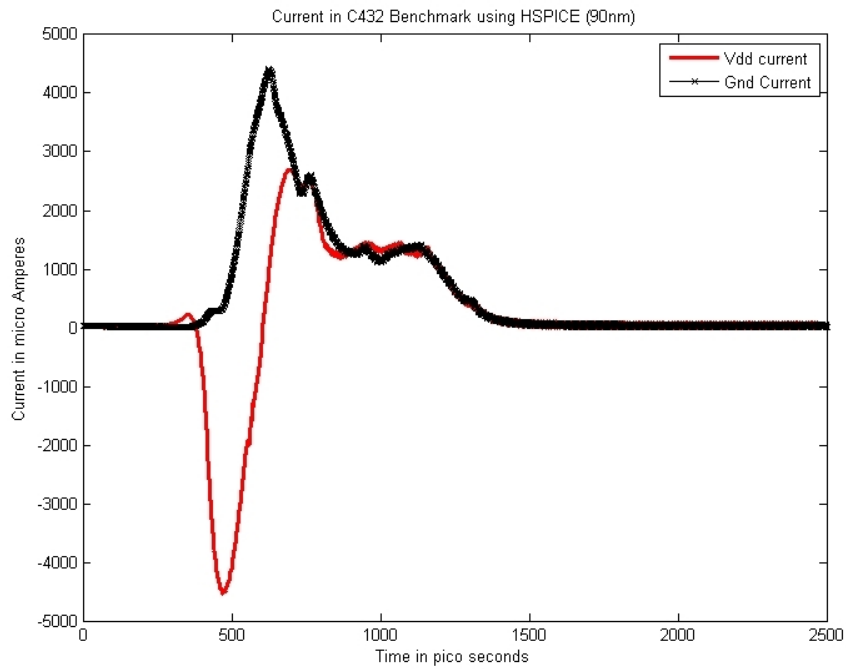


**Figure 49 Comparison of C432 Benchmark using Algorithm 2 in New Model and HSPICE (90nm)**

### 5.2.2.3 Simulation of C880 Benchmark

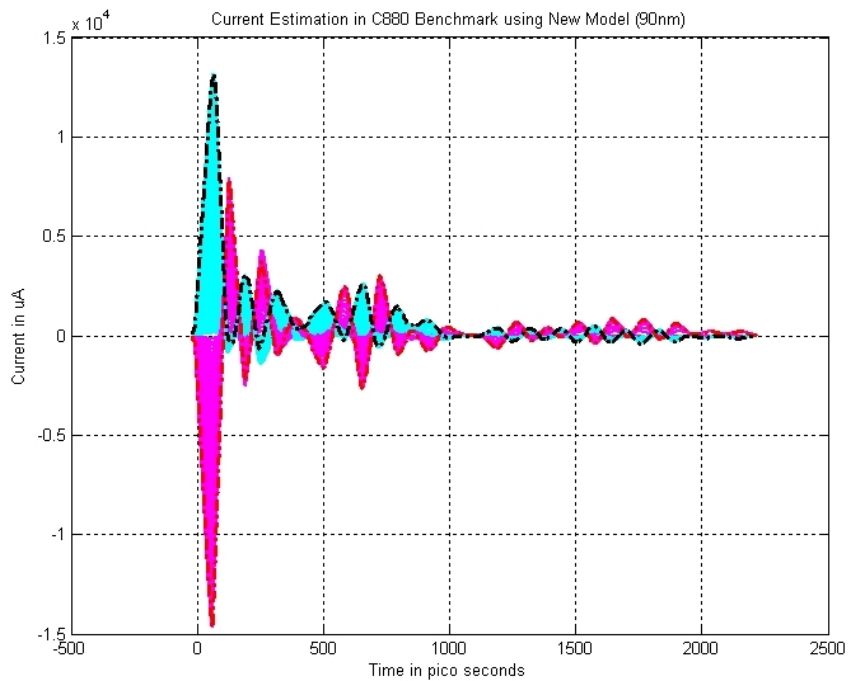
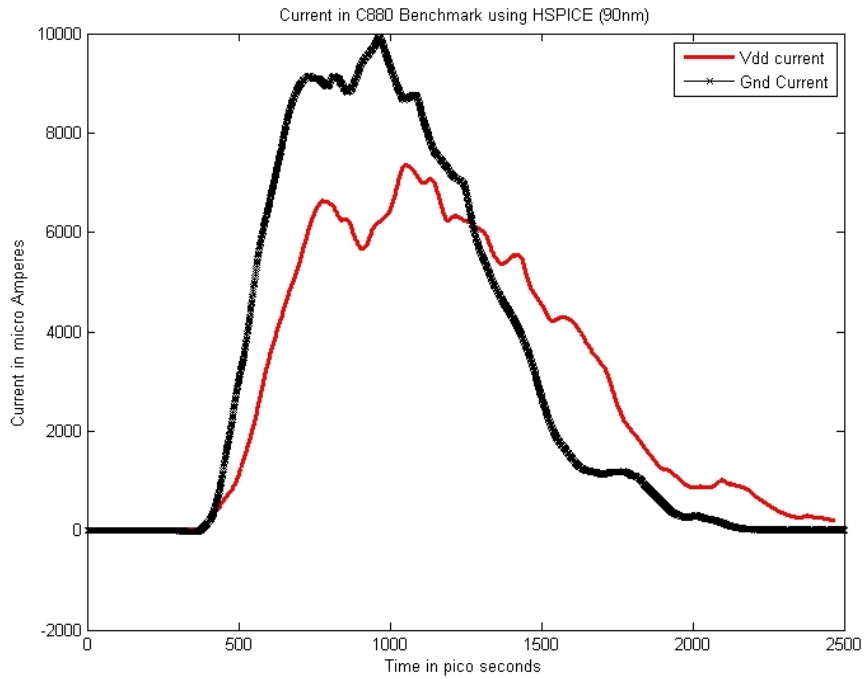


**Figure 50 Comparison of C880 Benchmark using Algorithm 2 in New Model and HSPICE (90nm)**



### 5.2.2.4 Simulation of C1908 Benchmark

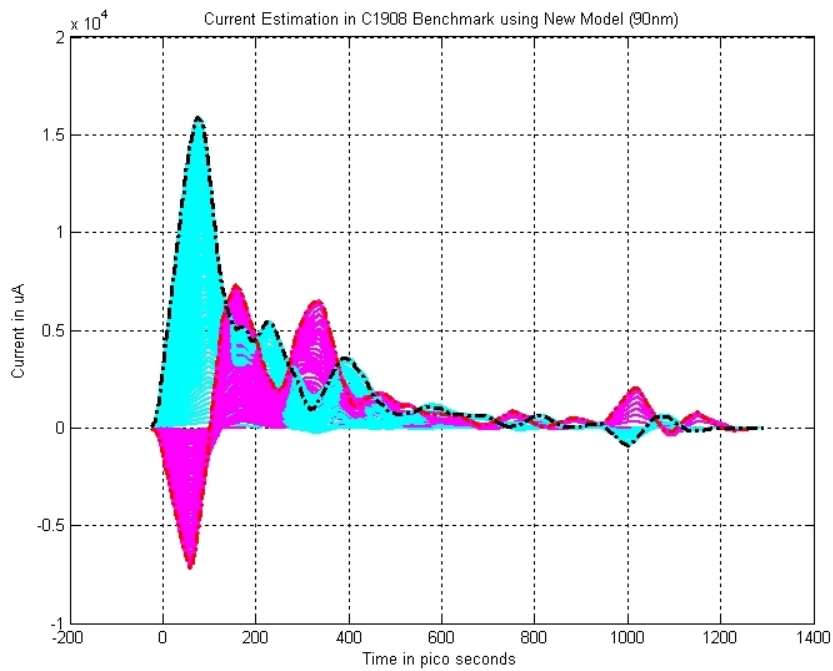
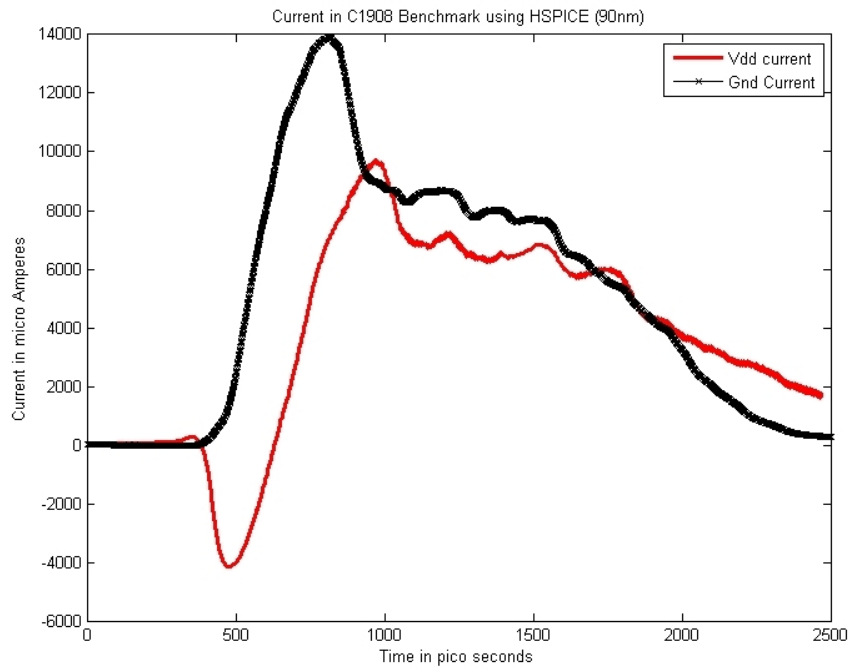


**Figure 51 Comparison of C1908 Benchmark using Algorithm 2 in New Model and HSPICE (90nm)**

### 5.2.2.5 Simulation of C2670 Benchmark

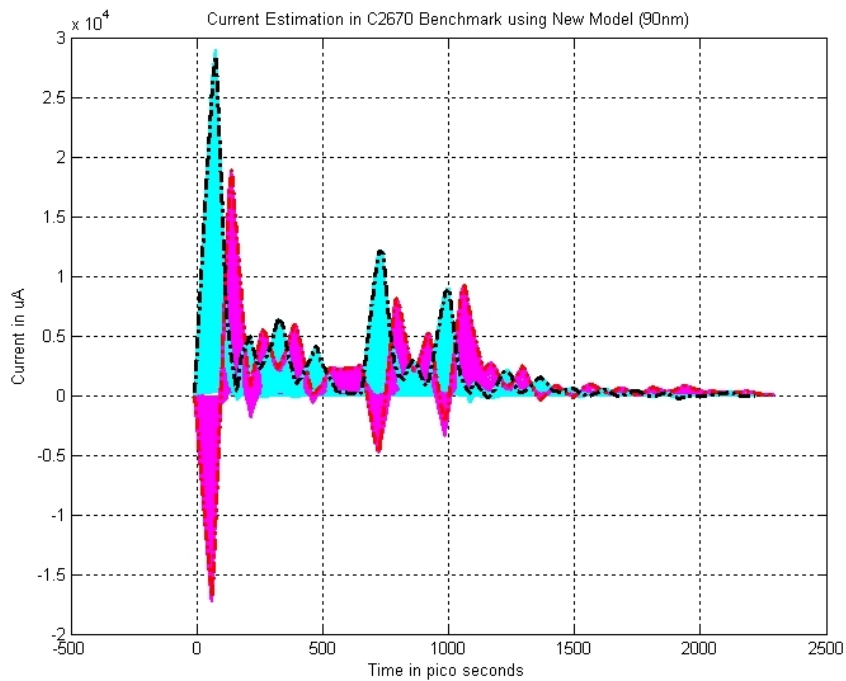
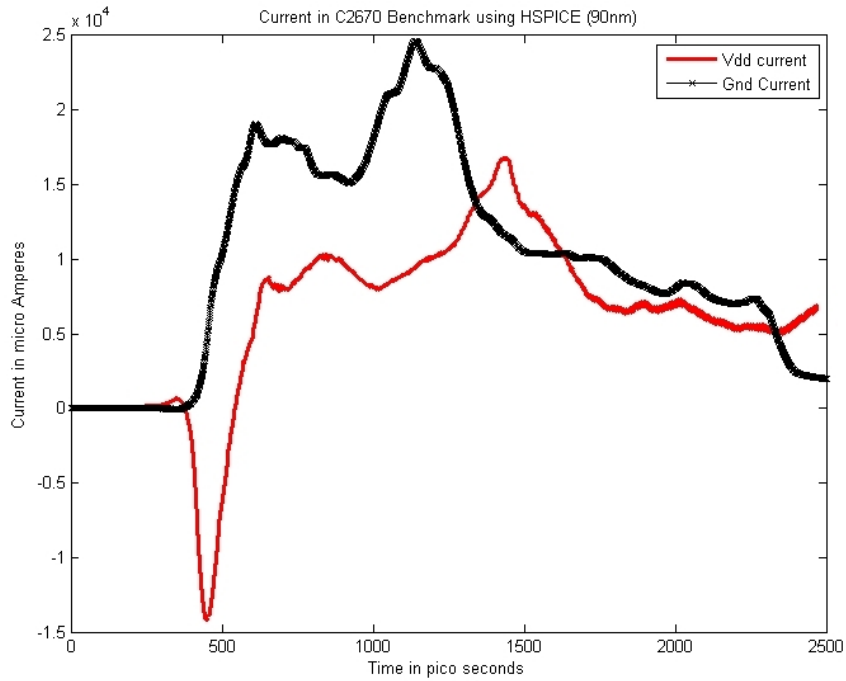


**Figure 52 Comparison of C2670 Benchmark using Algorithm 2 in New Model and HSPICE (90nm)**

### 5.2.2.6 Simulation of C3540 Benchmark

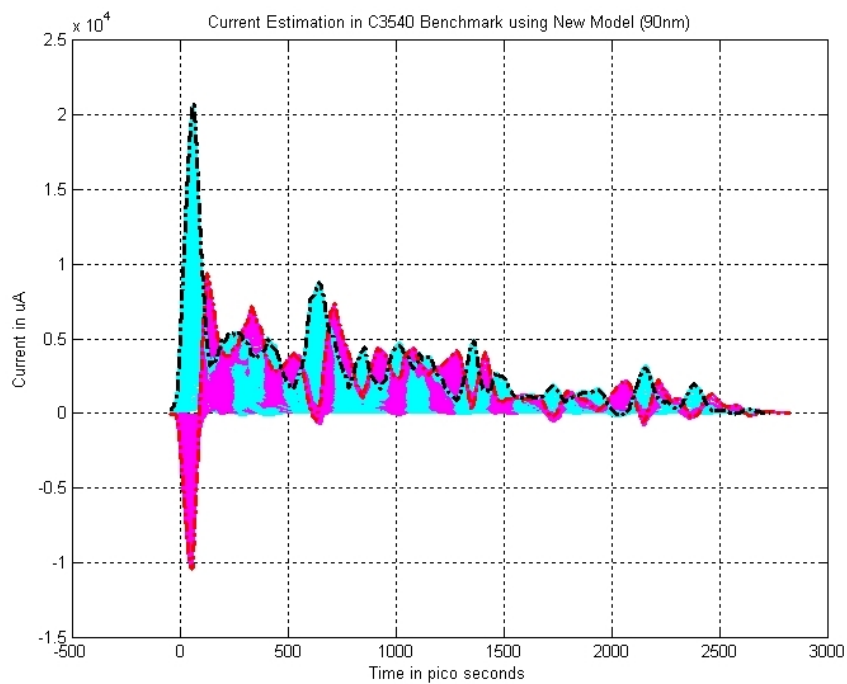
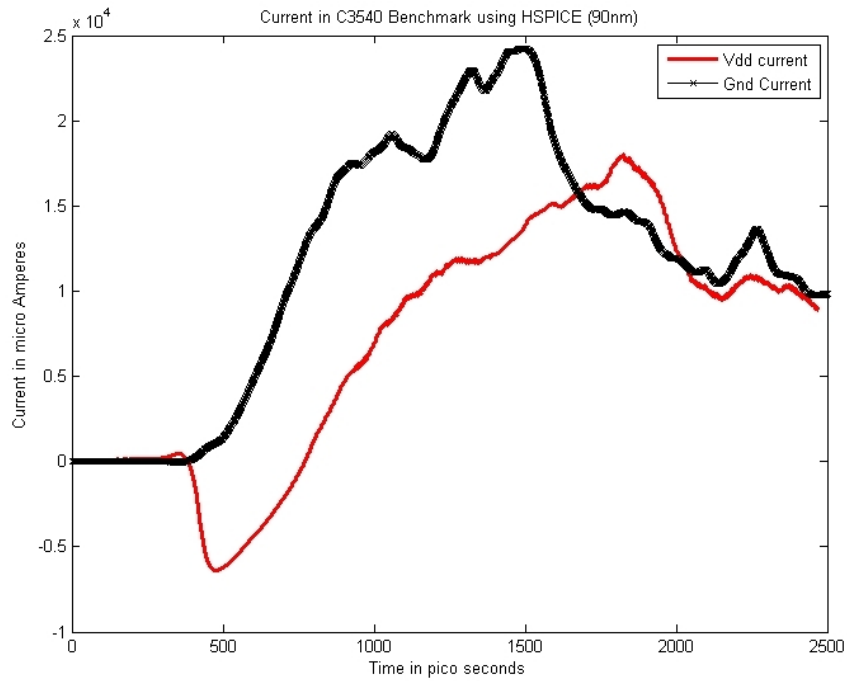


**Figure 53 Comparison of C3540 Benchmark using Algorithm 2 in New Model and HSPICE (90nm)**

### 5.2.2.7 Simulation of C6288 Benchmark

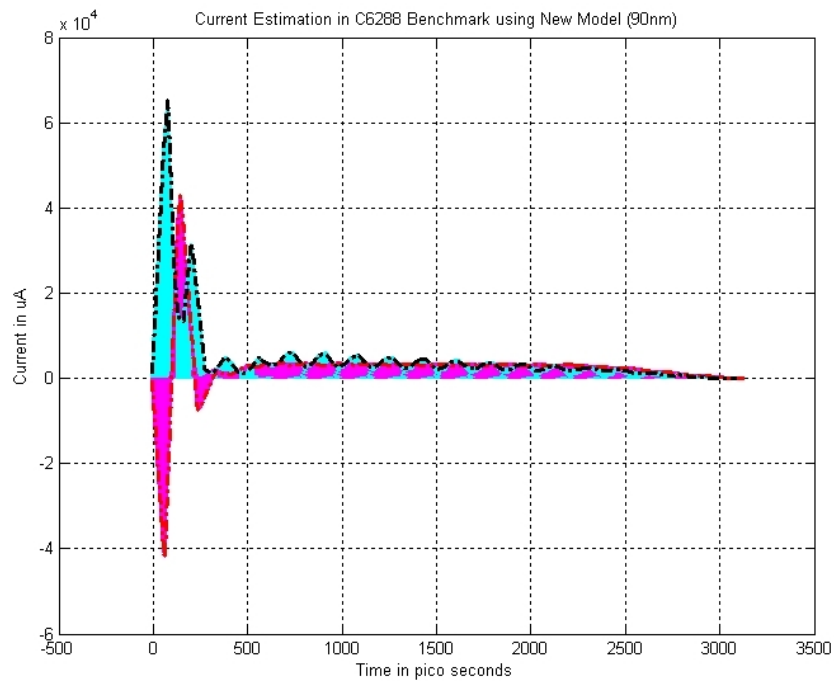
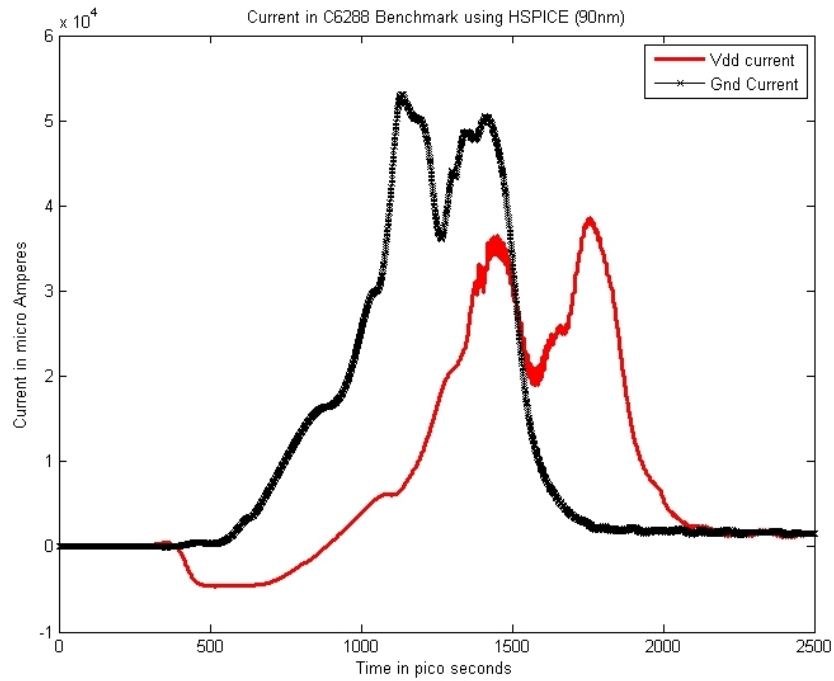


**Figure 54 Comparison of C6288 Benchmark using Algorithm 2 in New Model and HSPICE (90nm)**

### 5.2.2.8 Simulation of C7552 Benchmark

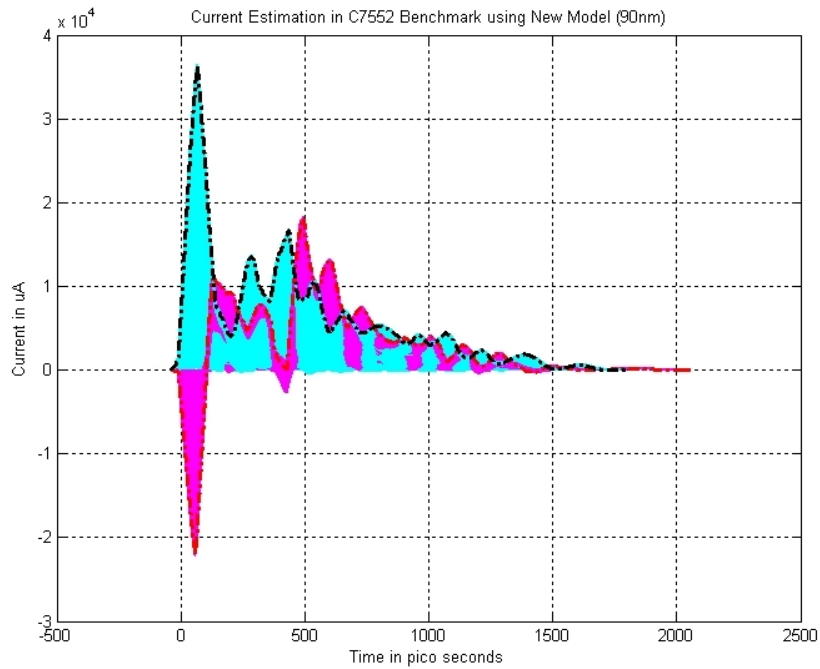
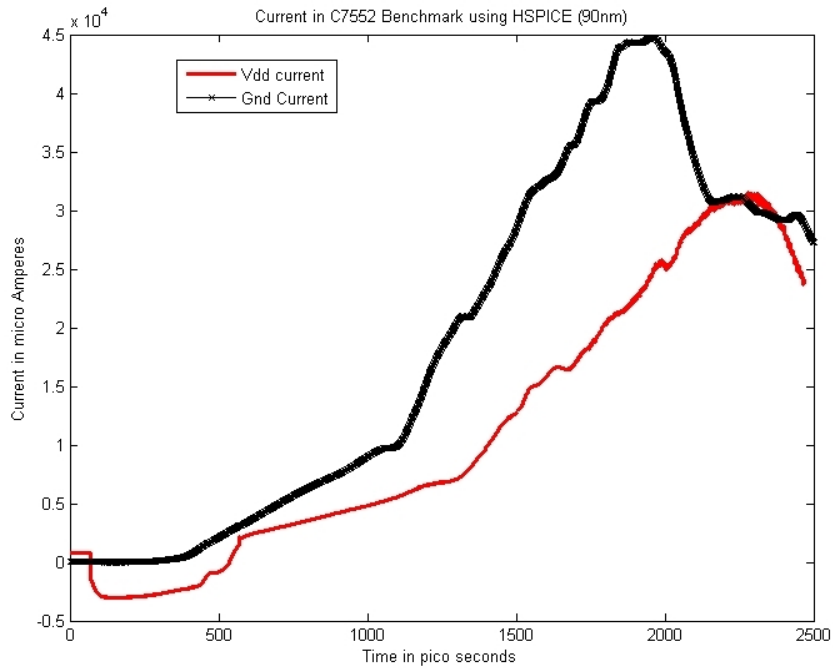


**Figure 55 Comparison of C7552 Benchmark using Algorithm 2 in New Model and HSPICE (90nm)**

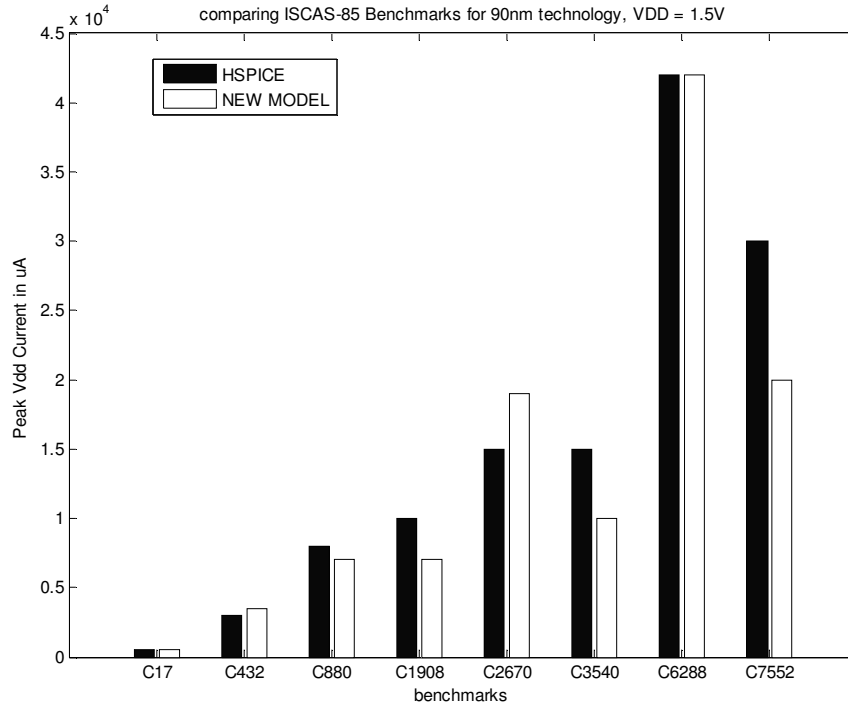


**Figure 56 Histogram of Comparison of vdd current using Algorithm2 in New Model and HSPICE (90nm)**

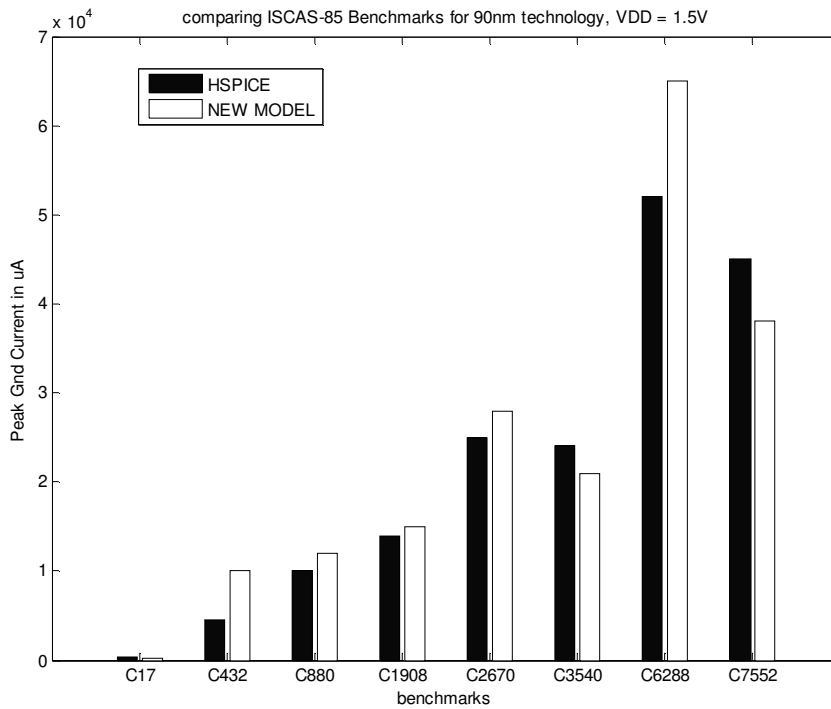


**Figure 57 Histogram of comparison of ground current using Algorithm2 in New Model and HSPICE (90nm)**

### 5.3 Simulation of ISCAS-85 benchmarks with 65nm technology (vdd = 1.5V)

#### 5.3.1 Simulation using Algorithm 2

##### 5.3.1.1 Simulation of C17 Benchmark

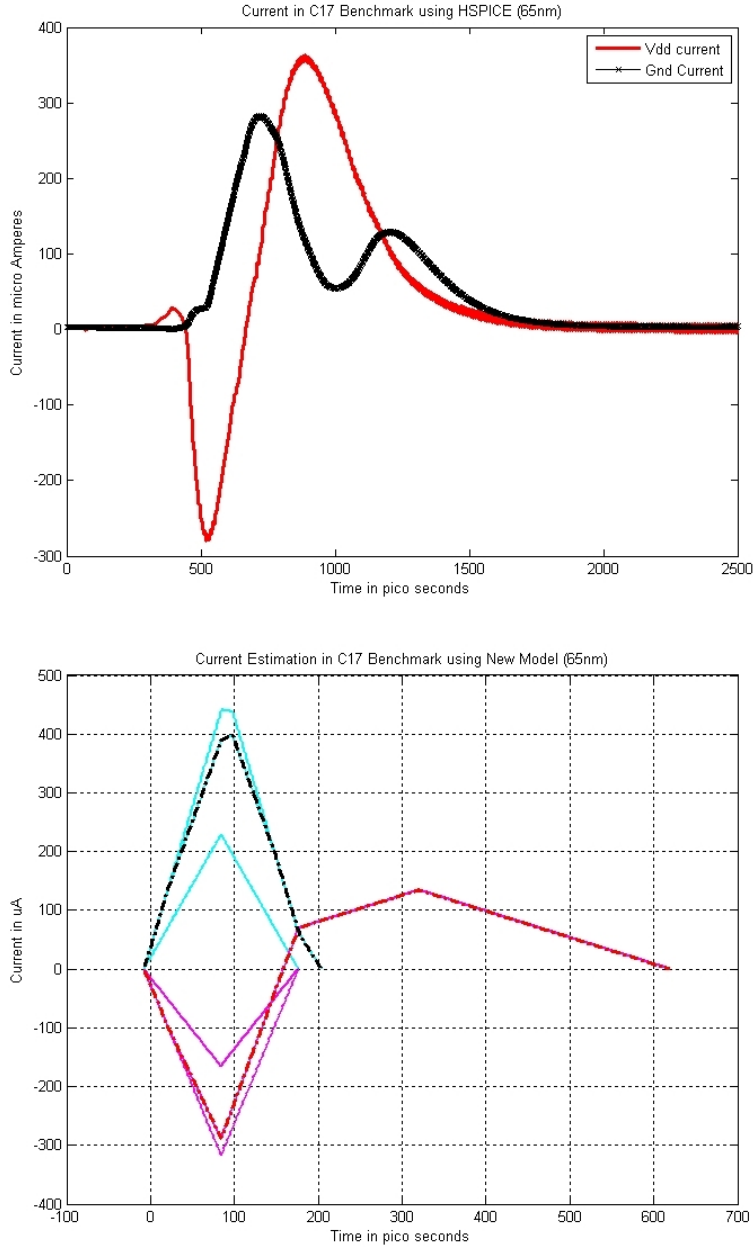


**Figure 58 Comparison of C17 Benchmark using Algorithm 2 in New Model and HSPICE (65nm)**

### 5.3.1.2 Simulation of C432 Benchmark

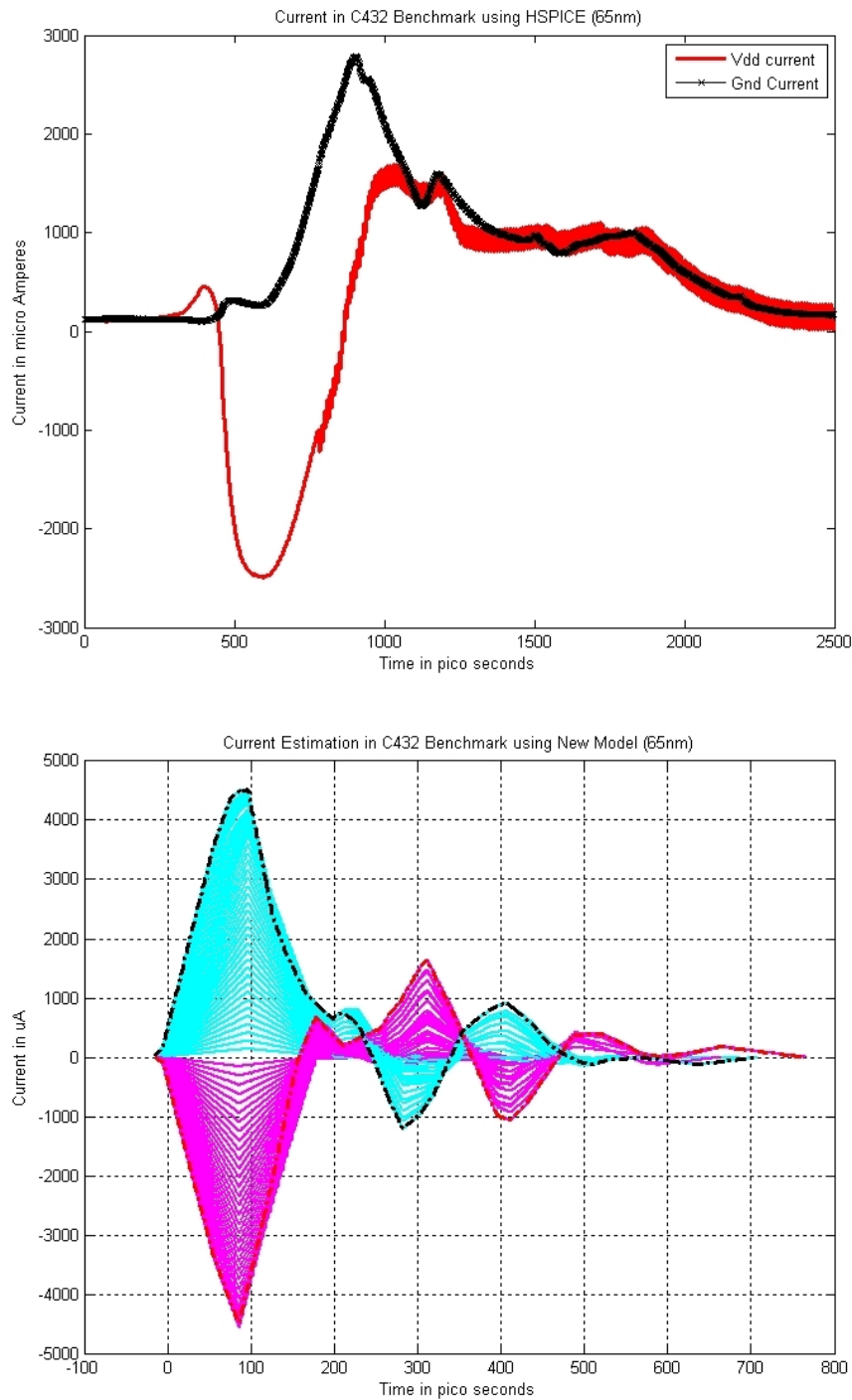


**Figure 59 Comparison of C432 Benchmark using Algorithm 2 in New Model and HSPICE (65nm)**



### 5.3.1.3 Simulation of C880 Benchmark

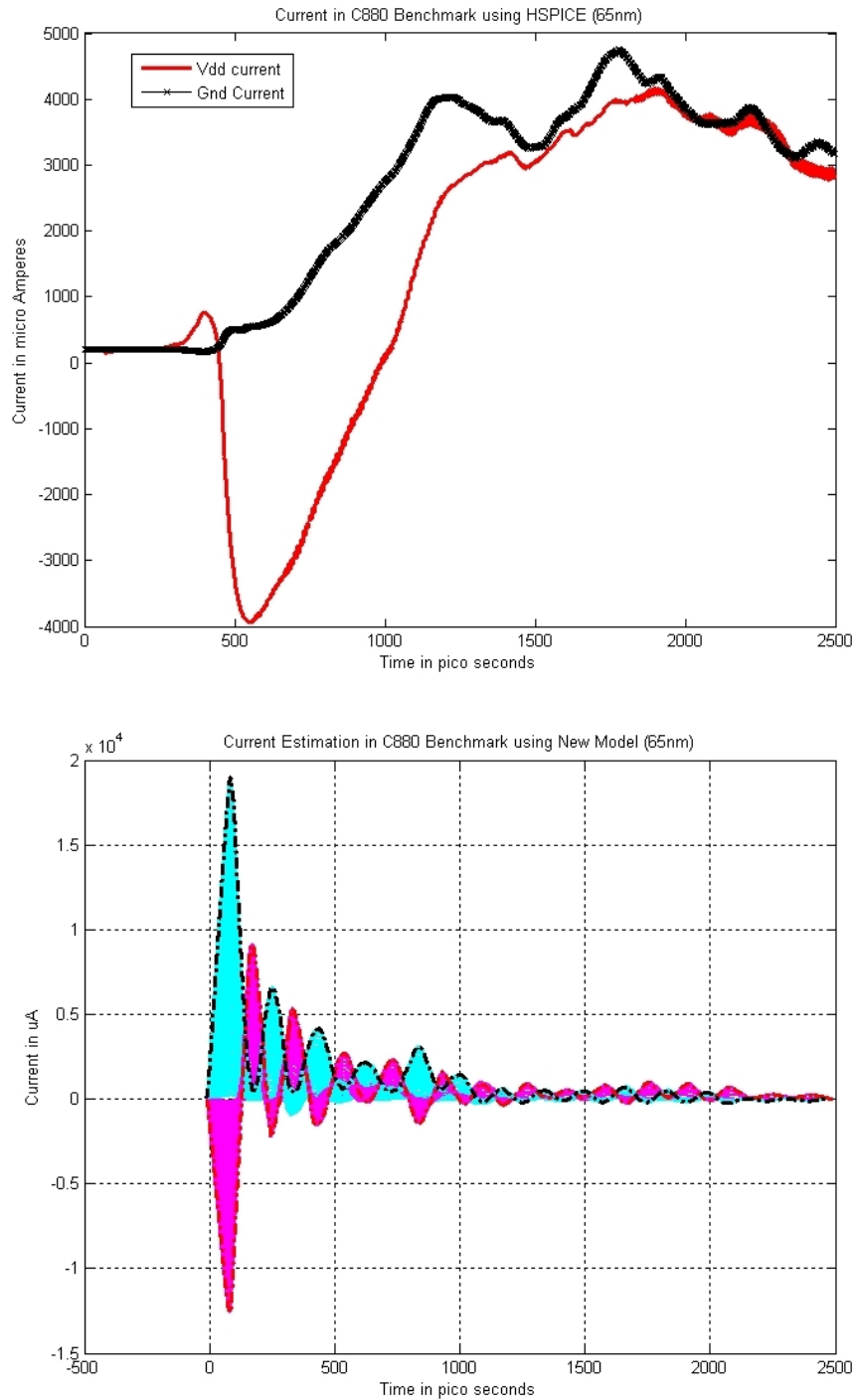


**Figure 60 Comparison of C880 Benchmark using Algorithm 2 in New Model and HSPICE (65nm)**

### 5.3.1.4 Simulation of C1908 Benchmark

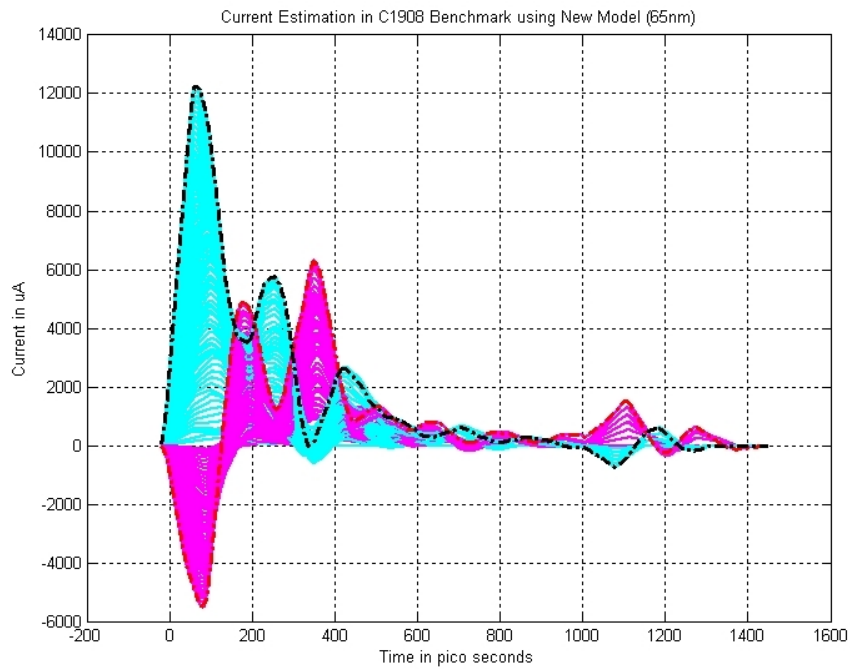
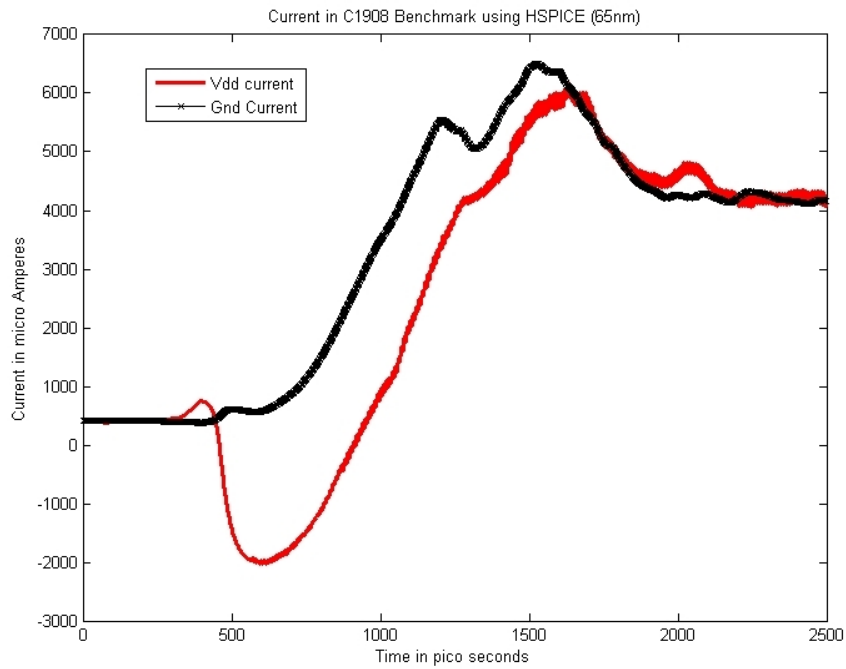


**Figure 61 Comparison of C1908 Benchmark using Algorithm 2 in New Model and HSPICE (65nm)**

### 5.3.1.5 Simulation of C2670 Benchmark

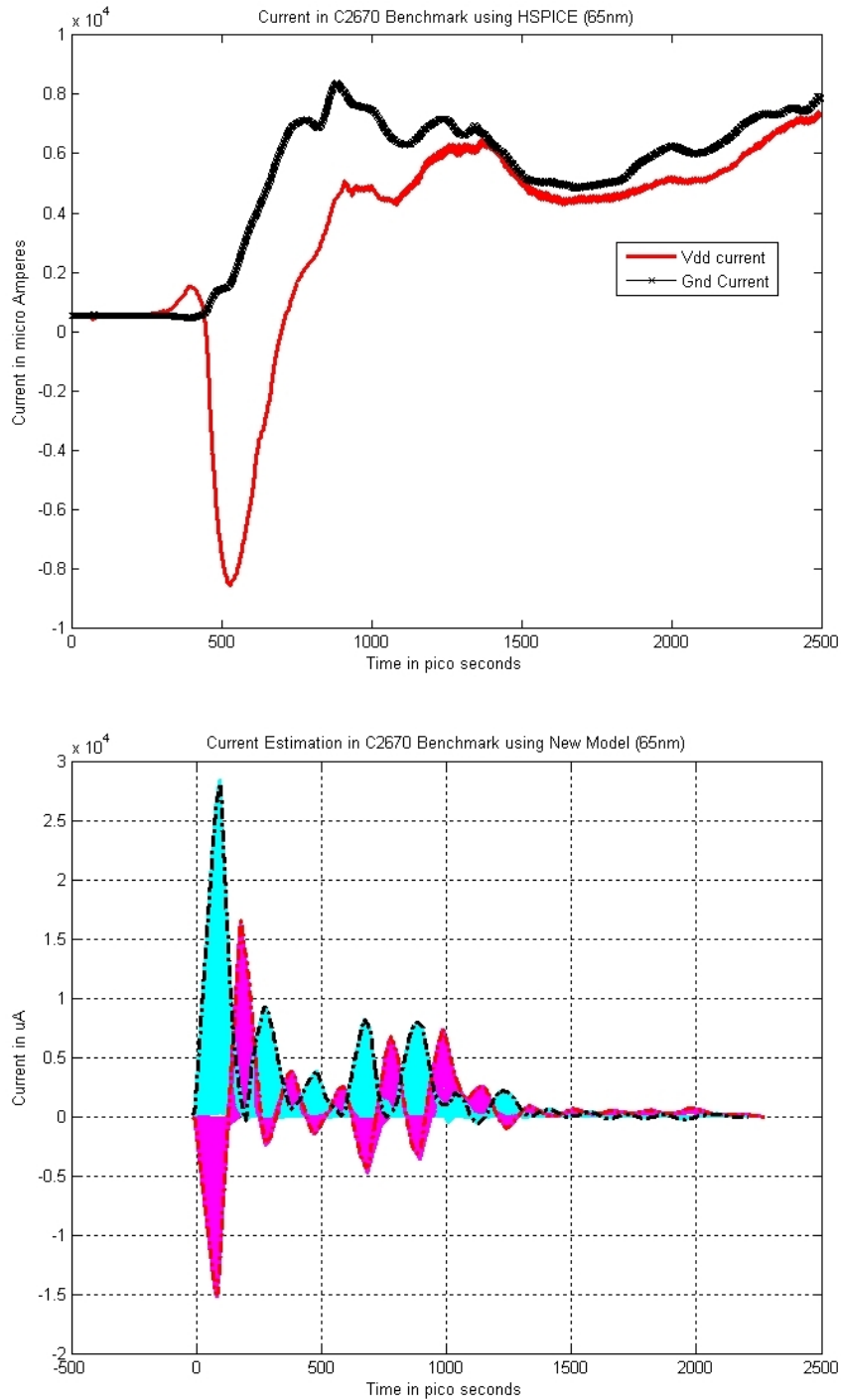


**Figure 62 Comparison of C2670 Benchmark using Algorithm 2 in New Model and HSPICE (65nm)**

### 5.3.1.6 Simulation of C3540 Benchmark

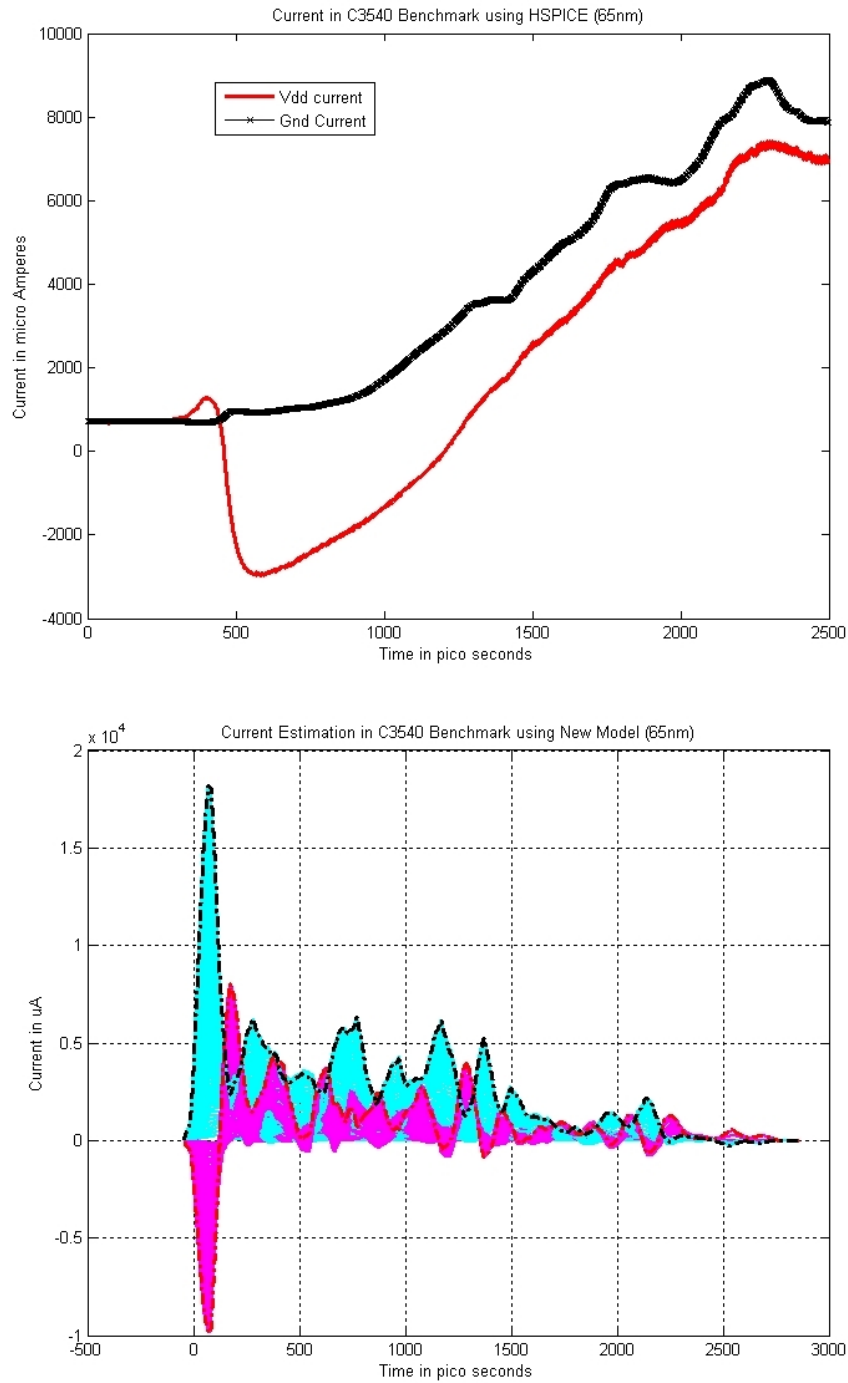


**Figure 63 Comparison of C3540 Benchmark using Algorithm 2 in New Model and HSPICE (65nm)**

### 5.3.1.7 Simulation of C6288 Benchmark

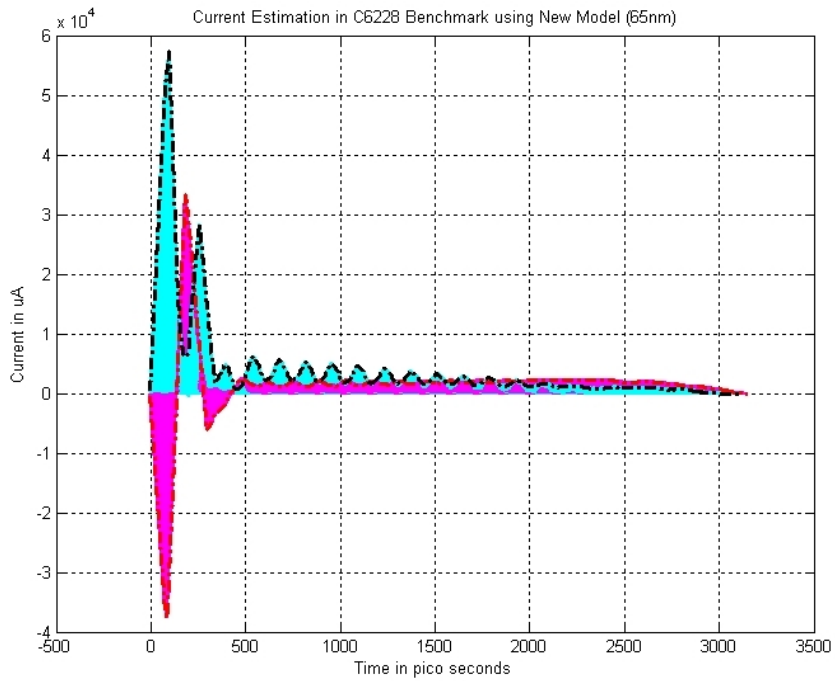
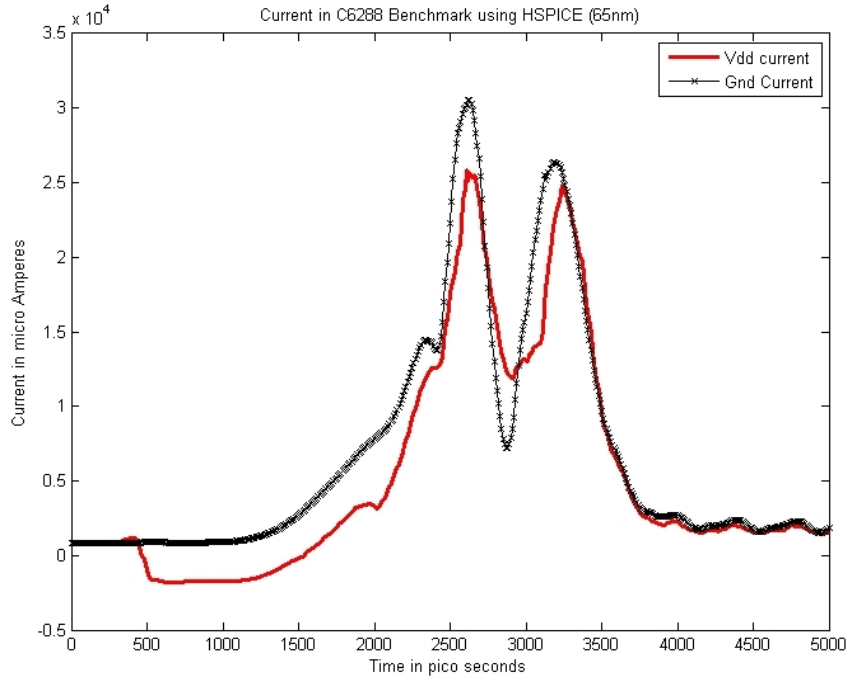


**Figure 64 Comparison of C6288 Benchmark using Algorithm 2 in New Model and HSPICE (65nm)**

### 5.3.1.8 Simulation of C7552 Benchmark

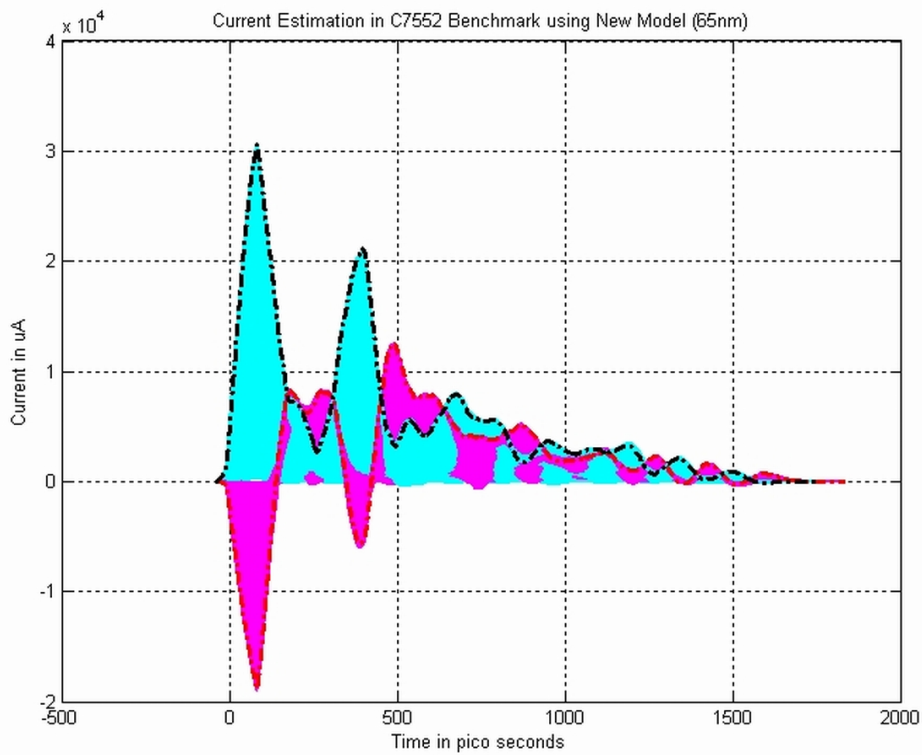
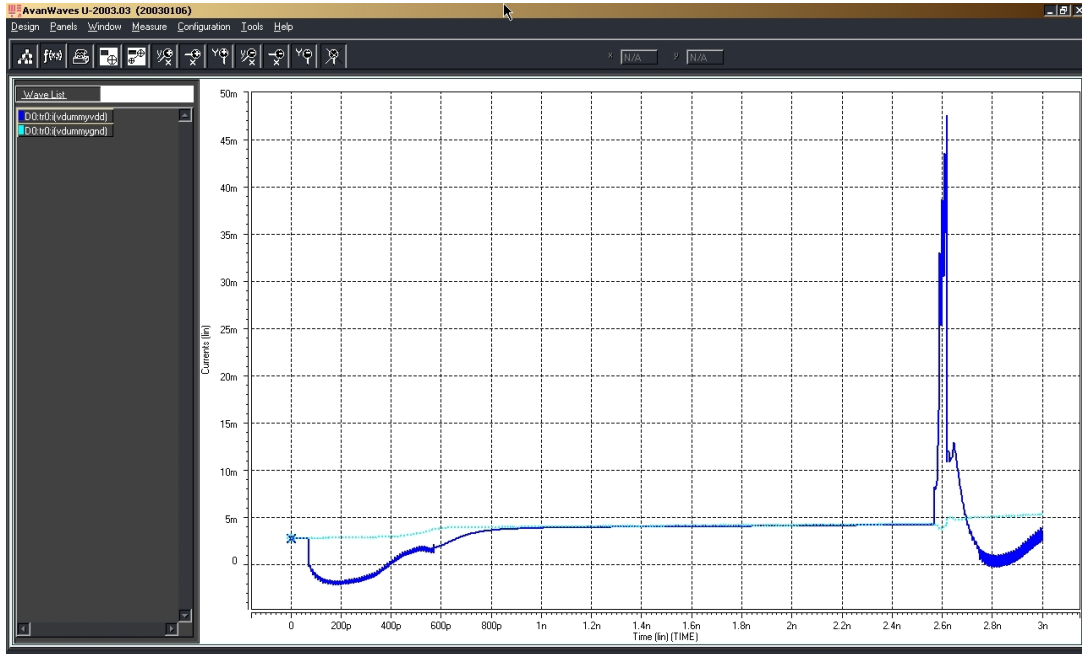


**Figure 65 Comparison of C7552 Benchmark using Algorithm 2 in New Model and HSPICE (65nm)**

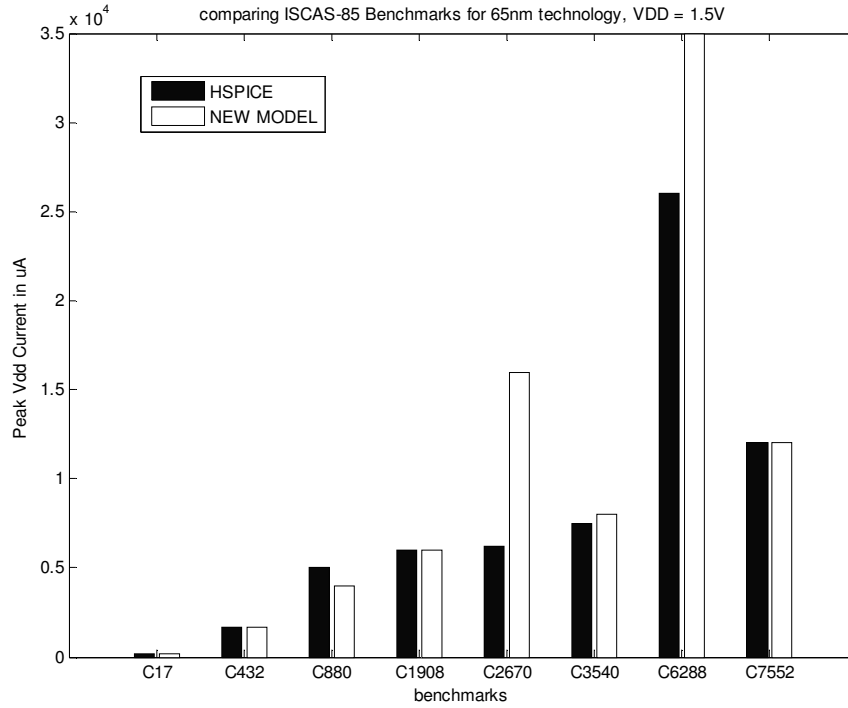


**Figure 66 Histogram of comparison of vdd current using Algorithm 2 in New Model and HSPICE for 65nm technology**

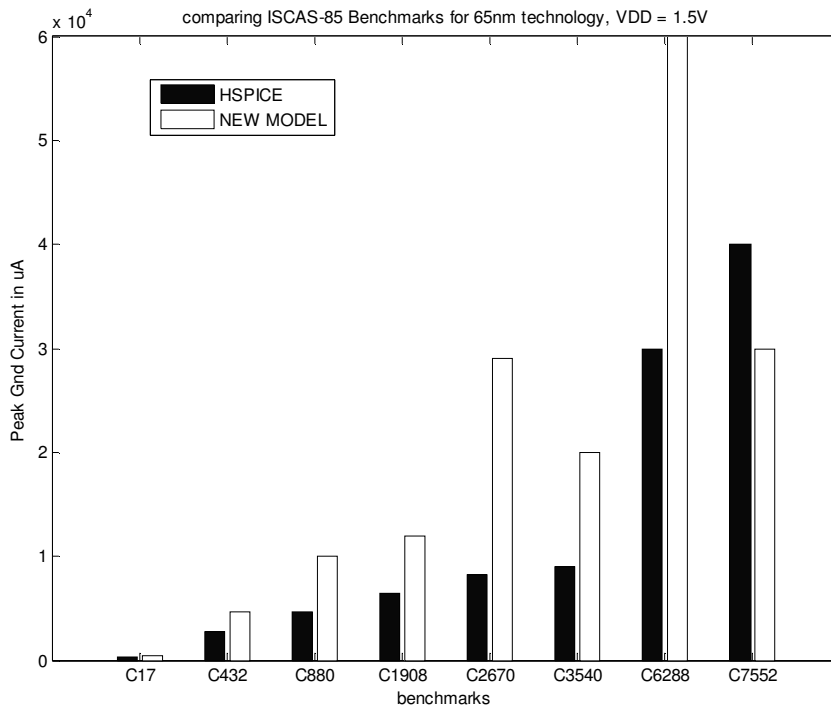


**Figure 67 Histogram of comparison of ground current using Algorithm 2 in New Model and HSPICE for 65nm technology**

# CHAPTER 6

## CONCLUSION

### 6.1 Comparing Run time of New Proposed Model with HSPICE

By running the simulations shown in the previous chapter, it is proved that the proposed new model's results are closer to HSPICE results. Further, slight variations of algorithm were introduced as algorithm 1 and algorithm2 While Algorithm 1 is sufficient for simulation, algorithm 2 goes one step further to reduce the simulation time. In 65nm technology, it was able to run simulation for benchmarks quicker than HSPICE for most of the benchmarks. The following histograms for the ISCAS-85 benchmarks illustrate this point.

#### 6.1.1 Comparing C432 Run time in HSPICE and New Model

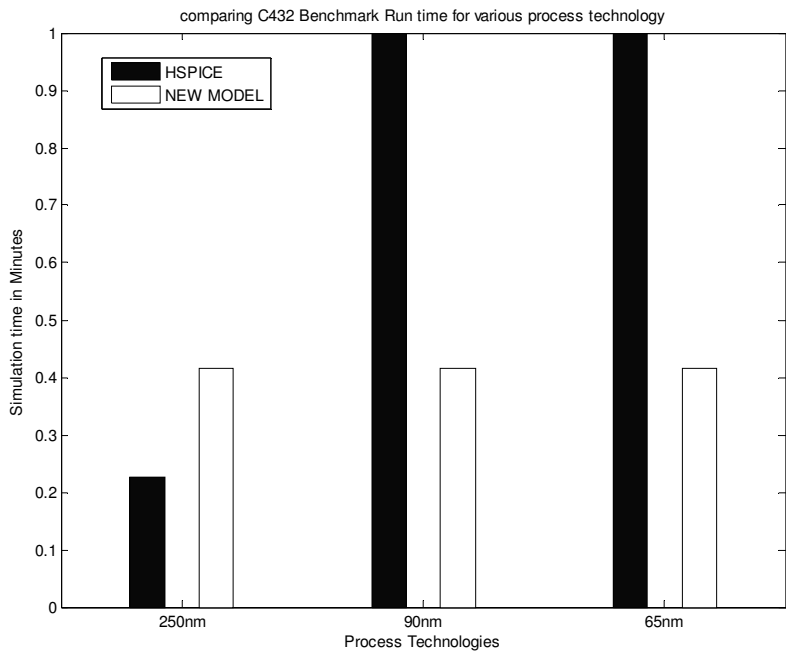




**Figure 68 Comparison of run time of C432 with HSPICE and New Model**

**6.1.2 Comparing C880 Run time in HSPICE and New Model**

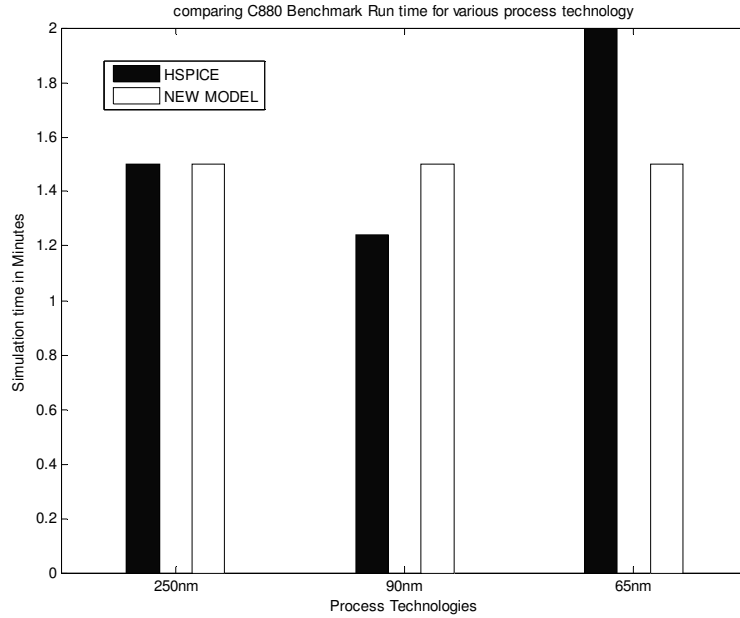


**Figure 69 Comparison of run time of C880 with HSPICE and New Model**

**6.1.3 Comparing C2670 Run time in HSPICE and New Model**

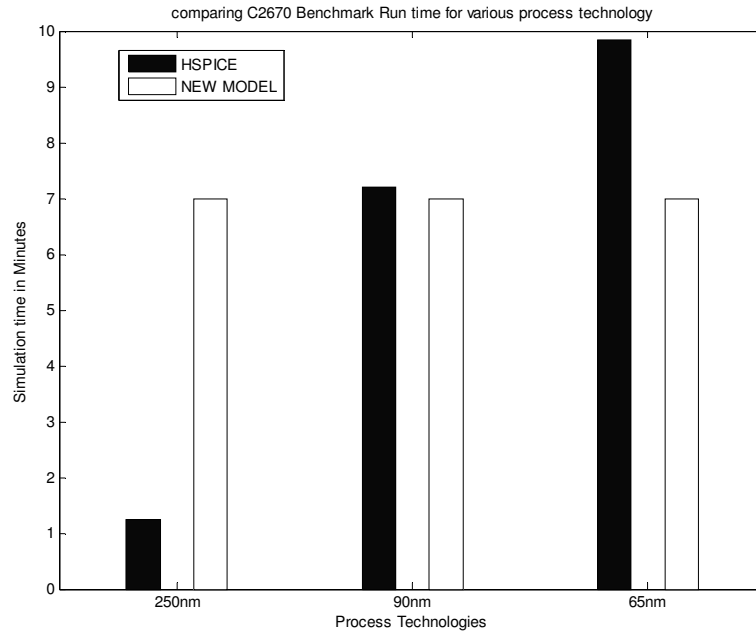


**Figure 70 Comparison of C2670 run time in HSPICE and New Model**

**6.1.4 Comparison C3540 run time in HSPICE and New Model**

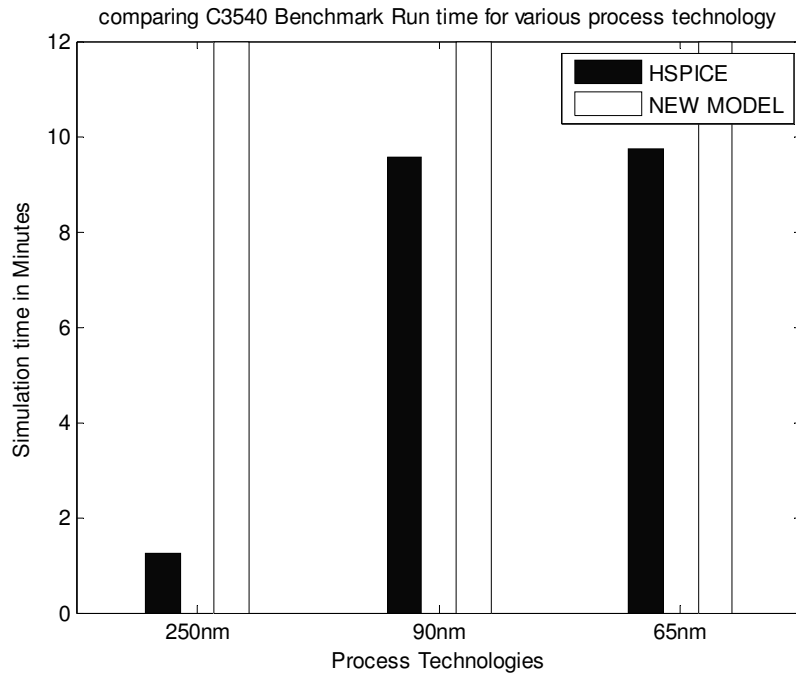


**Figure 71 Comparison of C354 runtime using HSPICE and New Model**

### 6.1.5 Comparison of C6288 run time in HSPICE and New Model

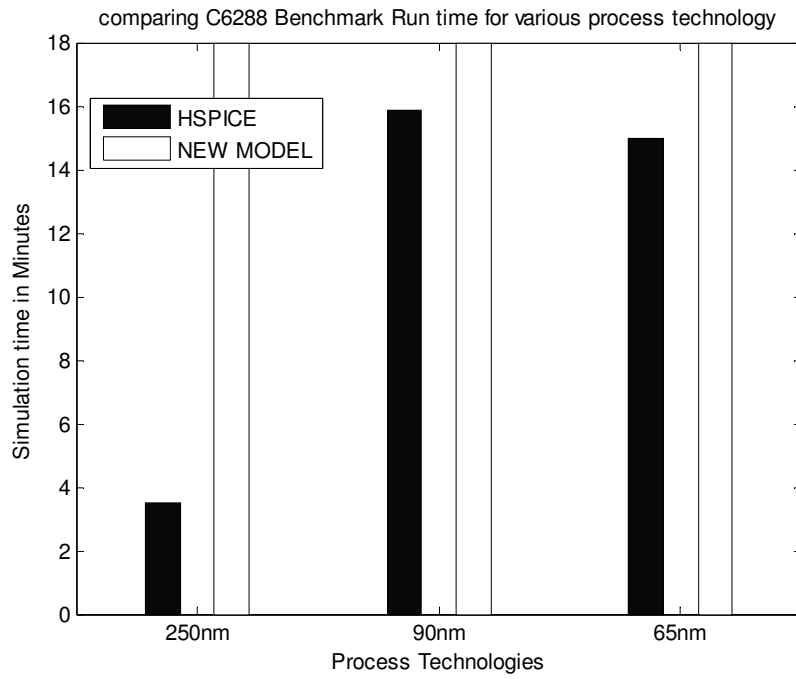
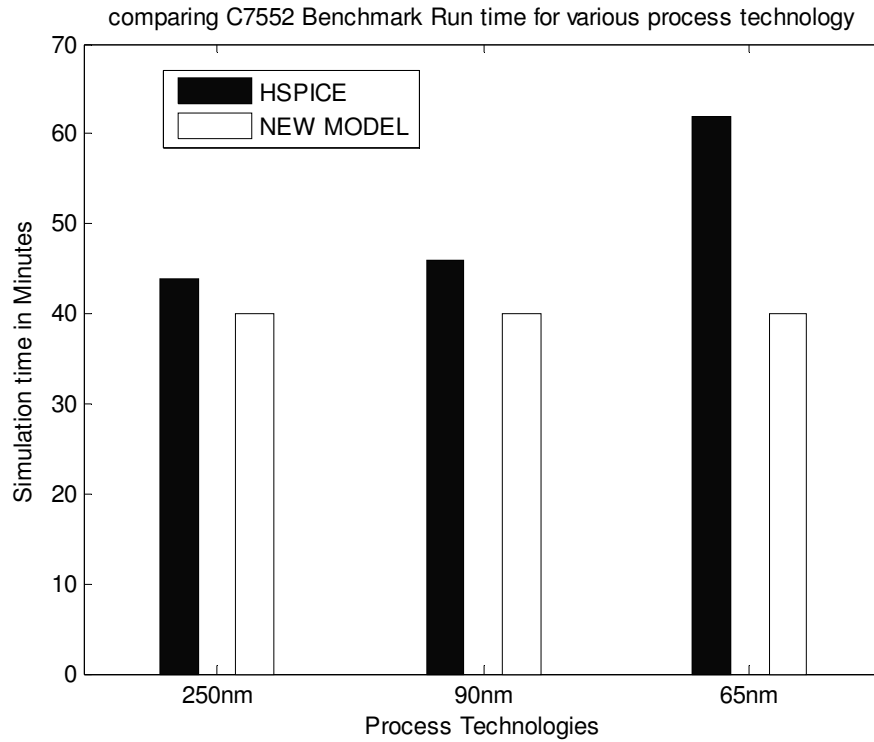


Figure 72 Comparison of C6288 run time using HSPICE and New Model.

### 6.1.6 Comparison of C7552 run time in HSPICE and New Model



**Figure 73 Comparison of C7552 run time in HSPICE and New Model**

## 6.2 Comparing accuracy of results between HSPICE and New Model

This is done by plotting the square root of mean square error for the simulation results between HSPICE and New Model. Following figures illustrate this.

**6.2.1 Comparing accuracy between HSPICE and Algorithm1 in New Model for 250nm technology**

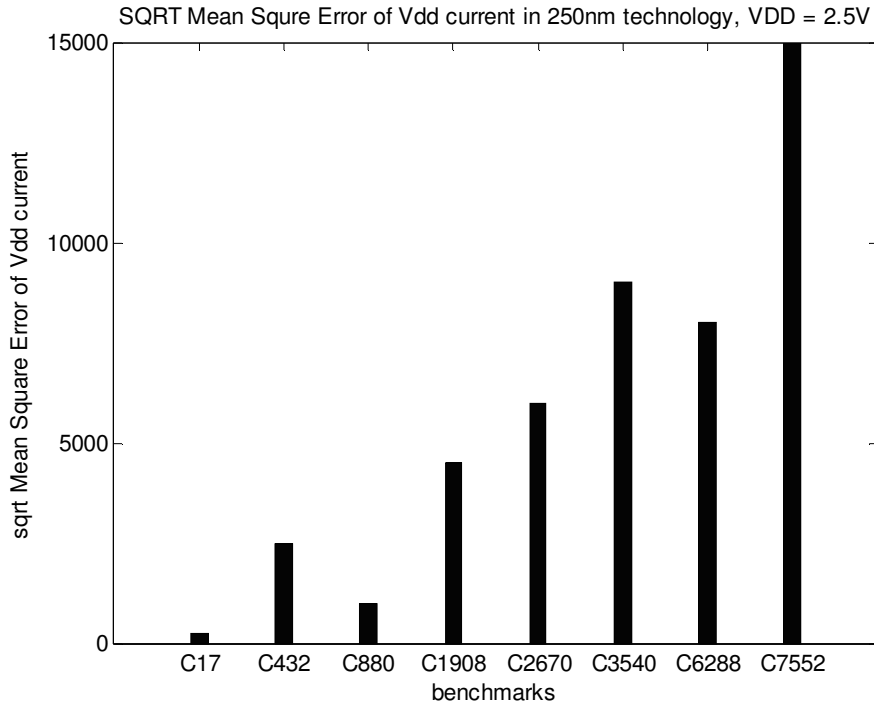


**Figure 74 Mean square error in vdd current between HSPICE and Algorithm 1 in New Model (250nm)**

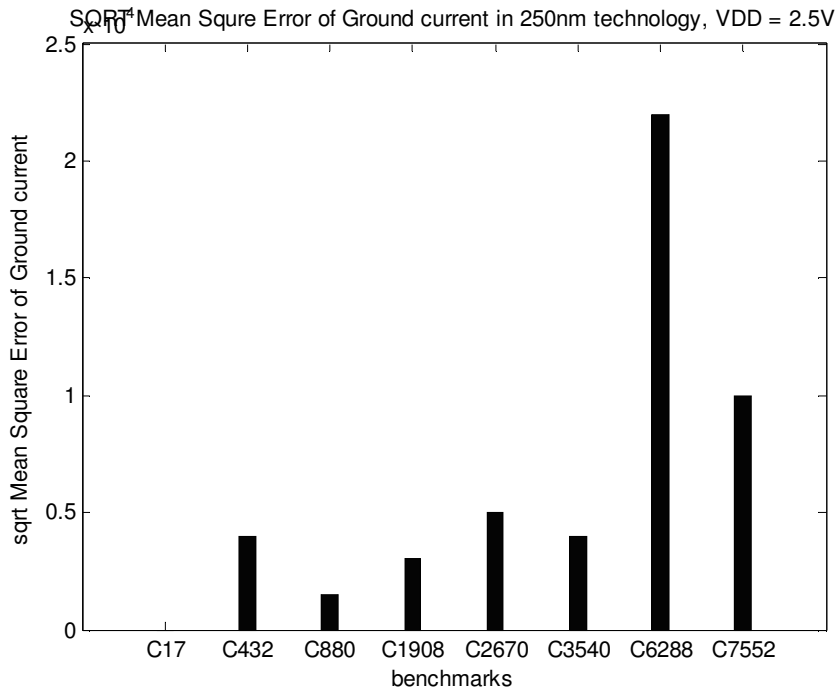


**Figure 75 Mean square error in gnd current between HSPICE and Algorithm1 in New Model (250nm)**

**6.2.2 Comparing accuracy between HSPICE and Algorithm2 in New Model for 250nm technology**

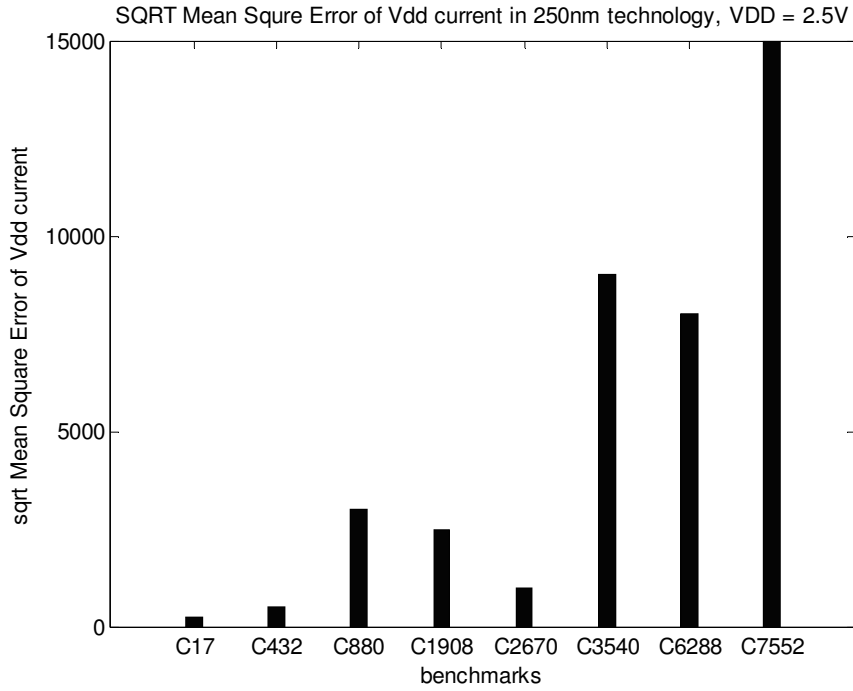


**Figure 76 Mean square error in vdd current between HSPICE and Algorithm2 in New Model (250nm)**

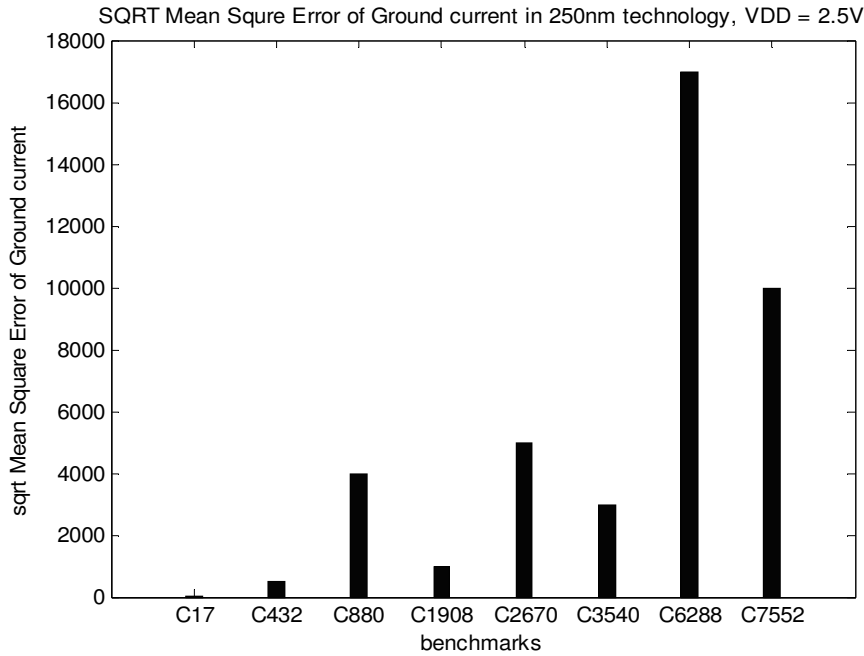


**Fig 77 Mean square error in ground current between HSPICE and Algorithm2 in New Model (250nm)**

### 6.2.3 Comparing accuracy between HSPICE and Algorithm1 in New Model for 90nm technology

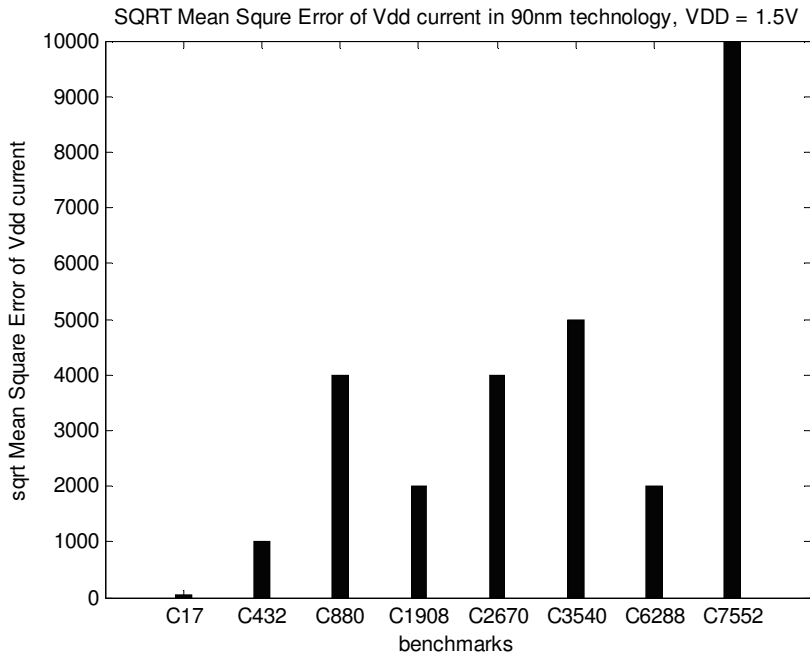


**Fig 78 Mean square error in vdd current between HSPICE and Algorithm1 in New Model (90nm)**

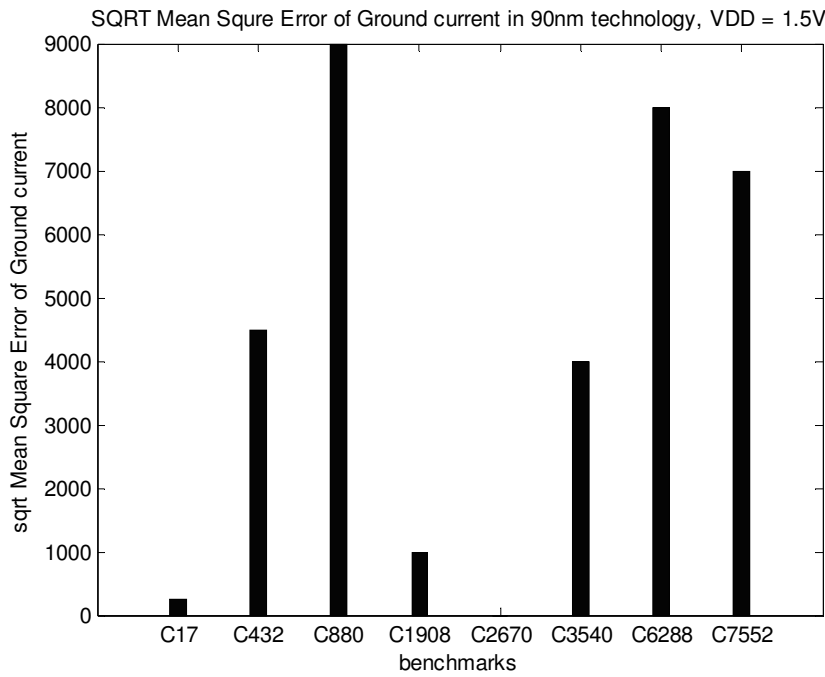


**Figure 79 Mean square error in ground current between HSPICE and Algorithm1 in New Model (90nm)**

### 6.2.4 Comparing accuracy between HSPICE and Algorithm2 in New Model for 90nm technology

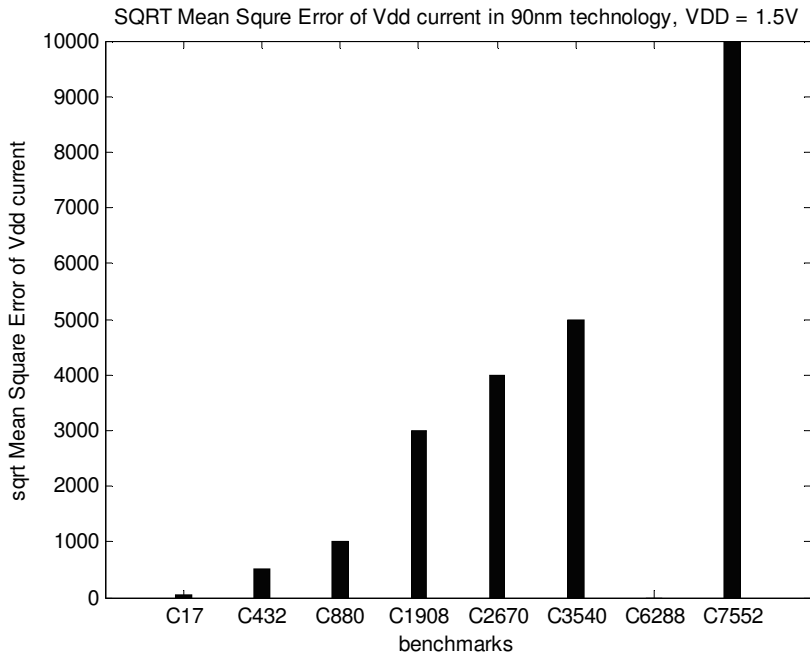


**Figure 80 Mean square error in vdd current between HSPICE and Algorithm 2 in New Model (90nm)**

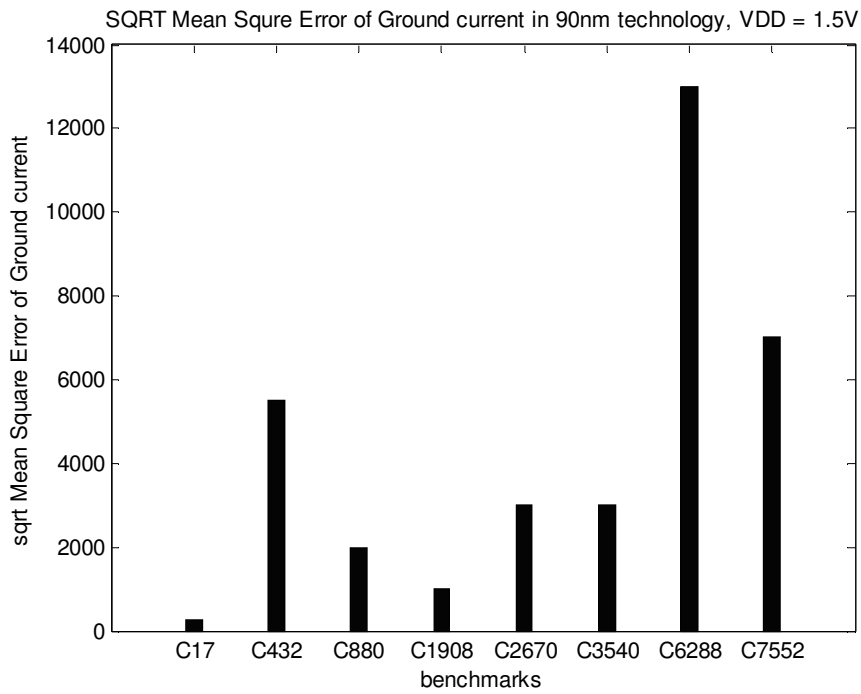


**Figure 81 Mean square error in ground current between HSPICE and Algorithm 2 in New Model (90nm)**



**6.2.5 Comparing accuracy between HSPICE and Algorithm2 in New Model for 65nm technology**

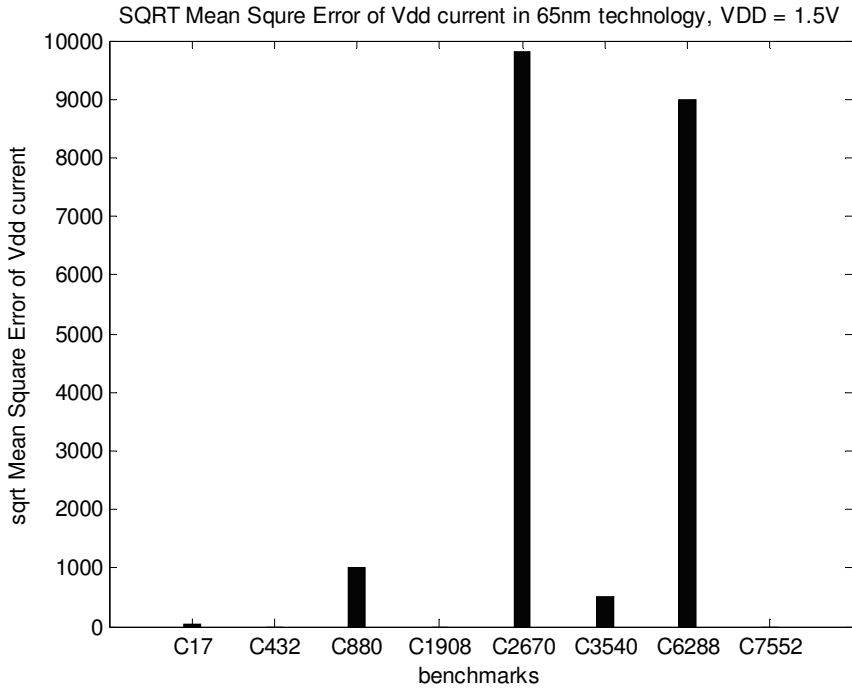


**Figure 82 Mean square error in vdd current between HSPICE and Algorithm 2 in New Model (65nm)**

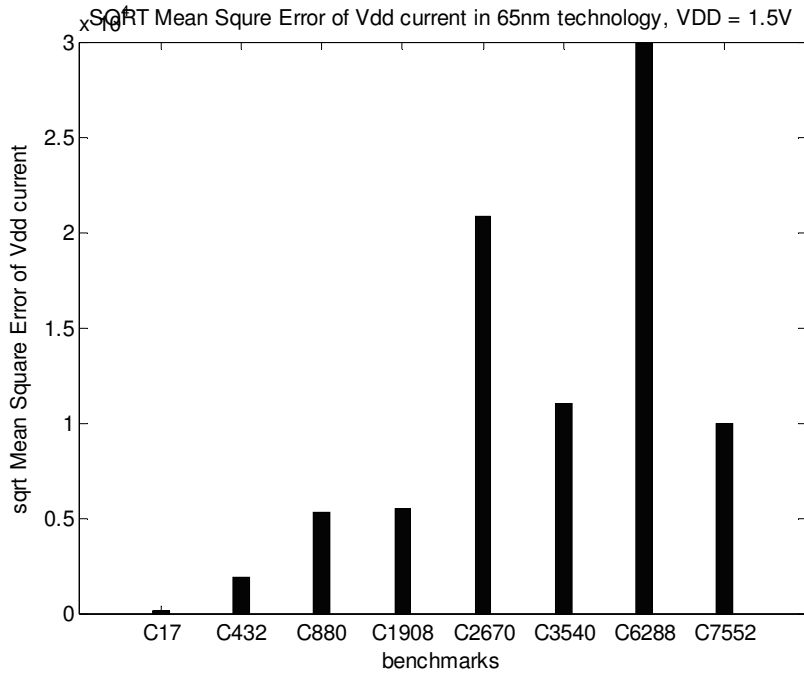


**Figure 83 Mean square error in ground current between HSPICE and Algorithm 2 in New Model (65nm)**

### **6.3 Future work**

Initially, this research project was started to see whether a simplified approach of modeling switching current works or not. Now that it has been shown that the approach works well, it can be extended. This work was based on a 2-input NAND gate. One can explore it for more than 2 input NAND gates. Further, one can do it for all other gate types. Secondly, in our proposed current model, simplified delay model has been used. One can work on that to improve it further. Thirdly, the case when both inputs switch and output does not switch in a 2 input NAND gate is not modeled in this work. So, one can model that as well. Lastly, one can write a faster algorithm to reduce computation time even further.

## BIBLIOGRAPHY

- [1] Sandip Kundu, Yi-Shing Chang, Chandra Trimurti, “a compact model for switching current waveform of CMOS gates”
- [2] Yi-Min Jiang, Angela Krystic, Kwang-Ting (Tim) Chang, “Estimation for Maximum Instantaneous current through supply lines for CMOS circuits,” *IEEE Transactions on VLSI systems*, Feb 2000.
- [3] Harish Kriplani, Farid Najm, Ibrahim Hajj, “Maximum current estimation in CMOS circuits,” *29<sup>th</sup> ACM/IEEE Design Automation Conference*, 1992
- [4] Anantha Chandrakasan, Jan M. Rabae, Borivoje Nikolic, “Digital Integrated circuits, a design perspective,” *2<sup>nd</sup> edition, Pearson Education, Inc.* 2003
- [5] Lavagno, Martin, and Scheffer, “A survey of the field of electronic design automation,” *Electronic Design Automation for Integrated Circuits Handbook, Taylor and Francis.* 2006
- [6] David Blaauw, Sanjay Pant, Rajat Chaudhry, Rajendran Panda, “Design and Analysis of Power Supply Networks,” chapter 20, vol II, *Electronic Design Automation for Integrated Circuits Handbook, Taylor and Francis.* 2006
- [7] Howard H. Chen, David D. Ling, “Power Supply noise analysis methodology for deep-submicron VLSI chip design,” *Design Automation Conference, Anaheim, CA* 1997
- [8] A. Chatzigeorgiou, S. Nikolaidis, “Efficient output waveform evaluation of a CMOS inverter based on short-circuit current prediction,” *John Wiley and Sons, Ltd*, 2002
- [9] Hedenstierna N, Jeppson KO, “CMOS circuit speed and buffer optimization,” *IEEE Transactions on Computer-Aided Design CAD-6(2):270–281*, 1987
- [10] Hirata A, Onodera H, Tamaru K, “Estimation of short-circuit power dissipation for static CMOS gates,” *IEICE Transactions on Fundamentals*, E79-A(3):304–311, 1996
- [11] Bisdounis L, Nikolaidis S, Koufopavlou O, “Analytical transient response and propagation delay evaluation of the CMOS inverter for short-channel devices,” *IEEE Journal of Solid-State Circuits*, 33(2):302–306, 1998
- [12] Sakurai T, Newton AR., “Alpha-power law MOSFET model and its applications to CMOS inverter delay and other formulas,” *IEEE Journal of Solid-State Circuits* 5(2):584–594, 1990
- [13] Chatzigeorgiou A, Nikolaidis S, Tsoukalas I, “A modeling technique for CMOS gates,” *IEEE Transactions on Computer-Aided Design of Integrated Circuits and Systems*, 18(5):557–575, 1999
- [14] Kong J-T, Hussain SZ, Overhauser D, “Performance estimation of complex MOS gates,” *IEEE Transactions on Circuits and Systems—I: Fundamental Theory and Applications* 44(9):785–795, 1997

- [15] A. Nabavi-Lishi and N.C. Rumin, "Inverter models of CMOS gates for supply current and delay evaluation," *IEEE Transactions on Computer Aided Design*, 13(10):1271-1279, 1994
- [16] Y.-H. Jun, K. Jun, and S.-B. Park, "An accurate and efficient delay time modeling for MOS logic circuits using polynomial approximation," *IEEE Transactions on Computer Aided Design*, 8(9):1027-1032, 1989.
- [17] Qi Wang and Sarma B.K. Vrudhula, "A new short circuit power model for complex CMOS gates," *Low power design proceeding*, 1999
- [18] F. Rouatbi, B. Haroun, and A. J. Al-Khalili, "Power estimation tool for sub-micron CMOS VLSI circuits," in *Proceedings of IEEE/ACM International Conference on Computer-Aided Design*, pp 204-209, Santa Clara, CA, November 8-12, 1992.
- [19] U. Jagau, "SIMCURRENT- an efficient program for the estimation of the current flow Of complex CMOS circuits," in *Proceedings of IEEE International Conference on Computer-Aided Design*, pp. 396-399, Santa Clara, CA, November 11-15, 1990.
- [20] A.-C. Deng, Y.-C. Shiau, and K.-H. Loh, "Time domain current waveform simulation of CMOS circuits," in *Proceedings of IEEE International Conference on Computer-Aided Design*, pp. 208-211, Santa Clara, CA, November 7-10, 1988.
- [21] S. Chowdhury and J. S. Barkatullah, "Estimation of maximum currents in MOS IC logic circuits," *IEEE Transactions on Computer-Aided Design*, vol. 9, no. 6, pp. 642-654, June 1990.
- [22] S. Devadas, K. Keutzer, and J. White, "Estimation of power dissipation in CMOS combinational circuits using Boolean function manipulation," *IEEE Transactions on Computer-Aided Design*, no. 3, pp. 373-383, March 1992.
- [23] Anas A. Hamoui, Nicholas Rumin, "An analytical model for current, delay and power analysis of submicron CMOS logic circuits," *IEEE Transactions of circuits and systems – II*, 2000
- [24] A. Nabavi-Lishi and N. Rumin, "Delay and bus current evaluation in CMOS logic circuits," *Proceedings of IEEE/ACM International Conference on Computer-Aided Design*, pp. 198-203, Santa Clara, CA, November 8-12, 1992.